EXPERIMENTAL AND MODELING STUDIES OF A DIRECT EXPANSION BASED AIR CONDITIONING SYSTEM HAVING A TWO-SECTIONED COOLING COIL (TS-DXAC) FOR IMPROVED INDOOR THERMAL ENVIRONMENTAL CONTROL

YANG LIU

PhD

The Hong Kong Polytechnic University

2021

The Hong Kong Polytechnic University

Department of Building Services Engineering

Experimental and Modeling Studies of a Direct Expansion Based Air Conditioning System Having a Two-Sectioned Cooling Coil (TS-DXAC) for Improved Indoor Thermal Environmental Control

Yang Liu

A thesis submitted in partial fulfillment of the requirements for the Degree of Doctor of Philosophy

May 2021

Certificate of Originality

I hereby declare that this thesis is my own work and that, to the best of my knowledge and belief, it reproduces no material previously published or written, nor material that has been accepted for the award of any other degree or diploma, except where due acknowledgement has been made in the text.

_____(Signed)

YANG Liu (Name of student)

Abstract

For buildings located in hot-humid climates, maintaining an appropriate level of indoor air humidity (RH_i) is important for improved indoor thermal comfort, better indoor air quality and a higher energy efficiency of air conditioning (A/C) systems. Direct expansion (DX) A/C systems have been widely used to control indoor thermal environments in small- to medium- scale buildings, because they are more energy efficient, require less space to install and cost less in operation and maintenance. However, it is a challenging task to control RH_i using a DX A/C system. This is because a single DX A/C system has to simultaneously handle the considerable changes in both sensible space cooling load and latent space cooling load. The commonly used temperature based On-Off control strategy for DX A/C systems can only be used for indoor air temperature (T_i) control, leaving RH_i control as a by-product of temperature control. In addition, currently, the design trend of a DX A/C system is to try to reduce its dehumidification capacity for improving its energy performances. Therefore, to meet the requirement of indoor moisture removal, an air-conditioned space is usually overcooled by having a lower T_i setting. Hence, there have been significant research efforts to address the inadequacies in air dehumidification when using DX A/C systems. However, in these efforts, additional dehumidification provisions leading to larger installation spaces, or complex controllers based on variable speed (VS) technology were usually required. Furthermore, for a VS DX A/C system, to output an enhanced dehumidification capacity, a lower supply air flow rate was usually required, leading to a reduced level of thermal comfort because of a lower supply air temperature and a poorer indoor air distribution.

Therefore, based on the previous related studies in developing novel A/C systems to provide an enhanced moisture removal capacity, a novel constant speed DX A/C system having a two-sectioned cooling coil (TS-DXAC) has been proposed. The two sections, with one section to mainly deal with the latent cooling load (LCL) and the other sensible cooling load (SCL), are arranged in parallel with their respective matching variable speed supply fans, and the mass flow rates for both refrigerant and air to each section could be adjusted. The total air flow rate of the system can be kept constant, so as not to affect indoor air distribution and occupants' thermal comfort.

A research project on developing such a TS-DXAC system using experimental and mathematical modeling approaches has been therefore carried out and the project results are presented in this Thesis.

Firstly, the establishment of an experimental TS-DXAC system, which was composed of two sub-systems, i.e., a DX refrigeration sub-system and an air-distribution sub-system, is reported. The experimental TS-DXAC system was placed inside an environmental chamber where air states can be controlled for experimental purposes. All the operating parameters of the experimental TS-DXAC system and the thermal environmental parameters in the chamber can be real-time monitored and recorded using high precision measuring devices. With availability of the experimental TS-DXAC system, its operational characteristics can be experimentally studied, a steady-state mathematical model for the experimental TS-DXAC system to be established also experimentally validated, and finally a control strategy to be developed to operate the experimental TS-DXAC system for improved indoor thermal environment control tested.

Secondly, the Thesis presents an experimental study on the inherent operational characteristics of the experimental TS-DXAC system. The study results showed that the variations in the mass flow rates of both refrigerant and air to the two sections would result in different combinations of the output total cooling capacity (TCC) and equipment sensible heat ratio (E SHR) from the experimental TS-DXAC system, and that the TCC - E SHR relationship was constrained within an irregular area. Furthermore, different inlet air temperatures and humidity levels to the experimental TS-DXAC system would also influence its inherent operational characteristics as reflected by the changes in the positions and shapes of the irregular areas, with the humidity levels influencing more on the operational characteristics.

Thirdly, the establishment of a steady-state physical-based mathematical model for the experimental TS-DXAC system is presented. The established model was experimentally validated using the data collected from the experimental TS-DXAC system, with the differences between the experimental and predicted results of being less than 6%. Using the validated TS-DXAC model, a follow-up modeling study was carried out on optimizing the relative sizes of the two sections. The modeling study suggested that a lower surface area ratio for the two sections can lead to a larger variation ranges of both output TCC and E SHR. For example, at the inlet state of 26 ℃ and 50% relative humidity, when the surface area ratio for the two sections was altered from 1:1 to 1:3, the variation range for output TCC was increased by 33%, and that for E SHR by 51%, which was beneficial to better dehumidification.

Finally, the Thesis reports the development of a control strategy to enable the experimental TS-DXAC system to be operated in hot-humid climates. The developed

control strategy included two control algorithms, i.e., Algorithm I and Algorithm II, enabling the experimental TS-DXAC system to be operated under two different indoor conditions, i.e., hot-humid and hot-dry, respectively. Controllability tests for the control strategy were carried out using the experimental TS-DXAC system. Two test sets with a total of six tests were organized for the two indoor air conditions. The controllability test results demonstrated that in all the tests, T_i could be directly controlled at the two indoor conditions using either of the two algorithms, while RH_i could be directly controlled at a hot-humid indoor condition using Algorithm I. The control strategy enabled the experimental TS-DXAC system to respond to the changes in either indoor settings or space cooling loads by outputting variable sensible and latent cooling capacities.

Publications Arising from the Thesis

I. Journal Papers

- **Yang Liu,** Yan Huaxia, Deng Shiming, Li weilin. An experimental investigation on the operational characteristics of a novel direct expansion based air conditioning system with a two-sectioned cooling coil. International Journal of Refrigeration, 2020, 118: 131-138. (Based on Chapter 5)

- **Yang Liu,** Weng Wenbing, Deng Shiming. A modeling study on a direct expansion based air conditioner having a two-sectioned cooling coil. Applied Energy, 2020, 278: 115688. (Based on Chapter 6)

- **Yang Liu**, Deng Shiming, Fang Guanyu, Li Weilin. Indoor thermal environmental control using a novel direct expansion based air conditioning system. Journal of Building Engineering, 2021, 43: 102920. (Based on Chapter 7)

II. Conference Papers

- **Yang Liu**, Deng Shiming. A modeling study on the inherent inherent operational characteristics of a direct expansion based air conditioning system having a two-sectioned cooling coil. International Conference on Applied Energy 2019. Västerås, Sweden, 2019, 8.

Acknowledgements

First of all, I must express my sincere gratitude to my supervisor, Prof. Deng Shiming from the Department of Building Services Engineering, The Hong Kong Polytechnic University, for providing me with the golden opportunity to pursue my Ph.D. His motivation, optimism and vision have inspired me deeply. He taught me patiently how to conduct research and how to present the research results clearly and accurately. It was a great honor to work under his guidance. I also want to express my thanks to Prof. Weng Wenbing from School of Environment and Architecture, University of Shanghai for Science and Technology, for his valuable help in the successful carrying out of my experimental research.

Secondly, I would like to thank my colleagues and friends in Hong Kong, Dr. Chen Wenjing, Dr. Yan Huaxia, Mr. Fang Guanyu, Ms. Liu Shengnan and Mr. Bai Xiaoxia for their support to my Ph.D. study.

Finally, I would dedicate this achievement to my wife, Dr. Li Weilin, and my parents and parents-in-law. Without their selfless dedication and the full support for the family, I would never be able to complete my work. I also want to dedicate this Thesis to my son, Yang Zhiyi, who made my research life more colorful and made this study period not difficult for me.

Table of Contents

List of Figures

Chapter 2

Chapter 4

Chapter 5

Chapter 6

Chapter 7

Appendix

List of Tables

Chapter 4

Chapter 5

Chapter 7

Nomenclature

Variable	Description	Unit
A	area	m^2
C_{pa}	specific heat of air	kJ/(kg·K)
h	specific enthalpy	kJ/kg
m	mass flow rate	kg/s
P	pressure	Pa
Q_s	output sensible cooling capacity	kW
R	ratio	DL
RH	relative humidity	%
RH_i	indoor air humidity	%
$RH_{i,s}$	the set-point of indoor air humidity	%
T	temperature	°C
T_{db}	air dry-bulb temperature	°C
T_i	indoor air temperature	°C
$T_{i,s}$	the set-point of indoor air temperature	°C
T_{wb}	air wet-bulb temperature	°C
ΔRH	relative humidity control dead-band	%
ΔT	temperature control dead-band	°C

Subscripts

a	air
com	compressor
con	condenser

ds	de-superheating
l	liquid refrigerant
r	refrigerant
sc	sub-cooling
sh	superheated
tp	two-phase
v	vapor refrigerant

List of Abbreviations

A/C	air conditioning
COP	coefficient of performance
DEAC	dual-evaporator air conditioning
DS	the degree of refrigerant superheat
DOAS	dedicated outdoor air system
EEV	electronic expansion valve
E SHR	equipment sensible heat ratio
HX1	the first section
HX2	the second section
IAQ	indoor air quality
LCC	latent cooling capacity
LCL	latent cooling load
LGU	load generating unit
MEAC	multi-evaporator air conditioning
RHC	radiant heating and cooling

SCC	sensible cooling capacity
SCL	sensible cooling load
SF	supply fan
SSLC	separating sensible and latent cooling
TCC	total cooling capacity
TS-DXAC	DX A/C system having a two-sectioned cooling coil
VS	variable speed

Chapter 1

Introduction

In buildings in the tropics and sub-tropics, the control of indoor air temperature (T_i) and that of indoor air humidity (RH_i) are equally important since both directly affect building occupants' thermal comfort, indoor air quality (IAQ) and the operating efficiency of building air conditioning (A/C) systems. In small- to medium- scale buildings such as residences, direct expansion (DX) based A/C systems are widely used for controlling indoor thermal environment because they are compact in volume, high in energy efficiency and low in operation and maintenance costs.

However, to simultaneously control T_i and RH_i using DX A/C systems is a great challenge because the current trend in the design of a conventional DX A/C system is to reduce its moisture removal capacity in an attempt to boost its energy efficiency ratings, and most DX A/C systems are equipped with single-speed compressors and fans, relying on On-Off control of compressors to only maintain T_i. Although additional dehumidification provisions such as a dedicated outdoor air system (DOAS) or an additional compression cycle or the use of desiccant may be employed for additional moisture removal capacities, these provisions are usually complicated and require additional installation space, and therefore are not suitable for use in small- to medium-scale buildings. On the other hand, the application of variable speed (VS) technology to DX AC systems can help achieve simultaneous control over T_i and RH_i without requiring additional space, so this is preferred for small- to medium- scale buildings. However, there are two problems associated with the application of the VS technology

to DX A/C systems control strategies being complicated and poorer indoor air velocity distribution adversely affecting indoor thermal comfort.

Hence, to address inadequacies in controlling indoor thermal environment using traditional DX A/C systems, based on the previous related studies on developing novel DX A/C systems to provide an enhanced moisture removal capacity, a novel DX based A/C system having a two-sectioned cooling coil or evaporator (TS-DXAC) has been proposed, without additional provision or complex control strategies to provide variable cooling capacities. A research project to develop the proposed TS-DXAC system has been carried out using experimental and mathematical modeling approaches, and the project results are presented in this Thesis.

To begin with, a comprehensive literature review on various issues related to the development of the proposed TS-DXAC system is presented in Chapter 2. Firstly, the fundamental issues on indoor thermal environmental control are detailed, including appropriate T_i for thermal comfort, sources of indoor moisture, the effects of different levels of RH_i on indoor thermal comfort and IAQ, and the influence of different supply air velocities on indoor thermal environment. Secondly, the existing problems of controlling indoor thermal environment using conventional DX A/C systems are reported. Thirdly, a review of different approaches, which may be grouped into three different categories to address these problems is presented. Fourthly, a review on previous modeling studies on DX A/C systems and their major components is reported. Lastly, the research gaps where further research attentions should be paid to are summarized.

In Chapter 3, based on the literature review presented in Chapter 2, a proposal for the research project presented in this Thesis, including the background, project title, objectives and research methodologies, is detailed.

Chapter 4 reports on the establishment of an experimental TS-DXAC system. This experimental TS-DXAC system are specifically established to carry out the research project proposed in Chapter 3. Firstly, the configuration of the experimental TS-DXAC system is detailed. Then the experimental TS-DXAC system and its major components are specified. This is followed by reporting various instrumentation and a data acquisition system for the experimental TS-DXA system. Finally, a supervisory program for operating and controlling the experimental TS-DXAC system using the LabVIEW platform is detailed.

Chapter 5 presents an experimental study on the inherent operational characteristics of the experimental TS-DXAC system, which were expressed by the relationship between its output total cooling capacity (TCC) and equipment sensible heat ratio (E SHR). In this experimental study, a constant compressor speed and a fixed total supply air flow rate were used. However, both the refrigerant and air flow rates to the two-sections can be varied. Extensive experimental work has been carried using the experimental TS-DXAC system, and experimental results are reported in this Chapter.

Chapter 6 presents the establishment of a physical-based steady-state mathematical model for the experimental TS-DXAC system. This mathematical TS-DXAC model was established by referencing to the previously developed sub-models for DX A/C systems. The established TS-DXAC model was validated using experimental results

from the experimental TS-DXAC system, with an acceptable modeling accuracy. Then, using the validated model, a follow-up modeling study on optimizing the relative sizes of the two sections for a TS-DXAC system was carried out, and modeling study results are presented.

In Chapter 7, the development of a control strategy to operate the experimental TS-DXAC system for improved indoor thermal environment is presented. The control strategy included two algorithms, i.e., Algorithm I and Algorithm II, for two typical indoor conditions in buildings in hot-humid climates. Extensive controllability tests for the control strategy have been carried out using the established experimental TS-DXAC system, and test results are presented.

Finally, the Conclusions of the Thesis and the proposed future work are given in Chapter 8.

Chapter 2

Literature review

2.1 Introduction

In buildings, maintaining a good indoor thermal environment at an appropriate level is important for the thermal comfort of occupants, indoor air quality (IAQ) [Toftum and Fanger, 1999] [Arens and Baughman, 1996; Berglund, 1998] and the energy efficiency of air conditioning (A/C) systems [Henderson Jr and Rudd, 2014]. This is particularly true for buildings located in hot-humid climates with a high ambient humidity for most of a year. On the other hand, in small- to medium- scale buildings such as residences and retails, direct expansion (DX) A/C systems are extensively used for controlling indoor thermal environments [Hernandez III and Fumo, 2020], because they are compact in volume, high in energy efficiency and low in operation and maintenance costs [Zhang et al., 2019a].

However, conventional On-Off controlled DX A/C systems only control T_i, leaving RH_i control as a by-product of T_i control. This is because the heat and mass transfers taking place in the cooling coil of a DX A/C system are highly coupled, leading to two highly coupled processes for controlling air temperature and humidity, respectively [Han and Zhang, 2011; Krakow et al., 1995]. In fact, conventional DX A/C systems unfortunately do not have the ability to decouple the two control processes, because of the inadequacies in their hardware and software provisions.

Although there have been research efforts on improving the dehumidification capability of conventional DX A/C systems, further studies are still considered necessary, so as to make these DX A/C systems not only more capable in dehumidification, but also smaller in size, less cost in manufacturing and operation, and simpler in control. To this end, a comprehensive literature review on a number of issues related to indoor thermal environmental control using DX A/C systems has been conducted and the review outcomes are presented in this Chapter. Firstly, the key parameters describing a thermal environment in an air conditioned space, such as air temperature, humidity and air velocity are discussed. Secondly, the indoor thermal environmental control in various buildings using A/C systems are reviewed. This is followed by reviewing various approaches adopted to address the inadequacies of indoor thermal environmental control using DX A/C systems. Fourthly, the previous related studies on modeling DX A/C systems and their components and the methods of solving the mathematical models for DX A/C systems are reviewed. Finally, the conclusions of the literature review where research gaps are identified are presented.

2.2 The thermal environment in an air conditioned space

It has been well known that there are three key environmental parameters that can be used to describe the thermal environment in an air conditioned space, i.e., T_i, RH_i and indoor air velocity, and that these parameters may be directly modulated by the use of A/C systems. In this section, these parameters are respectively discussed, as follows.

2.2.1 Air temperature

In buildings, without the presence of an environmental control system, such as an A/C system or a space heating system, T_i is affected by both the external heat sources such as solar heat gain, heat transfer through building envelopes due to the difference between indoor and outdoor air temperature, and the internal sources such as the heat gain from occupants and equipment, etc. It is commonly acknowledged that T_i is the most important environmental factor that influences an indoor thermal environment. Previous studies have demonstrated that the performances of occupants were affected primarily by T_i, not only directly through the heat exchange between indoor air and a human body, but also indirectly through the impacts of air temperature on either the prevalence of sick building syndrome symptoms or the satisfaction with indoor air quality [Fang et al., 2004]. The occupant performances would decrease as T_i was deviated from a so called comfort range, or when T_i was frequently changed [Lan et al., 2009]. For most mental tasks, the optimum T_i was 24 ℃, while for perceptual tasks, a conversed U-curve for temperature – performance was observed, with the best performance achieved at 27 ℃. In addition to the influences on human work performances, T_i also had an impact on human mental state. A warmer environment was more harmful to both human performances and motivations than a colder environment. A thermal environment from slightly cold to neutral has been recommended because the performances of occupants did not change significantly. An improvement in indoor thermal environments can also make people more motivated and their performances would increase due to a higher motivation [Lan et al., 2010; Lorsch, 1994]. Although many studies have suggested that T_i ranges would change

according to different working scenarios, an optimum T_i range existed for people to achieve their best performances [Heating et al., 2004; Niemel äet al., 2002].

2.2.2 Air humidity

Human beings were very good at sensing skin moisture from perspiration [Berglund, 1994], and their skin moisture levels would correlate well with their thermal sensations. An appropriate level of RH_i would lead to a good indoor thermal environment, and the setting of T_i can also be increased correspondingly without affecting occupants' thermal sensation, thus saving energy. Moreover, RH_i may also impact occupants' health.

There were internal and external sources of indoor moisture [Liu et al., 2019]. Internal sources of indoor moisture mainly include occupants and indoor activities like cooking, and external sources the ventilation and infiltration of outdoor air [McGahey, 1998; Sekhar, 2016]. The moisture content of outdoor air can significantly influence RH_i level [Sekhar, 2013]. In particular, for buildings located in hot-humid climates, at part load conditions, the moisture from outdoor air had greater impact on RH_i level than at full load conditions [Aynur et al., 2008; Seo et al., 2014].

Appropriate RH_i level was necessary to achieve an indoor environment that was beneficial to human thermal comfort and health. Firstly, as far as occupants' thermal comfort was concerned, the requirements for RH_i control were not very precise [Standard, 2010]. A low level of RH_i can lead to dry skin and mucous surfaces, causing discomfort to eyes and throat, and dry nose and skin [Wyon et al., 2006]. On the other hand, a high level of RH_i would prevent effective evaporative cooling of a human body,

and increase the thermal discomfort [Berglund and Cunningham, 1986] caused by the feeling of the moisture itself from skin, which increased the friction between skin and clothing, making clothing feel less comfortable and fabrics feel more coarse [Gwosdow et al., 1986]. To sustain a good indoor thermal environment, it has been recommended that indoor relative humidity level not exceed 60% [Nevins et al., 1975].

Secondly, regarding human health, a low RH_i may lead to the chapping and irritation of throat and other sensitive areas. In particular, in winter, respiratory illness and absenteeism would increase with a decrease in RH_i [Green, 1982]. On the other hand, a high RH_i may cause heat exhaustion or heat stroke and possible death [Toftum et al., 1998a, b]. In addition, for the direct influences on human health, RH_i may also affect people indirectly. For example, many organisms and the products of various chemical reactions can cause discomfort to, and even illness of occupants, while the growth rates of these organisms and the speed of chemical reactions were largely determined by the combinations of T_i and RH_i.

Many studies have demonstrated that the maximum growth of fungus occurred at above 95% but almost ceased at below 80% relative humidity, and that indoor mite populations were directly related to air relative humidity with a strong increasing trend at above 60% relative humidity. In addition, certain individuals were at risk for undesirable health effects caused by the exposure to either high (above 60%) or low (below 30%) relative humidity. For example, exposing to low RH_i increased the health problems of asthmatics, individuals with allergies, newborns and the elderly, who were more susceptible to respiratory infections. On the other hand, exposing to high RH_i

increased the risk for individuals with allergies or with a poorly functioning thermal regulatory system, such as the elderly and people with cardiovascular diseases.

Therefore, in buildings located in hot-humid climates, to maintain a suitable indoor thermal environment and to avoid the above-mentioned health problems caused by inappropriate RH_i levels, RH_i should be maintained at between 30% and 60%.

2.2.3 Air velocity

Indoor air velocity distribution affected not only indoor thermal environment but also indoor air quality [Zhang et al., 1990].

Indoor air velocity should be kept within a specific range, because low air velocities may limit off-gassing from evaporatively controlled emitters thus having an adverse effect on pollutant discharge. In addition, it was inadequate for quantitative passive monitoring of pollutant vapors. 10% and 50% reductions in sampling rates were reported for passive monitors at air velocities ranging from < 0.7 to 25 cm/s and from < 0.7 to 2 cm/s, respectively [Matthews et al., 1989].

On the other hand, the effects of air movements on human thermal comfort have also been studied. In occupied zones, air velocities were usually small (0 to 0.5 m/s), and the acceptable velocities were varied at different indoor air temperatures or occupant work conditions. In cool and moderate indoor thermal environments, for example, with T_i up to 23 ℃, there was a risk that sedentary occupants would feel discomfort even when indoor air velocity was low. To maintain a suitably low air velocity in occupied

zones, the supply air velocity from an air diffuser should be high enough to ensure air was adequately mixed and to keep the air flow in its desired direction [Zhang et al., 1990]. Although a high air velocity can increase the cooling effect, at an T_i of over 23 ℃, occupants can feel warmer, so that they actually did not feel draught at typical indoor air velocities (up to around 0.4 m/s). Moreover, when T_i was around 30 ℃, indoor air velocity up to 1.6 m/s was acceptable [Toftum, 2004]. In addition, the fluctuations in indoor air velocity can also affect occupants' thermal comfort since velocity fluctuations with a frequency of up to 1 Hz in occupied zones can significantly increase occupants' discomfort caused by draft [Arens et al., 2009].

2.3 Indoor thermal environmental control using air conditioning systems

Various A/C systems have been used to maintain a desirable indoor thermal environment in different types of buildings. Generally speaking, in large buildings, central A/C systems are widely used, while in small- to medium- scale buildings, DX A/C systems such as roof top units or split-type units are more preferable.

2.3.1 The variations in space cooling loads

The sources for indoor cooling loads in a conditioned space can be divided into internal and external ones. The former included indoor occupants, lighting and equipment, and did not change much during the operating period of an A/C system [Li et al., 2006]. The latter included the heat transfer from ambient air through convection and conduction, outdoor infiltration and solar radiation, etc. and would however change

significantly during the operating period of an A/C system that may last for 7 months in a year from April to October in hot-humid climates [Lam, 1993].

For an A/C system, two important parameters, i.e., total cooling capacity (TCC) and equipment sensible heat ratio (E SHR), can be used to describe its ability to deal with the space cooling loads. The output TCC value was the output total cooling capacity from an A/C system while the E SHR value was the ratio of the output sensible cooling capacity (SCC) to the output TCC from an A/C system. On the other hand, there were also two key parameters to describe the characteristics of space cooling loads, i.e., total cooling load (TCL) and application SHR (A SHR), with the latter being the ratio of the space sensible cooling load (SCL) to the space TCC in an air conditioned space. For achieving the precise T_i and RH_i control, E SHR and TCC of an A/C system should match exactly A SHR and TCL, respectively [Li and Deng, 2007b]. However, as stated earlier, external cooling loads can be actually varied significantly throughout the period of air conditioning in a year. For example, in hot-humid climates, the values of A SHR for a conditioned space could vary between 0.6 and 0.8, and those of E SHR for an A/C system stayed normally unchanged [Lin and Deng, 2004]. There have been many studies on the mismatch between values of A SHR / TCL in a conditioned space and those of E SHR / TCC from an A/C system, leading to uncontrolled indoor humidity levels [Amrane et al., 2003; Andrade and Bullard, 2002; Harriman III, 2002; Hourahan, 2004; Lstiburek, 2002; Murphy, 2002; Shirey III et al., 2006].

Therefore, it was hard for a conventional A/C system to achieve the desirable indoor thermal environment control when the space cooling load in a conditioned space was

subject to significant changes, leading to a poorer indoor thermal environment which was conductive to the health problems mentioned in Section 2.2.

2.3.2 Indoor thermal environmental control using central A/C systems in large buildings

In large buildings such as hotels and offices, chilled water based central A/C systems have been widely used. Generally speaking, in large buildings, because there was enough installation space, it was therefore possible for conventional central A/C systems to incorporate additional novel equipment or technologies that have been extensively used to achieve the enhanced moisture removal [Zhang et al., 2011], one example being a temperature and humidity independent control (THIC) A/C system.

Zhao et al. [2011] studied a THIC A/C system installed in an office building, with its schematic diagram shown in Fig. 2.1. In this THIC A/C system, heat pump driven liquid desiccant assisted outdoor air processors were employed to handle the latent cooling load (LCL) from outdoor air for the whole building to control RH_i, and chilled water at the temperature of 17.5 ℃ was supplied to dry fan coil units (FCU) and radiant panels to control T_i. There were two subsystems in the THIC A/C system. In Fig. 2.1, the temperature control subsystem which consisted of a high-temperature water chiller, a cooling tower, cooling / chilled water pumps and indoor terminal devices (FCU and radiant panels) is shown on the left hand side and the humidity control subsystem which consisted of the liquid desiccant outdoor air processors that supplied adequate dry fresh air into occupied spaces on the right hand side. In the heat pump driven outdoor air processor, the exhaust heat from its condenser was used to heat the diluted solution

from dehumidification modules. After that, the diluted solution was turned into a hot concentrated solution which was cooled by passing it through a heat exchanger before entering the dehumidification modules for removing moisture from outdoor air. In addition to controlling RH_i using the outdoor air processor, the energy from indoor exhaust air can also be recovered using a total heat recovery device installed in the outdoor air processor to reduce the energy consumption of the THIC A/C system. The Coefficient of Performance (COP) of the THIC A/C system could reach 4.0 and its energy consumption for the office building was at 32.2 kWh/(m^2yr), which showed that its energy efficiency was much higher than that of conventional central A/C systems.

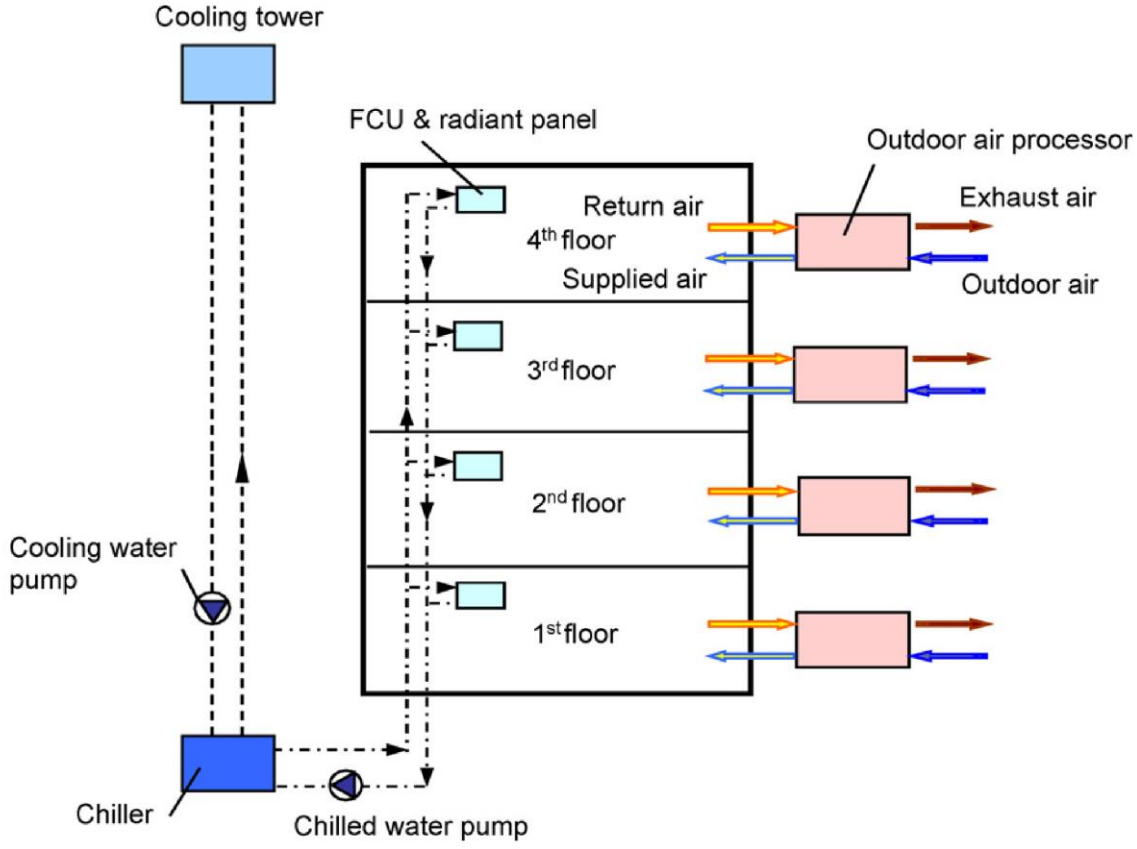

Fig. 2.1 Schematic diagram of the THIC A/C system [Zhao et al., 2011]

Furthermore, in the workshop of an industrial factory [Guan et al., 2020], a full outdoor air A/C system with a liquid desiccant dehumidifier (DEH) was used to achieve a precise control of both T_i and RH_i. Because pollutants were produced in the workshop during its operation, return air could not be reintroduced to the A/C system. Therefore, a full outdoor air A/C system using an air handing unit (AHU) with a DEH was used to handle outdoor air to control the indoor thermal environment. Fig. 2.2 shows the full outdoor air A/C system and the detailed configurations of the AHU. There were three cooling coils, i.e., Cooler 1, Cooler 2 and Cooler 3, using high-temperature chilled water at 14 -18 ℃ to process the SCL of the workshop for controlling T_i, while the DEH in the AHU powered by a heat pump was used to handle the moisture of outdoor air and other space LCLs for controlling RH_i. In Fig. 2.2, outdoor air at the state of A_{in} flowed into the AHU and was divided into two streams. The first passing through Cooler 1 was further cooled to the state of $A1$, whereas the second passing through Cooler 2 and DEH was processed to the state of $A3$. These two outdoor air streams were then mixed and finally cooled by Cooler 3 to the required state of A_{out} and supplied to the workshop. The use of DEH could not only help the A/C system achieve the simultaneous control of T_i and RH_i but also decrease the energy grade required for cooling, and avoid reheating as compared with conventional A/C systems.

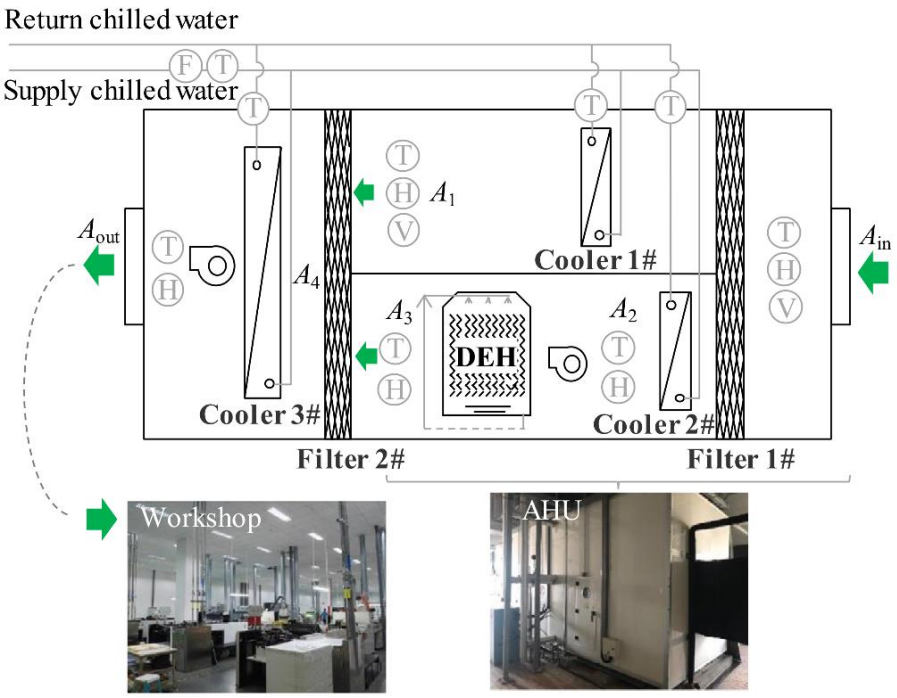

Fig. 2.2 Schematic diagram of a full outdoor air A/C system for a workshop [Guan et al., 2020]

In a museum storeroom, a novel THIC device was developed and installed in the cooling coil of a conventional central A/C system to achieve simultaneous control of T_i and RH_i [Zhang et al., 2012]. The schematic diagram of the central A/C system with the THIC device is shown in Fig. 2.3. Although the cooling and dehumidification were two coupled processes in a cooling coil, the cooling and dehumidification capacity from the coil could be separately adjusted. It can be seen from Fig. 2.3 that before chilled water was supplied to the cooling coil, it first flowed to the THIC device where both its mass flow rate and temperature may be changed. The changes in mass flow rate would be used to control the cooling capacity, and those in temperature the dehumidification capacity of the cooling coil. Consequently, T_i and RH_i can be controlled independently. Furthermore, a split-range control strategy was developed purposely for the central A/C

system with the THIC device to prevent the dehumidification and re-humidification to save energy. Field tests for the central A/C system with the THIC device showed that T_i and RH_i were well controlled within the required range with a high precision under different operating conditions. The energy performances of the A/C system were also tested and compared with those of a conventional central A/C system using the TRNSYS platform. The comparison results showed that the central A/C system with the THIC device can achieve an energy saving of 30–50%.

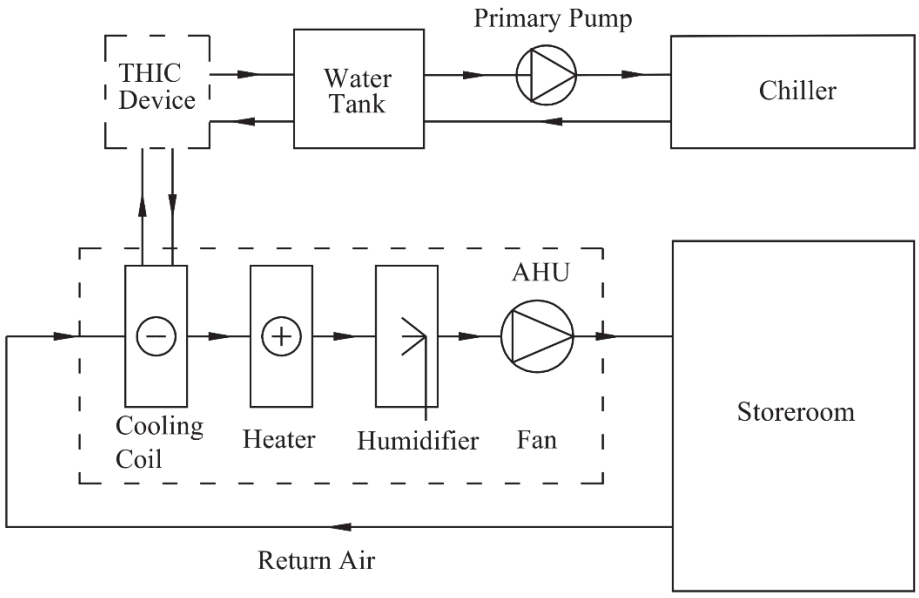

Fig. 2.3 Schematic diagram of a central A/C system with a THIC device for the storeroom in a museum [Zhang et al., 2012]

As seen from the above mentioned studies, in large buildings, simultaneous control of T_i and RH_i may be achieved by using chilled water central A/C systems that incorporated additional dehumidification technologies or provisions. This was easy to realize in large buildings where sufficient installation spaces for additional technologies / provisions were available.

2.3.3 Indoor thermal environmental control using DX A/C systems in small- to medium- scale buildings

As shown in Fig. 2.4, a conventional DX A/C system was composed of four key components, i.e., a compressor, a condenser, an expansion device and a DX evaporator, which were connected in series by pipelines to form a refrigerant circuit. There were also a supply air fan and a condenser air circulation fan. For the DX A/C system, the refrigerant directly exchanged heat with the air passing through the DX evaporator. Therefore, an intermediate medium of working fluid between refrigerant and air such as water used in water chillers was no longer needed, and a DX A/C system can therefore be made more compact, requiring less installation space. In addition, DX A/C systems were usually of a higher energy efficiency because of the direct heat exchange between air and refrigerant. Furthermore, DX A/C systems were normally of package types, such as roof top or spilt-type, and needed no connecting air ducts, requiring less maintenance work. Therefore, the initial costs, operating and maintenance costs for DX A/C systems were generally low, as compared to those of central chilled water based A/C systems.

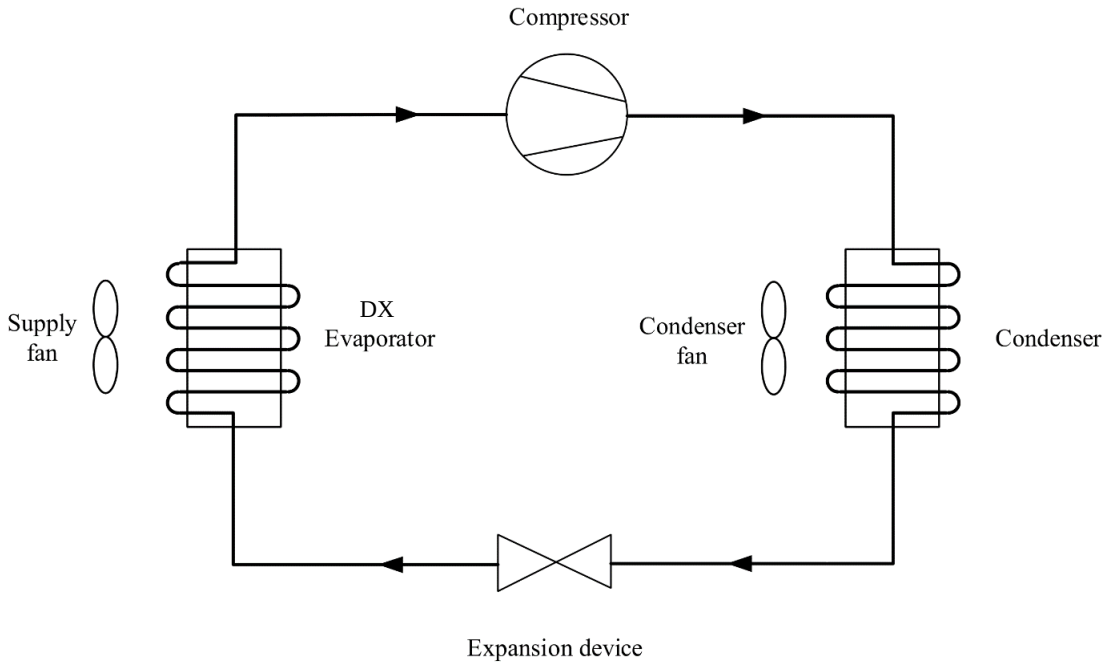

Fig. 2.4 Schematic diagram of a conventional DX A/C system

Unlike large buildings, in small- to medium- scaled buildings, installation spaces for A/C systems / units were actually limited and central chilled water based A/C system less preferred, but DX A/C systems were more suitable to be used for controlling indoor thermal environments. However, using DX A/C systems to control indoor thermal environment in small- to medium- scale buildings may also encounter some problems as follows.

Firstly, the current designs for DX A/C systems with respect to dehumidification were inadequate. For the cooling process taking place on the surface of a cooling coil, when air temperature was lower than air dew-point, water vapor condensation occurred. For obtaining a high moisture-removal efficiency, a cooling coil needed to be designed accordingly by using the following three methods: reduce evaporating temperature; reduce air face velocity; and increase its surface area, so that the outlet air from the

cooling coil would have a lower temperature and moisture content. However, a cooling coil so designed may not remove SCL efficiently. As a matter of fact, the current design trends for DX A/C systems were rather to obtain a higher energy efficiency ratings (EER) and COP, while the dehumidification capacity was weakened [Kittler, 1996]. This could therefore potentially lead to a situation where a DX A/C system would provide the desired T_i control but not the required RH_i control [Murphy, 2002; Shirey, 1993; Westphalen, 2004]. The situation would be even worse in buildings where space SCLs were lower and the shutdown time of DX A/C systems longer, resulting in a significantly reduced dehumidification capacity for these DX A/C systems [Rudd et al., 2005]. Furthermore, it was shown by [Kurtz, 2003] that to save operating costs for DX A/C systems, people would rather increase T_i set points in summer, which would further increase indoor humidity levels.

Secondly, there were also inadequacies for controlling DX A/C systems. Most DX A/C systems were operated with a single-speed compressor and supply fan, relying on On-Off control of the compressor to control T_i only. The compressor would be shut down when the setting of T_i was reached, but the moisture removal by the DX A/C system was also stopped at the same time. The RH_i level may be significantly increased when the compressor was shut down, but the supply fan was continuously operated. This was because the condensate remaining the surface of a cooling coil would evaporate into supply air stream again due to the continuous operation of the supply fan [Amrane et al., 2003; Shirey III et al., 2006]. Therefore, RH_i cannot be controlled at a moderate level using On-Off controlled DX A/C systems. In addition, RH_i would be higher for buildings located in hot-humid climates where space LCL was higher. This situation would in particular be worse in envelope-efficient buildings, where SCLs were low and

DX A/C systems were shut down over the large time period of air conditioning [Harriman III, 2002].

If an On-Off controlled DX A/C system was used to control RH_i, the setting of T_i had to be lower to increase its moisture removal capacity. Then an oversized DX A/C system may have to be employed to increase its output TCC, which would inevitably overcool indoor air and increase the initial and operation costs [Huh and Brandemuehl, 2008].

2.4 Measures to address the inadequacies of indoor thermal environmental control using conventional DX A/C systems

In Section 2.3.3, the problems for maintaining a suitable indoor thermal environment using DX A/C systems are briefly summarized. To overcome these problems, many efforts have been made and can be in general grouped into the following three major approaches [Xu et al., 2018].

2.4.1 Applying additional provisions

The first major approach was to apply additional provisions to conventional DX A/C systems to achieve suitable indoor thermal environmental control. For conventional DX A/C systems, as stated in Section 2.3.3, their dehumidification capacities were questionable. Therefore, the primary concern for applying additional provisions was to enhance their moisture removal abilities. The simplest and most straightforward method was to employ a stand-alone dehumidifier to deal with the space LCL

[Henderson Jr and Rudd, 2014; Rudd, 2013]. However, it was hard to achieve the desirable humidity control only using a stand-alone dehumidifier. Therefore, for improving the dehumidification performances of a stand-alone dehumidifier, an integrated ducted air dehumidifier with A/C systems can be employed. However, such A/C systems with ducted dehumidifier actually required additional installation space, which was thus not suitable for use in most small- to medium- scale buildings.

A reheating coil, which was usually an electric heating one, may also be added to a conventional DX A/C system, as shown in Fig. 2.5 [Mazzei et al., 2005]. The air was subcooled to significantly reduce its moisture content, and then reheated to a suitable temperature before supplying it into a space. The simultaneous cooling and reheating processes enabled the DX A/C system to control RH_i, but was costly and energy inefficient, in particular when outdoor air temperature and humidity were very high.

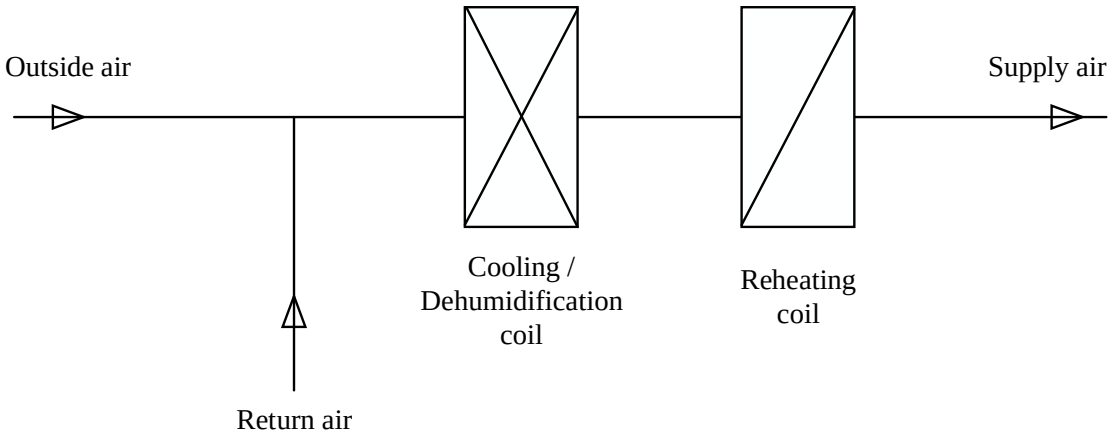

Fig. 2.5 A DX A/C system with a reheating coil [Mazzei et al., 2005]

To address the issue of high energy, use of a DX A/C system with a reheating coil, solid [Jeong et al., 2010; Pramuang and Exell, 2007] or liquid desiccant subsystems [Burns et al., 1985; Jia et al., 2006; Mart ńez et al., 2017; Worek and Chung-Ju, 1986; Xiao et al., 2011; Yadav, 1995] may be added to DX A/C systems. Furthermore, if the waste heat from the condenser of a DX A/C system or other renewable energy can be used for desiccant regeneration, more energy may be saved. However, these subsystems would inevitably increase the complexity and costs of these integrated systems [Jain and Bansal, 2007].

Because most of the space LCL come from ventilation air, a dedicated outdoor air system (DOAS) can be integrated to a DX A/C system. A DX A/C system with an integrated DOAS can be used adequately to handle indoor space sensible and LCLs at a high efficiency. The configuration of a conventional DOAS is shown in Fig. 2.6. As seen, outdoor air was processed in a cooling coil firstly to remove moisture, and then reheated to an appropriate temperature before supplying to a conditioned room. A DOAS could deal with all the space LCL, while the space SCL was handled using a parallel indoor terminal to achieve simultaneous control over T_i and RH_i [Mumma, 2001a]. However, the operation of a conventional DOAS was very inefficient. Consequently, an improved arrangement for a DOAS was proposed, as shown in Fig. 2.7, which represented also the current general arrangement of a DOAS.

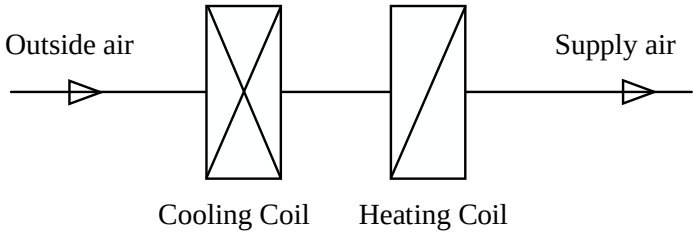

Fig. 2.6 Schematic diagram of a conventional DOAS [Mumma, 2001a]

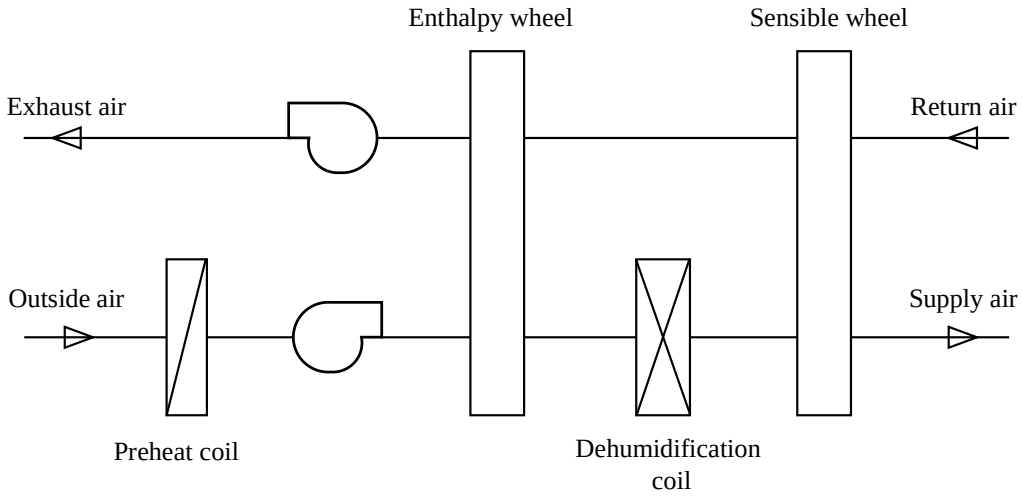

Fig. 2.7 The general arrangement of a DOAS [Mumma, 2001b]

In the improved general arrangement of a DOAS, an enthalpy wheel was used to precondition outdoor air, and the heating coil in a conventional DOAS was replaced by a sensible wheel [Mumma, 2001b]. Applying such an improved DOAS to a conventional DX A/C system could efficiently deal with indoor space SCLs and LCLs, and improve the indoor thermal environment. In addition, because outdoor air was handled independently, it could also satisfy the requirements of indoor air quality. However, a DOAS was always complex and additional provisions were required which would increase the initial costs and requiring more installation space. To fully take

advantages of a DOAS and integrate it with DX A/C systems more conveniently, a highly energy efficient DOAS using novel vapor-compression refrigeration cycles was proposed. As shown in Fig. 2.8 [Zhang et al., 2019b], this novel DOAS was featured by a fine combination of two-stage DX dehumidification, subcooled liquid-to-air reheating and exhaust air heat recovery. This novel system was optimally designed and analyzed with a detailed mathematical model. A prototype was also setup and tested. The research results indicated that the supply air can be processed to desirable states and its energy efficiency reached 5.42 under rated cooling conditions, which was 26% higher than that of a the conventional DOAS.

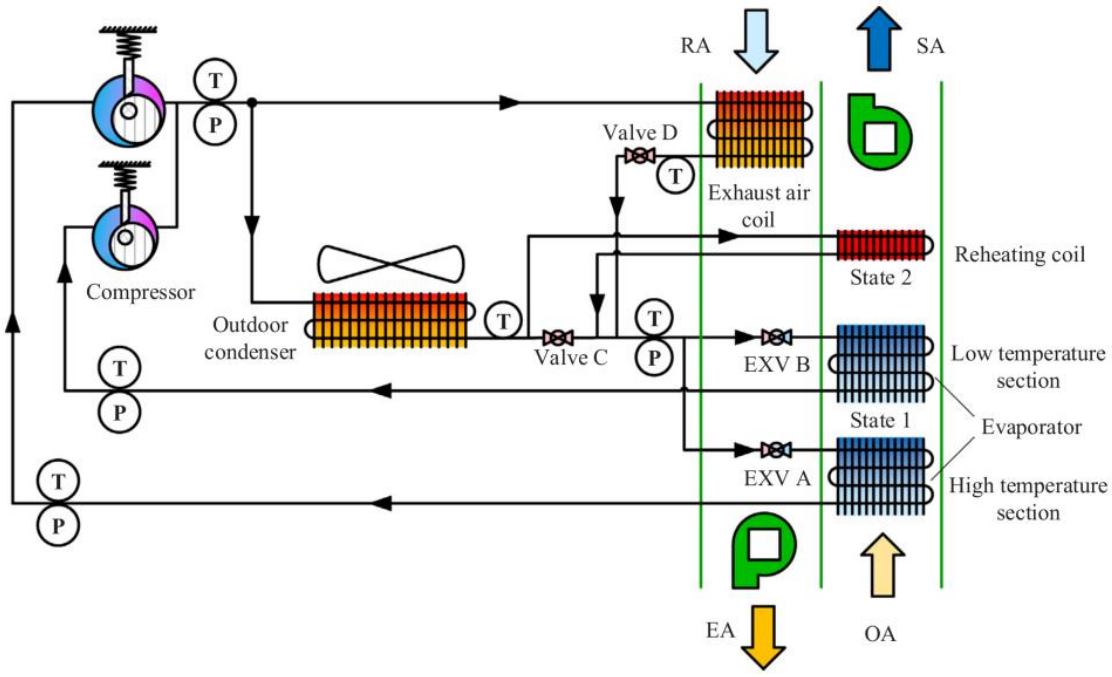

Fig. 2.8 Schematic diagram of the proposed DOAS [Zhang et al., 2019b]

When a DOAS was integrated into a DX A/C system, the LCL of the system was handled separately [Lowenstein, 2008; Rambhad et al., 2016]. Therefore, the air conditioning terminal in a conditioned room only needed to deal with the SCL [Hu and

Niu, 2012; Saber et al., 2016]. Because there was no dehumidification requirement for the terminal in the conditioned room, it could be operated at a dry condition. The most commonly adopted method for dry cooling was to employ a radiant terminal [Mumma, 2002].

Li et al. [2017] developed a novel DX based radiant A/C system integrating an outdoor air dehumidifier (OAD) used in the highly humid Yangtze River region in China. As shown in Fig. 2.9, the novel DX based radiant A/C system was composed of three main parts, i.e., a VRF plant, an OAD unit and a radiant A/C terminal.

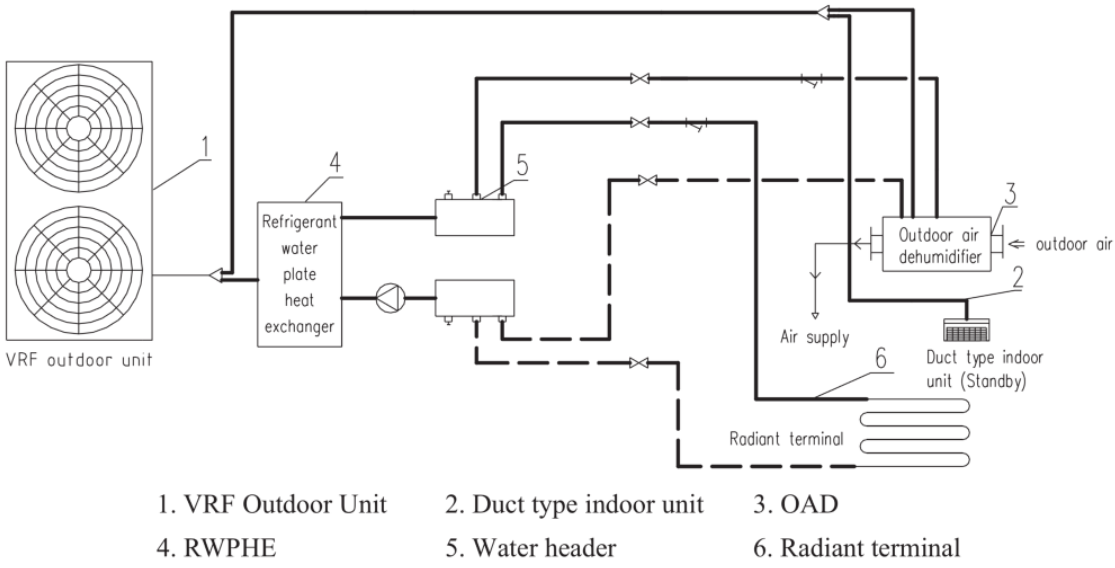

Fig. 2.9 The configuration of the DX based radiant A/C system [Li et al., 2017]

In this novel system, one refrigerant cycle was assigned to the OAD unit to cool and dehumidify outdoor air and the other to the heat exchanger to provide radiant terminals with chilled water. Therefore, the OAD unit handled indoor LCL by processing outdoor

air and the radiant terminal handled indoor sensible load, so as to achieve the simultaneous control of T_i and RH_i [Zhu et al., 2014a; Zhu et al., 2014b].

The experimental results for this novel DX based radiant A/C system demonstrated that in summer and transitional seasons, the supply air temperature was maintained at its set point with a fluctuation of less than 2 ℃. The supply air moisture content was maintained at within 8–10 g/kg, which was set in accordance with the supply air moisture content recommended by ASHRAE [Standard, 2010], suggesting a satisfactory performance of temperature and humidity control. Furthermore, the supply chilled water temperature in the summer condition was maintained at its set point with a moderate fluctuation less than 2 ℃. In addition, the supply air temperature from the OAD unit also met the requirement of the occupant in winter condition, which suggested a stable year-round operation of the novel system.

Thereafter, a follow-up simulation study on the energy performance of the proposed DX based radiant A/C system was also conducted [Li et al., 2018]. Compared to a conventional air source heat pump (ASHP) based system [Qu et al., 2012; Song et al., 2014], the proposed DX based radiant A/C system achieved an energy saving of 19.34% annually. With a higher energy efficiency, the proposed DX based radiant A/C system, can be used to provide a promising approach for radiant A/C systems to achieve the simultaneous control over T_i and RH_i in small- to medium- scaled buildings. However, this novel DX based radiant A/C system required a precise control of chilled water temperature to avoid the potential condensation indoors, which would cause severe damages to buildings [Rhee et al., 2017]. In addition, the additional radiation panels and heat exchangers also increased the initial and maintenance costs.

As seen from the above studies, all these novel DX A/C systems assisted by additional provisions could be used to achieve simultaneous control over T_i and RH_i. However, they actually required additional provisions thus installation spaces. Therefore, together with high capital and operational costs, it was not suitable for use in small- to medium-scale buildings.

2.4.2 Modifying configurations

To address the inadequacies when applying additional provisions such as a DOAS to the DX A/C system and meet the requirement of enhanced dehumidification, the second major approach, i.e., modifying configurations of conventional DX A/C systems without requiring additional provisions was studied. A typical modification for the DX A/C system was the separating sensible and latent cooling (SSLC) system shown in Fig. 2.10 [Ling et al., 2010; Ling et al., 2011, 2013]. For a SSLC system, one vapor compression cycle was used to handle the SCL and the other the LCL from internal and external.

In the SSLC system, the latent cooling cycle was actually a conventional vapor compression cooling cycle, while the sensible cooling cycle having a higher evaporating temperature was of a higher energy efficiency compared to the latent cooling cycle. Therefore, the whole SSLC system was expected to have a higher energy efficiency than a conventional DX A/C system. Compared to the integrated systems introduced in Section 2.4.1, the SSLC system could also obtain desirable supply air states without additional provisions. However, because two refrigeration cycles were actually required for the SSLC system, its initial costs would be higher and the system

more complicated, which was unsuitable for the application in small- to medium- scale buildings either.

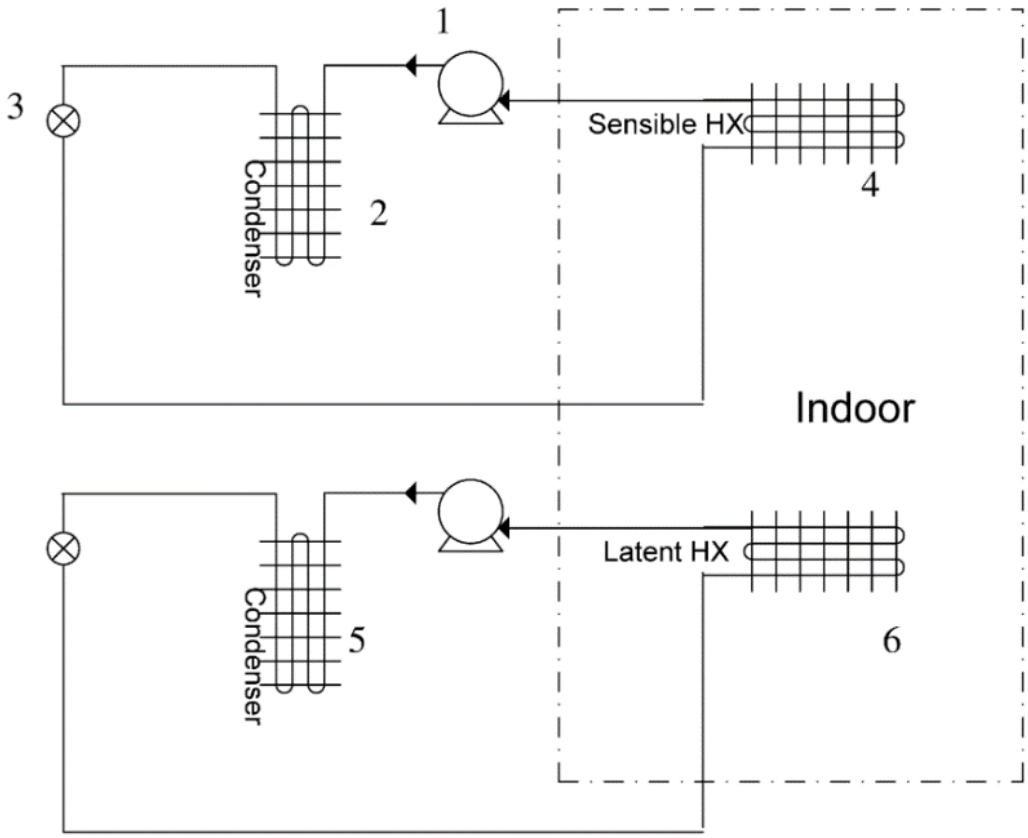

Fig. 2.10 Refrigeration cycle of the SSLC system [Ling et al., 2010]

In contrast to the SSLC system, the strategy of multi-heat exchangers used in one cooling cycle was more applicable and has been applied to DX A/C systems to achieve simultaneous control of T_i and RH_i. The main principle of the multi-heat exchanger strategy was employing an additional heat exchanger working as a cooling coil or a heating coil at different conditions.

For example, Han et al. [2013] developed a novel DX isothermal dehumidification system having two indoor units connected in series, one indoor unit acting as a reheating coil or an evaporator and the other as a normal evaporator by valve arrangements, with the schematic diagram shown in Fig. 2.11. In this novel system, two heat exchangers were used, i.e., Coil 1 and Coil 2. The arrangement of valves could realize two different working statuses for the DX isothermal dehumidification system. If Valve 1 and 4 are open, while Valve 2 and 3 are closed, the system will work with reheating function, and air was firstly processed in Coil 1 and then was reheated in Coil 2. On the other hand, if Valve 1 and 4 are closed, while Valve 2 and 3 are open, the system will work as a conventional DX A/C system, and both Coil 1 and Coil 2 will work as evaporators. According to the characteristics of the system, it was very suitable for use in the transition season when SCL was low but LCL high. The experimental results demonstrated that this system can meet the isothermal dehumidification demand at a capacity of 1.08 - 3.2 kg/h, and the outlet air temperature from the system fluctuated within 1 ℃. As stated earlier, this novel system was intended to achieve an isothermal dehumidification in transitional seasons. However, in hot-humid areas such as Hong Kong, the usefulness of such a system was in doubt, because cooling and dehumidifying an indoor space were equally important for most of a year.

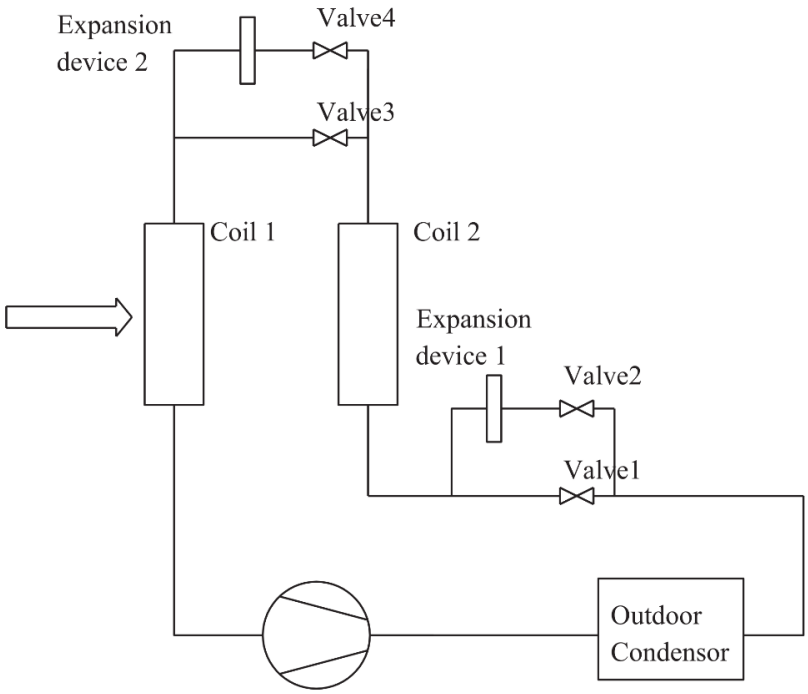

Fig. 2.11 The schematic diagram of a novel DX isothermal dehumidification system [Han et al., 2013]

Fan et al. [2014] developed a multi-unit heat pump system to simultaneously control T_i and RH_i for all-year-round operation. The schematic diagram of the multi-unit heat pump system is shown in Fig. 2.12. Two parallel connected condensers, i.e., HE2 and HE3 are employed in the system, while HE2 was located at the back of the indoor evaporator, HE1, and HE3 used as the outdoor unit. The system could be operated in four modes, i.e., heating, cooling, dehumidification without and/or with partial or total condensing heat recovery by regulating the four-way-valve and electric valves. In addition, both the indoor air flow rate and the outdoor air flow rate could be varied using Fan1 and Fan2, respectively, with the former directly influencing the evaporator performance and the latter the condenser performance. Furthermore, the supply air temperature and humidity could be simultaneously controlled by adjusting the indoor and outdoor air flow rates.

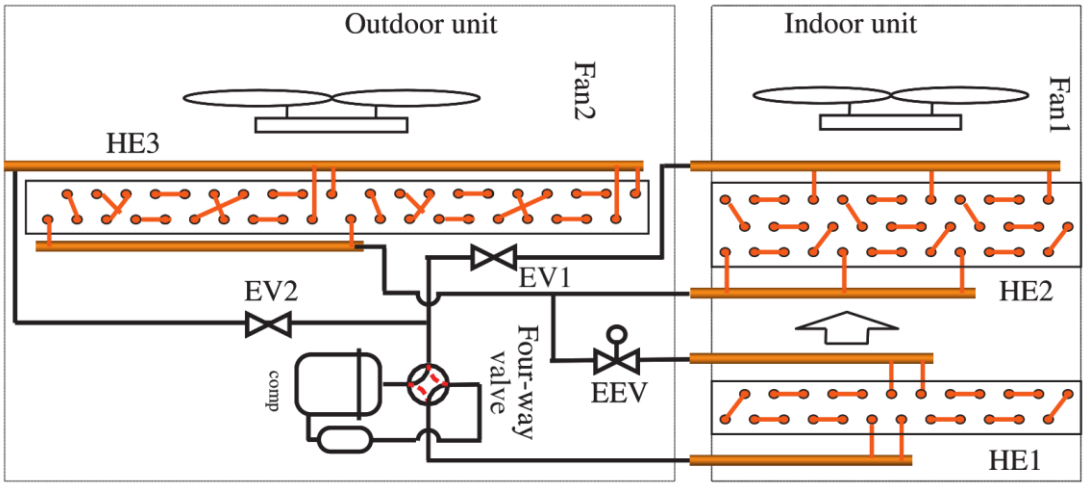

Fig. 2.12 Schematic diagram of the multi-unit heat pump system [Fan et al., 2014]

The experimental results revealed that variable cooling and dehumidification capacities could be obtained at a high energy efficiency by adjusting indoor and outdoor air flow rates. However, the variation in indoor air flow rates directly related to the cooling and dehumidification capacity of the multi-unit heat pump system. Because of the requirement of indoor thermal environment, the indoor air flow rates cannot be varied greatly, leading to the limitation of cooling and dehumidification capacity from the system.

Chen et al. [2018b] proposed a DX A/C system with enhanced dehumidification (EDAC) to achieve improved indoor thermal environmental control with a constant supply air flow rate for all-year-round operation. The proposed EDAC system is shown in Fig. 2.13. As seen, the multi-evaporate technology was used and two parallel-connected evaporators existed, i.e., HX1 and HX2 with their corresponding two electronic expansion valves (EEVs), i.e., EEV1 connected to HX1 and EEV2 to HX2. The refrigerant flow rates passing through two EEVs could be adjusted by varying the

opening degree of EEV1 while EEV2 was adjusted accordingly to maintain a constant superheat at the suction of the compressor. In addition, different operation models could be obtained by using different arrangements of three modulating valves (SV1 to SV3) installed on refrigerant pipelines. Furthermore, air flow passing through the two evaporators could also be changed by adjusting two air volume control dampers (VCDs) installed in the duct. Consequently, the EDAC system can achieve the all-year-around operation in hot-humid climates by switching different modes.

The operating characteristics of the EDAC system has been experimentally investigated [Chen et al., 2018c]. When employing fixed speeds of the compressor and supply fan in the experimental EDAC system, different combinations of TCC and E SHR could be obtained under a fixed air state with varied refrigerant and air flow rates to the two evaporators. For example, at an inlet air state of 26 ℃ and 50% RH, the range of the output TCC values was from 4.5 kW to 5.32 kW and that of E SHR was from 0.63 to 0.7. Furthermore, TCC and E SHR were correlated and mutually constrained within an irregular area in a TCC - E SHR diagram, and the shape and position of the irregular area would be influenced by different inlet air states. From the experimental results, it was possible for the EDAC system to achieve simultaneously control of T_i and RH_i with its ability to output variable TCC and E SHR.

Although the proposed EDAC system may be used to simultaneously control T_i and RH_i without additional equipment, the two evaporators were placed in series, thus the total air side flow resistance would be increased, and a longer air flow path was needed to process the supply air, resulting in more fan energy consumption and requiring more installation space.

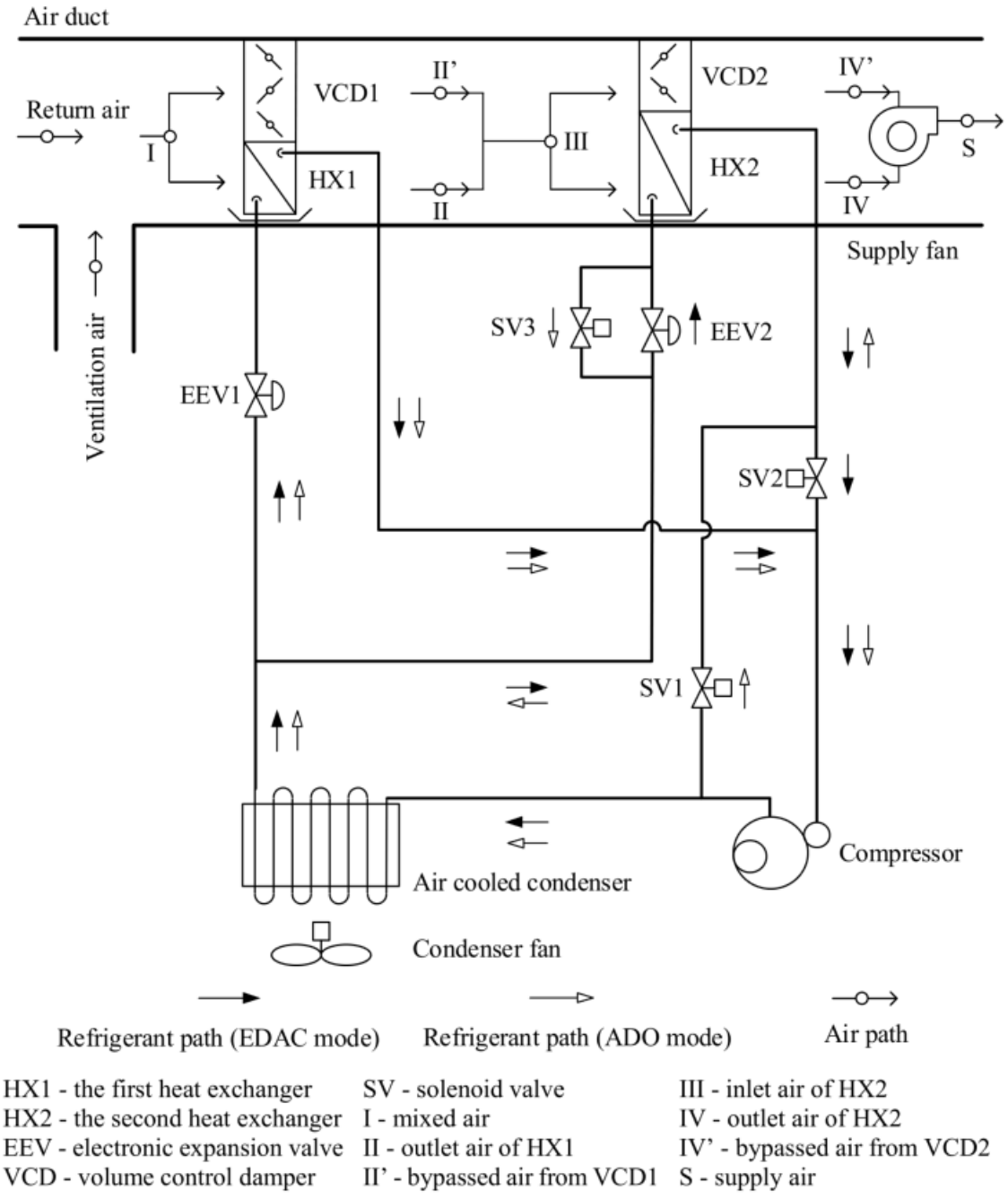

Fig. 2.13 Schematic diagram of the proposed EDAC system [Chen et al., 2018a]

2.4.3 Applying variable speed technology

The last major approach was to apply variable speed (VS) technology to conventional DX A/C systems. As mentioned in Section 2.4.1, it was hard for conventional DX A/C systems to control T_i and RH_i simultaneously, and the T_i had to be reduced to an adequate lower level to remove more moisture from a conditioned space. This was because the processes of cooling and dehumidification taking place on the surface of a cooling coil were coupled. In addition, both the supply air flow rate and refrigerant mass flow rate passing through a DX cooling coil would influence its cooling and dehumidification behaviors. The former would change the heat and mass transfer coefficients between air and the cooling coil surface, and the latter the temperature difference between air and the cooling coil surface. As a result, the output TCC and E SHR from a DX A/C system could also be varied when the supply air flow rate and refrigerant mass rate were altered through changing the speeds of both supply fan and compressor. Such has provided an opportunity to decouple the cooling and dehumidification process in a DX cooling coil so as to simultaneously control T_i and RH_i.

The use of VS technology enabled a DX A/C system to be variable speed operated for its compressor and supply fan. Previous studies on the inherent characteristics of a DX A/C system when it was VS operated. Li and Deng [2007b] experimentally investigated the inherent operational characteristics of an experimental VS DX A/C system and the experimental results are shown in Fig. 2.14 and Fig. 2.15. As seen, under a fixed inlet air state, different output TCC and E SHR from the experimental VS DX A/C system could be obtained by varying both of the speeds of the supply fan and compressor. In

addition, to obtain a greater output TCC from the experimental VS DX A/C system, higher supply fan and compressor speeds were expected. On the other hand, to achieve an enhanced dehumidification capacity, i.e., a lower value of E SHR, the speed of compressor should be higher while that of supply fan lower. Furthermore, it could be observed that the speed of compressor influenced more on output TCC value, and that of supply fan more on E SHR value.

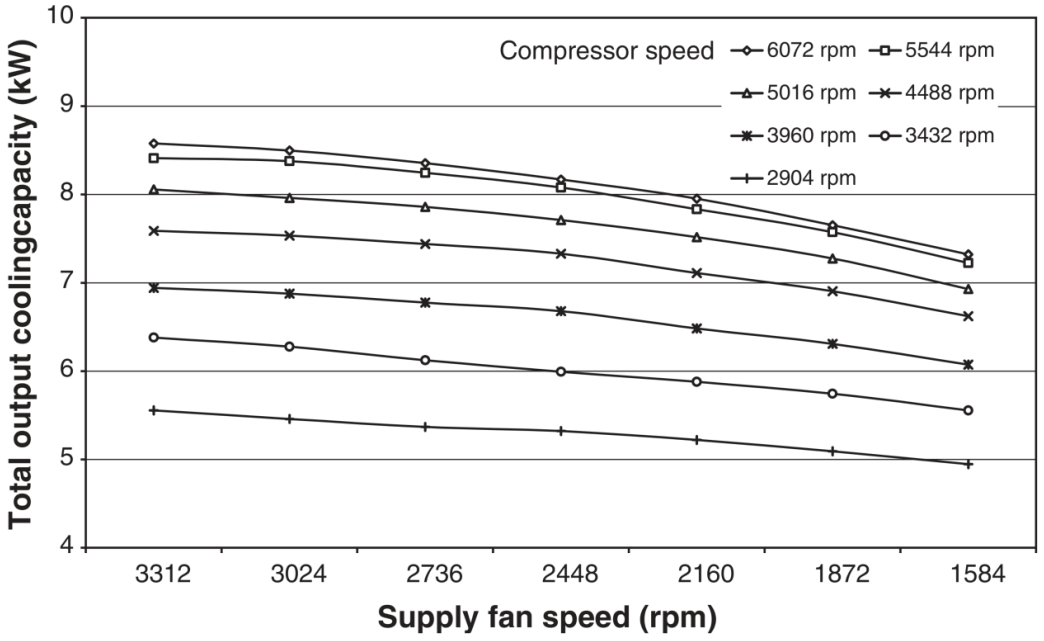

Fig. 2.14 The variations in TCC at different speeds of supply fan and compressor under a fixed inlet air state [Li and Deng, 2007b]

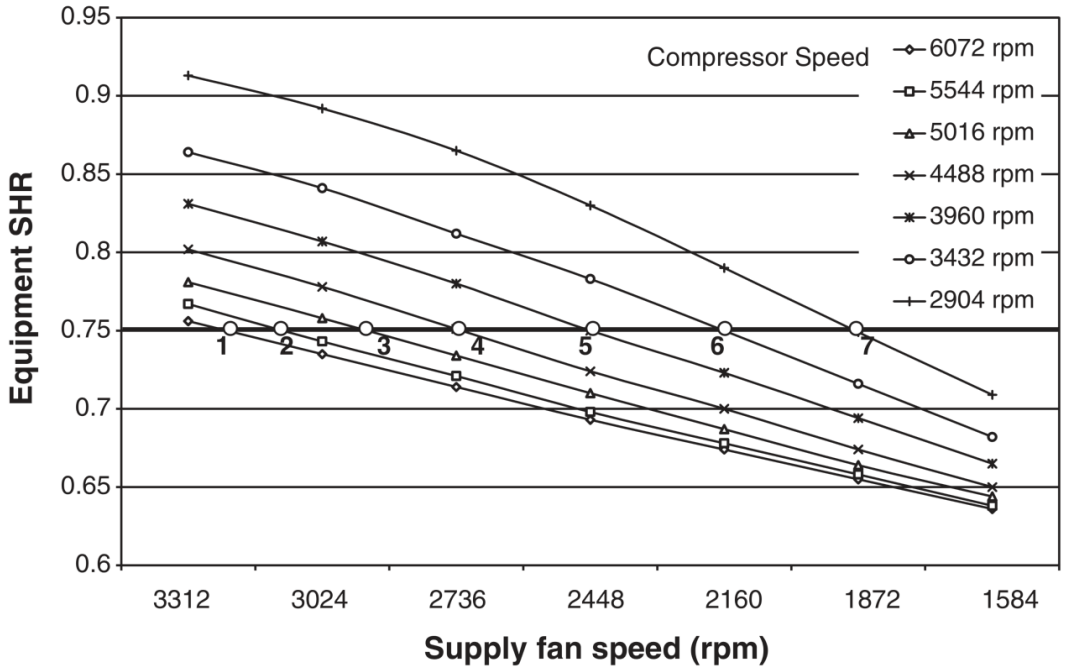

Fig. 2.15 The variations in E SHR at different speeds of supply fan and compressor under a fixed inlet air state [Li and Deng, 2007b]

Xu et al. [2010] demonstrated that the values of output TCC and E SHR of a VS DX A/C system were strongly coupled and mutually restrained within a trapezoid plotted in a TCC - E SHR diagram, as shown in Fig. 2.16. In other words, a VS DX A/C system can only output the values of TCC and E SHR located within the trapezoid. Li et al. [2014] carried out a further experimental study and the study results showed that both the temperature and relative humidity of inlet air to a DX A/C system would significantly influence the relationship between output TCC and E SHR, as reflected by the trapezoids shown in Fig. 2.17 and Fig. 2.18, respectively. It can be seen from the two figures that, varying the inlet air temperature or relative humidity would influence not only the position but also the shapes of the trapezoids. The experimental results demonstrated that a VS DX A/C system can indeed output different cooling and dehumidification capacities. As mentioned in Section 2.3.1, to simultaneously control

T_i and RH_i in a conditioned space, the output TCC and E SHR from a DX A/C system should match exactly the TCL and A SHR of a conditioned space. Therefore, applying VS technology to conventional DX A/C systems can be a promising approach to achieve a desirable indoor thermal environmental control.

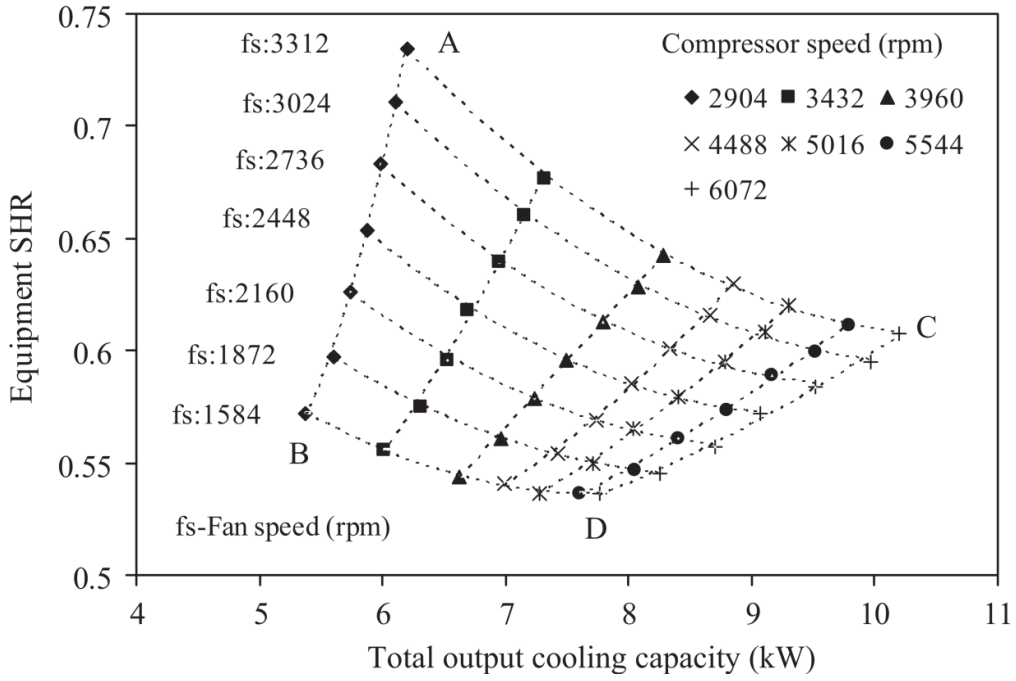

Fig. 2.16 The relationship between the output TCC and E SHR under VS operation [Xu et al., 2010]

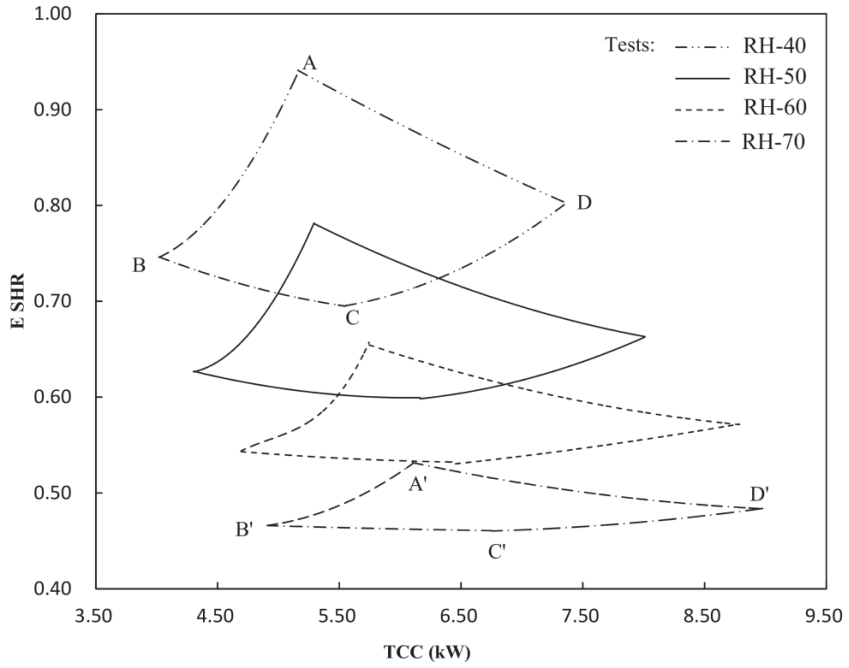

Fig. 2.17 Relationships between output TCC and E SHR of the variable speed operation DX A/C system at constant inlet air temperature [Li et al., 2014]

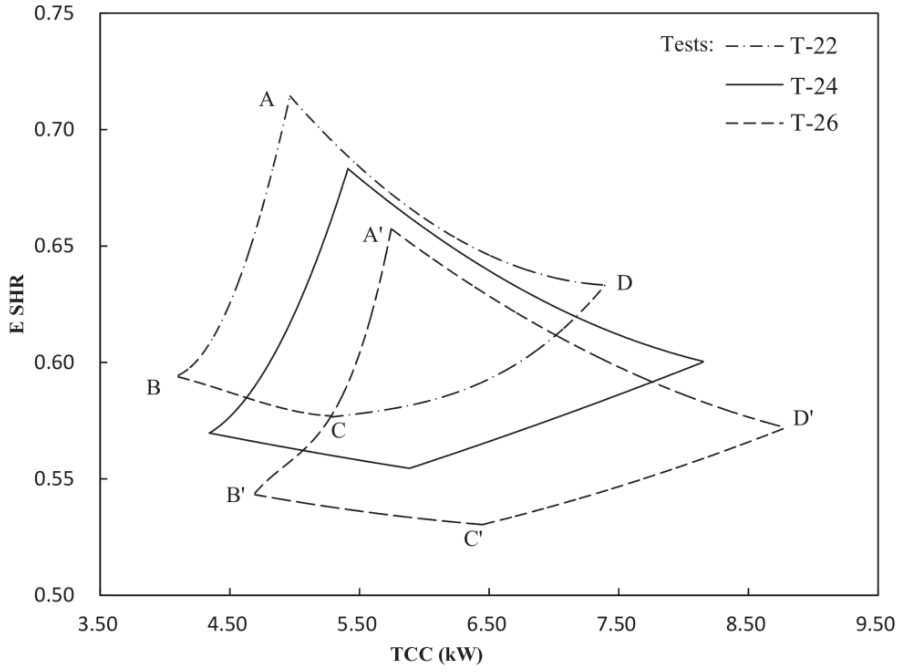

Fig. 2.18 Relationships between output TCC and E SHR of the variable speed operation DX A/C system at constant inlet air RH [Li et al., 2014]

Based on these previous studies [Li and Deng, 2007b; Li et al., 2014; Xu et al., 2010] many advanced controllers, either model based [Li et al., 2012; Li et al., 2013; Li and Deng, 2007a; Muñoz et al., 2017; Qi and Deng, 2008, 2009; Xia et al., 2018; Yan et al., 2016] or black-box based [Li et al., 2015a, b; Yan et al., 2018; Zhong et al., 2017], for the simultaneous control over T_i and RH_i using a VS DX A/C system have been developed. For example, Li et al. [2012] developed an artificial neural network (ANN) based dynamic model which was obtained by training the inherent correlations of a VS DX A/C system, and a controller based on the ANN model to achieve simultaneous control over T_i and RH_i using the VS DX A/C system. The controllability of this ANN-based controller was experimentally carried out. Furthermore, directly based on the inherent correlations between output TCC and E SHR for a VS DX A/C system, a fuzzy logic controller was developed [Yan et al., 2018]. The trapezoid which represented the operational characteristic of a DX A/C system shown in Fig. 2.16 was divided into nine zones (zones I-IX) as shown in Fig. 2.19. Nine representative points, i.e., Points A to J, were assigned to indicate their corresponding zones, and represented the operating speeds of both compressor and supply fan. If the compressor and supply fan were required to be operated within Zone I, the compressor and fan would operate at the representative Point A. In addition, if compressor and supply fan were required to be operated between Zones I and II, either Point A or Point B might be selected as the operating point. Furthermore, if the required operating statuses for compressor and supply fan were outside the trapezoid, the nearest point may be assigned. For example, in Fig. 2.19, if the required operating point was at Y which was outside the trapezoid, the nearest point on the borderline of the trapezoid, i.e., Point H may be selected. This fuzzy logic controller was tested by experiments and the test results demonstrated that it could achieve the simultaneous control over T_i and RH_i.

Although the controllers mentioned above could be used to achieve the simultaneous control of T_i and RH_i, they were indeed very complicated and required complex mathematical calculations. In addition, they were developed based on specific DX A/C systems and therefore cannot be directly applied to other DX A/C systems. Furthermore, to obtain an enhanced dehumidification capacity, as stated earlier, a lower supply air velocity was required which would result in a poorer indoor air distribution and adversely affect occupants' thermal comfort.

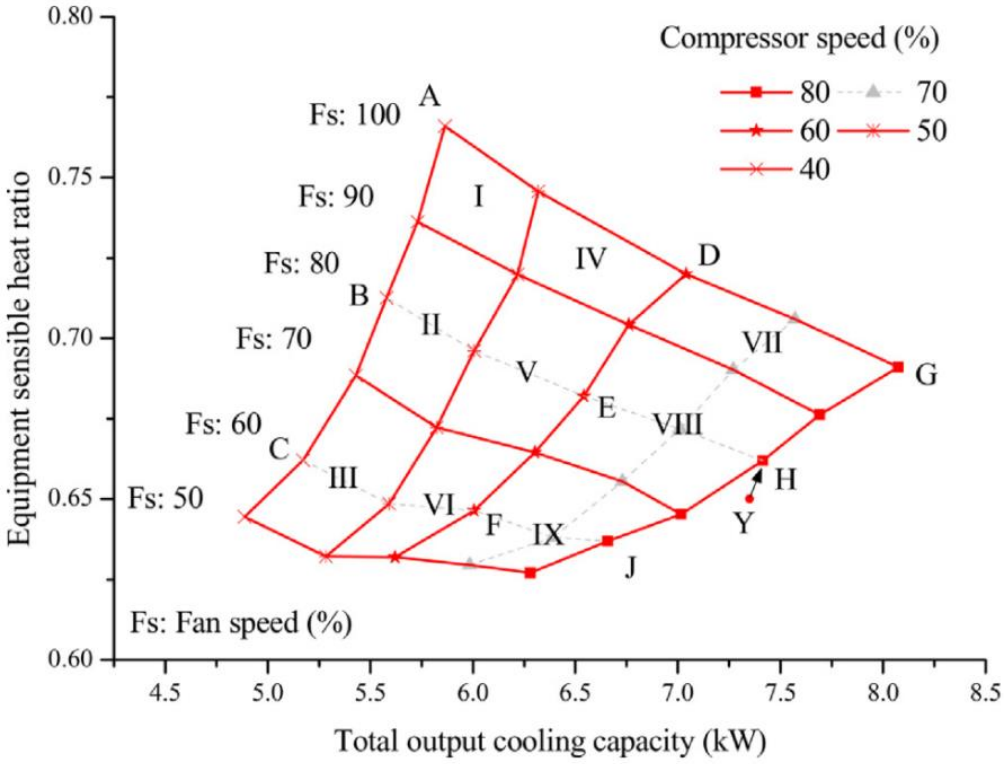

Fig. 2.19 Proposed zoning with nine representative points in the trapezoid [Yan et al., 2018]

2.5 Modeling of DX A/C systems

In addition to experimental studies, mathematical modeling studies for DX A/C systems have also been extensively carried out. Compared to experimental studies, using mathematical modeling to study DX A/C systems may be more time-efficient and cost less. In addition, it could also help obtain detailed understandings of the operating characteristics of DX A/C systems at both component and system levels [Sami, 1993; Sami and Zhou, 1995]. Consequently, for a DX A/C system, through a modeling study, its operations and configuration scan be optimized, and its controllers developed and its operating faults detected and removed.

Existing mathematical models for DX A/C systems can be divided into two broad categories, i.e., steady-state and transient models. A steady-state model for a DX A/C system has been widely used to investigate its steady-state operating characteristics and to optimize its configurations. However, in contrast to transient models, steady-state models cannot capture the transient responses of DX A/C systems to disturbance, which was however essential in developing controllers for the DX A/C systems.

On the other hand, existing models for DX A/C systems, being whether steady-state or transient, can also be separated into two broad categories: physical and empirical models. A physical model for a DX A/C system was developed based on its detailed physical information, with lumped-parameter modeling and distributed-parameter modeling being two commonly used approaches for developing a physical model. Generally speaking, lumped-parameter modeling was simpler and it only used some specific parameters which were space volume averaged to form a model. Distributed-

parameter modeling not only considered several specific parameters, but also took into consideration the system size and space coordinates for these parameters. Therefore, the distributed-parameter modeling was expected to be more accurate, but it was time-consuming with possible calculation instability, while the lumped-parameter modeling was simpler but failed to reflect the distributed nature of these parameters along the dimensions of a system. For different study objectives, two modeling approaches may be employed accordingly.

As for an empirical model for a DX A/C system, it was usually developed based on the statistical correlation of the system performances without requiring its detailed physical information, thus having a stronger adaptability. Many methods may be used to establish an empirical model, such as ANN [Kreider et al., 1992; Kumlutaş et al., 2012], expert system, graph theory and fuzzy algorithm, etc. [Diaz et al., 1999; Liu et al., 2004; Pacheco-Vega et al., 2001]. However, many technically hidden problems may be brought in for a complete empirical model because of the imperfection of the model itself and the user's limited understandings of empirical modeling. For the practical application of modeling DX A/C systems, there has been a trend of merging the two modeling approaches to overcome their respective problems. For example, using artificial intelligence technology to adaptively adjust the empirical parameters of a theoretical model could lead the predicted results closer to the actual experimental data [Ding et al., 2004b].

Since there were a number of key components on the refrigerant side of a DX A/C system, modular-based modeling for these components was usually adopted to derive

sub-models for these components, and finally a complete DX A/C system can be obtained by linking these sub-models

2.5.1 Sub-models for a DX A/C system

A complete DX A/C system was composed of four key components: a compressor, a condenser, an expansion device and a DX evaporator. Therefore, sub-models of these components expressed by a set of differential or algebraic equations should be firstly derived. Previous studies have reported the development of sub-models for these components [Chen and Deng, 2006; Elliott and Rasmussen, 2008, 2013; Shah et al., 2004; Tuo et al., 2012; Xu et al., 1996; Yan et al., 2016]. In the following sub-sections, the reviews on developing the sub-models for these key components are given separately.

2.5.1.1 Compressor

In the compressor of a DX A/C system [Ndiaye and Bernier, 2010], both heat and mass transfer processes would take place, and these processes can be different for different types of compressor. Therefore, it was ideal to establish mathematical sub-models for different types of compressor accordingly. When modeling a complete DX A/C system, the thermal performances of its compressor in terms of refrigerant mass flow rate, input power, discharge and suction temperatures (or pressure), compressor speed in rpm, etc., were very important. As mentioned earlier, the sub-models for the compressors in DX A/C systems may also be of transient type and steady-state type.

Theoretically, only a transient compressor sub-model [Chi and Didion, 1982] considering the dynamic performances of all its components could be used to predict correctly the transient characteristic of a compressor, and it was necessary to use such a transient sub-model in a dynamic model for a DX A/C system. However, general speaking, a transient model was very complicated, and it would consume much more computation time for solving a transient model. Therefore, unless it was about studying the dynamic performances of a DX A/C system for control purpose, a transient sub-model of compressor was not necessarily required.

On the other hand, a steady-state sub-model for a compressor in a DX A/C system was merely composed of steady-state equations for its thermal calculations [Browne and Bansal, 1998; Domanski and McLinden, 1992; Jolly et al., 1990]. In a steady-state sub-model for a compressor, only those necessary parameters such as poly-tropic index, refrigerant mass flow rate, coefficient of output refrigeration capacity and electric efficiency needed to be considered. Actually, a steady-state sub-model for a compressor in a DX A/C system can be naturally used for not only steady-state modeling [Rasmussen and Alleyne, 2004], but also transient modeling, because the time constant of a compressor in a compression process was much shorter than that of a heat exchanger. However, it was also necessary to consider the start-up of the compressor, which may take some time. The start-up process for a compressor could be treated as a linear element or a first order inertial element, which could greatly improve the modeling accuracy for the dynamic process of the start-up and enhance the modeling stability. When developing an empirical steady-state sub-model of the compressor in a DX A/C system, its performance date could be used to establish the empirical correlations, based on curve fitting or regression analysis [Li, 2013]. For a specific

compressor, such an empirical sub-model could be actually used for better modeling accuracy.

2.5.1.2 Heat exchanger

Both an evaporator and a condenser in a DX A/C system were actually heat exchangers, the reviews of their modeling are presented together here. In general, for heat exchanger modeling, there were also two types: steady-state modeling and transient modeling.

A steady-state model of a heat exchanger can be used to describe and predict its steady-state operating performances, and may be divided into the following three types: a lumped-parameter model, a distributed-parameter model and finally a partial-lumped-parameter model.

For a heat exchanger without phase transition for its working medium, its steady-state performances could be predicted using a lumped-parameter model [Chi and Didion, 1982; Elmahdy et al., 1977; Jacobi and Goldschmidt, 1990; Rasmussen and Alleyne, 2004; Vargas and Parise, 1995]. However, if there was a phase transition in a heat exchanger, the use of its lumped-parameter model would result in a poorer modeling accuracy. and distributed-parameter modeling [Bensafi et al., 1997; MacArthur, 1984] for the heat exchanger should be employed. When using distributed-parameter modeling, a heat exchanger was divided into a number of control volume, and then a lumped-parameter modeling approach would be adopted for each control volume. Compared to lumped-parameter modeling, distributed-parameter modeling was more accurate but obviously required more computational time. Therefore, as a compromise

to the first two modeling approaches, the third one, a partial-lumped-parameter modeling approach for a heat exchanger in a refrigeration system, was proposed [Domanski, 1991; Shiming, 2000]. According to refrigerant status, a heat exchanger, i.e., an evaporator or a condenser, could be divided into several zones. Inside an evaporator, there can be two refrigerant statuses, two-phase and superheated vapor, and therefore, there should be two corresponding zones in an evaporator. Similarly, a condenser may be divided into three zones, i.e., de-superheating, two-phase and subcooled based on the refrigerant statuses [Rasmussen and Alleyne, 2004]. In each divided zone, a lumped-parameter model could be established. Due to its nature, the modeling accuracy for a partial-lumped-parameter model was between that of a distributed-parameter model and that of a lumped-parameter model, and could be very close to that of a distributed-parameter model with a greatly improved computational speed.

On the other hand, a transient model for a heat exchanger may be used to describe its dynamic responses to the changes in the operating conditions. A transient model was usually used to assist the development of controllers for a dynamic system such as a DX A/C system. Similarly, a transient model for a heat exchanger in a refrigeration system could also be established using distributed-, lumped- or partial-lumped parameter modeling approaches [Ataer et al., 1995; Shah et al., 2004; Wang and Touber, 1991].

2.5.1.3 Expansion device

The functions of an expansion device in a DX A/C system were to reduce the refrigerant pressure when passing through it and to regulate the refrigerant mass flow rate. The commonly used expansion devices included capillary tubes, thermostatic expansion valves and electronic expansion valves (EEVs), etc. Although a capillary tube was simpler and of low cost, its regulating range was limited and therefore it was not suitable for use in DX A/C systems if precise refrigerant flow rate control was required [Xia et al., 2019]. Furthermore, a thermostatic expansion valve regulated thermo-mechanically the degree of superheat (*DS*) at evaporator outlet, but it was hard to be used to vary the refrigerant mass flow rate because of its long response time. Finally, an EEV responding to electronic signals had a high sensitivity and could be adequately used to alter refrigerant flow rate by changing it degree of opening.

The expansion process in an EEV could be treated as adiabatic or isenthalpic, then isenthalpic orifice equations could be applied to EEVs [MacArthur and Grald, 1987]. For modeling expansion device, empirical- and physical-modeling approaches could also be used. Because of the complex geometry configurations of EEVs, physical-modeling approaches were mainly applied to capillary tubes and thermostatic expansion valves. For EEVs, empirical modeling was applied [Damasceno et al., 1990; Park et al., 2007]. Ye et al. [2007] established an empirical correlation model for an EEV's mass flow rate based on experimental date. Park et al. [2007] established an empirical model to predict the mass flow rate of an EEV using a modified single-phase orifice equation after incorporating the EEV's geometries parameters and operating conditions. Xue et al. [2008] developed a regressive expression for the flow factor of an EEV using multivariate analysis, and found out that the flow factor was related to the geometry parameters of an EEV, refrigerant inlet temperature and pressure, and

thermo-physical properties of refrigerant. Furthermore, it was revealed that the modeling results predicted by an empirical model for an EEV were always smaller than experimental results, which was likely due to the fact that a homogeneous flow rather than a metastable flow of refrigerant was assumed.

2.5.1.4 Refrigerant pipework

Refrigerant pipework modeling was important to ensure the modeling accuracy of a complete DX A/C system. This was particular true as the refrigerant pressure drop along the pipework would significantly affect the operating performances of the entire DX A/C system [Lu et al., 2009]. The pressure drop of refrigerant flow along the pipework was influenced by various factors, such as refrigerant viscosity, heat transfer coefficient and the roughness of the internal surface of a pipe. In general, the refrigerant pressure loss along a pipework could be calculated by Darcy-Weisbach Equation [McKeon et al., 2004]. For example, Pan et al. [2012] studied the refrigerant pressures drops in a dual-evaporator DX A/C system, and investigated the effect of pipe length on the system performances. A similar study was also carried out by Lu et al. [2009]. In these studies, according to refrigerant statuses, i.e., single-phase and two-phase, different flow regions inside a pipework should be determined, and the calculation of friction coefficient in a sub-model for refrigerant pipework would be different depending on refrigerant statuses and the changes in kinetic energy of refrigerant due to phase change would also be different. Furthermore, the roughness of pipeline should also be considered by using appropriate coefficient in a sub-model for refrigerant pipework.

2.5.2 Solving a complete DX A/C system model

To solve a complete DX A/C system model, firstly, all sub-models for system components and pipework needed to be solved. Secondly, the coupled relationships for the input / output parameters to / from all the sub-models for all system components along the refrigerant / air flow directions should be established. Therefore, solving a complete model for a DX A/C system was more complex than solving a single sub-model, with the following two common solving methods:

The first was to solve all the model equations and the equations, for initial and boundary conditions simultaneously. The available numerical methods included the Euler Method, the Newton-Raphson Method and the Runge-Kutta Method, etc. [Chi and Didion, 1982; Tian et al., 2004]. Although solving all equations simultaneously had a high versatility, there was no specific physical meaning for a calculation process, and it was hard to find out the cause of calculation error which might result in inefficient debugging and calculation instability. On the other hand, the flexibility of this method was also questionable since additional sub-models were hard to be inserted into a complete system model when using this method.

The second was the sequential modular method [Ding et al., 2004a; Jin et al., 2011; Lu et al., 2004]. Specific equilibrium conditions, such as mass balance, can be used as the convergence criterion. After assuming a set of initial values, such as refrigerant mass flow rate and temperature at compressor inlet, the calculation for the compressor was started. Other related parameters for the compressor were then calculated based on these assumed values. Thereafter, along the refrigerant mass flow direction, all the

parameters for the condenser, the expansion device such as an EEV and the evaporators were calculated sequentially. If the convergence conditions were not met, the previous assumed values were updated or replaced. The advantage of this method was that the intermediate process of a calculation had a clear physical meaning, which was easy to debug, and calculation stability was easy to guarantee. However, its versatility was not high, because it was often necessary to adjust or redesign the calculation flow in combination with the actual physical cycle process.

2.6 Conclusions

Extensive previous studies on indoor thermal environmental control using DX A/C systems and other related issues have been carried out and the study results have demonstrated the importance of maintaining a suitable indoor thermal environment which would greatly affect the thermal comfort of occupants, IAQ and the operating efficiency of DX A/C systems. In small- to medium- scale buildings located in hot-humid climates, DX A/C systems have been widely used to control the indoor thermal environment because they were compact in volume, high in energy efficiency and low in operation and maintenance costs. However, there existed three main inadequacies in the design and operation of DX A/C systems for indoor thermal environmental control in buildings located in hot-humid climates, as follows. Firstly the current design trends for DX A/C systems were to obtain a higher EER and COP with therefore an impaired dehumidification capacity, leading to potentially a situation where the use of a DX A/C system might provide only the desired T_i control but not the required RH_i control; Secondly, the significant changes in space cooling loads in a conditioned space made it difficult for a conventional DX A/C system to achieve the desirable indoor thermal

environment control; Lastly, for spaces where an On-Off controlled single-speed DX A/C system was used for thermal environmental control, T_i had to set low enough to increase its moisture removal capacity. Therefore, an oversized DX A/C system may have to be employed to increase its output TCC, which would inevitably overcool indoor air and increase the initial and operating costs.

Many efforts have therefore been tried to deal with the above three inadequacies to obtain the desirable indoor thermal environmental control, and can be broadly grouped into three main approaches. The first approach was to add extra provisions to conventional DX A/C systems, which actually required additional installation spaces and increased initial and operating costs. Therefore, it was not suitable for use in small- to medium- scale buildings. Then, for the second approach of applying VS technology to conventional DX A/C systems, the previous related studies suggested that variable cooling and dehumidification capacities may be achieved when DX A/C systems were VS operated. However, VS technology was more costly, and the associated controllers developed based on VS technology were indeed very complicated and required complex mathematical calculations. In addition, these controllers were developed based on specific DX A/C systems and therefore cannot be directly applied to other DX A/C systems. Furthermore, at a fixed compressor speed, reducing the supply air flow rate for improved dehumidification capacity would result in a poorer indoor air distribution and adversely affect occupants' thermal comfort. Hence, applying VS technology to DX A/C systems for indoor thermal environmental control may not be the best option for small- to medium- scale buildings. Lastly, for the third approach of modifying the configuration of conventional DX A/C systems, although previously a novel EDAC system with two evaporators was developed without additional provisions and costly

VS technology, the two evaporators were actually arranged in series. As a result, there were a few drawbacks as follows. Firstly, the air flow path within such an EDAC system was longer, leading to a larger system size. Secondly, the air-side resistance was increased because supply air needed to pass through the two evaporators, leading to an increased fan energy consumption. Lastly, since the two evaporators were placed in series, the total air flow including fresh air flow would pass through both. Hence, it was not possible to designate one of the two evaporators to process specifically fresh air for more effectively moisture removal.

On the other hand, there have been extensive studies on the modeling of DX A/C systems. Mathematical models / sub-models for both a complete DX A/C system and its main components have been readily available and can be used to assist the developments of both novel DX A/C systems for improved indoor thermal environmental control and new controllers for better control accuracy and improved energy efficiency of DX A/C systems.

The literature review presented in this Chapter has identified that it became highly necessary to further optimize the arrangement of two evaporators to address the above-mentioned drawbacks. Consequently, a novel DX A/C system having a two-sectioned cooling coil (TS-DXAC) was to be proposed and studied by both experiments and mathematical modeling. In addition, a novel controller to specifically operated the TS-DXAC was also to be developed. These are the main objectives of the research project presented in this Thesis.

Chapter 3

Proposition

3.1 Background

The literature review presented in Chapter 2 has identified a number of inadequacies of indoor thermal environmental control when using DX A/C systems in small- to medium- scale buildings located in hot-humid climates. As a result, a number of approaches have been attempted to address these inadequacies. However, for these approaches, there were still issues such as requiring additional provisions or complex control strategies based on the expensive VS technology to maintain a desirable indoor thermal environment. In addition, although a previous EDAC system with two evaporators was developed without requiring additional provisions and costly VS technology, the two evaporators were actually arranged in series. As a result, there existed also a few drawbacks such as a larger system size and an increased air-side flow resistance, etc.

3.2 Project title

To address specifically the drawbacks associated with the EDAC system, a novel DX A/C system having a two-sectioned cooling coil (TS-DXAC) was proposed and studied by experiments and mathematical modeling in the research project presented in this Thesis. The research project to be reported in this Thesis is therefore entitled "Experimental and modeling studies of a direct expansion based air conditioning

system having a two-sectioned cooling coil (TS-DXAC) for improved indoor thermal environmental control”

3.3 Aims and objectives

The aims and objectives of the research project were as follows:

1) To propose conceptually a novel DX A/C system having a two-sectioned cooling coil (TS-DXAC) without requiring extra provisions and complex VS technology based controllers to provide variable cooling and dehumidification capacities and improved indoor air distribution;

2) To build an experimental TS-DXAC system to investigate its inherent operational characteristics expressed in terms of the relationship between its output total cooling capacity and equipment sensible heat ratio and to evaluate its operating performances for indoor thermal environmental control;

3) To develop and experimentally validate a steady-state physical-based mathematical model of the experimental TS-DXAC system, and to further study its inherent operational characteristics and optimize the configuration of the TS-DXAC system using the validated model;

4) To develop a control strategy for the experimental TS-DXAC system to operate it at different indoor conditions in buildings located in hot-humid climates.

3.4 Research methodologies

Both experimental and mathematical modeling approaches will be employed in this research project reported in this Thesis.

Firstly, an experimental TS-DXAC system will be established in a laboratory. There were two chambers, and each chamber had an independent DX based VS A/C system and a load generation unit (LGU), to create and maintain the indoor or outdoor experimental thermal environment. All of the operating parameters of the experimental TS-DXAC system and the thermal environmental parameters of the two chambers can be real-time monitored and recorded.

Secondly, a steady-state physical-based mathematical model for the experimental TS-DXAC system will be developed, with reference to the existing system models for various DX A/C systems and the existing sub-models for key components in a DX A/C system. The physical-based mathematical model will be experimentally validated using the experimental TS-DXAC system.

Finally, a control strategy consisting of two algorithms will be developed to enable the experimental TS-DXAC system to be operated at different indoor conditions in buildings located in hot-humid climates to obtain an improved indoor thermal environmental control. Controllability tests for the strategy will be carried out to evaluate the operating performance of the developed control strategy.

Chapter 4

The experimental TS-DXAC system

4.1 Introduction

As stated in Chapter 3, to address specifically the drawbacks associated with the previously developed EDAC system, a research project to study a novel DX A/C system having a two-sectioned cooling coil (TS-DXAC) by experiments and mathematical modeling is going to be carried out. Therefore, an experimental TS-DXAC system has been purposely established to enable carrying out the research project. In the experimental TS-DXAC system, advanced technologies such as a VS compressor, electric expansion valves (EEVs), as well as a computerized data measuring, logging and control unit have been included.

This Chapter reports on the developments of the experimental TS-DXAC system. Firstly, a conceptual description of the novel TS-DXAC system is given. Secondly, detailed descriptions of the experimental TS-DXAC system and its major components are presented. This is followed by describing a computerized instrumentation and data acquisition system including sensors and measuring devices for all operating parameters of the experimental TS-DXAC system. Finally, a computerized monitoring and controlling program for the experimental TS-DXAC system is detailed.

4.2 A conceptual description of the novel TS-DXAC system

Fig. 4.1 shows a conceptual diagram of the novel TS-DXAC system. As seen, in this novel system, its DX evaporator, or cooling coil, was divided into two sections, HX1 and HX2. Unlike in an A/C system with a dual-evaporator where two indoor units were normally separated, here, the two sections were actually housed inside one single unit and arranged in parallel on its airside. Two EEVs, i.e., EEV1 and EEV2, were connected to HX1 and HX2, respectively. On the air side, in order to be able to independently vary the supply air flow rate passing through each of the two sections, each section had its own matching VS supply fan, SF1 and SF2, as shown in Fig. 4.1.

In the current design, HX2 was of a larger size and hence intended to be a main cooling and dehumidification section, and HX1 of a smaller size a supplementary one to provide additional latent cooling capacity (LCC) when necessary. The ratio of the refrigerant mass flow rates to the two sections could be changed by varying the opening degree of EEV1, while that of EEV2 was adjusted accordingly to maintain a constant *DS* at compressor suction. The ratio of the supply air flow rates passing through the air sides of both HX1 and HX2 could also be varied by adjusting the operating speeds of the two supply fans, but a constant total supply air flow rate was maintained. In the TS-DXAC system, when the refrigerant mass flow rates or supply air flow rates to HX1 and HX2 were different, they would operate at different evaporating pressures thus different evaporating temperatures, and therefore different output SCCs and LCCs from the TS-DXAC system could be obtained. On the other hand, when the surface temperature of a cooling coil was lower than air dew point temperature, air cooling and dehumidification occurred simultaneously. Therefore, two different surface

temperatures in HX1 and HX2, respectively, can be provided, with the surface temperature in HX1 being normally lower than that in HX2, since HX1 was designated to provide additional LCC. In addition, with a constant total supply air flow rate, the supply air temperature could be maintained at a moderate level even if the surface temperature of HX1 was very low for better dehumidification.

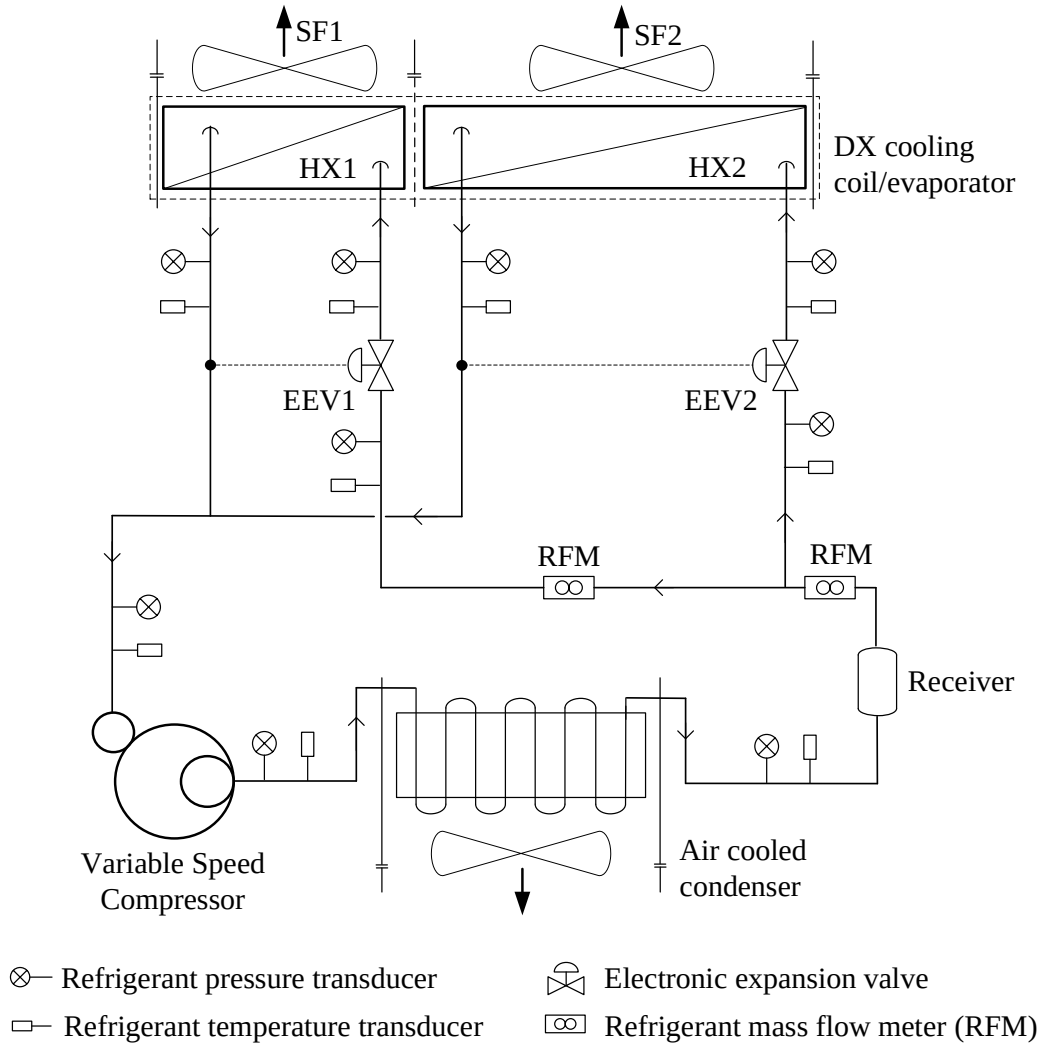

Fig. 4.1 A conceptual diagram of the novel TS-DXAC system

4.3 Descriptions of the experimental TS-DXAC system and its major components

An experimental TS-DXAC system, according to the conceptual diagram shown in Fig. 4.1 was established in a laboratory, as detailed in Fig. 4.2. As seen, in the experimental system, there were two chambers, one as an indoor space and the other as an outdoor space. Each environmental chamber was measured at 5m (L) × 3 m (W) × 2.5m (H). In each chamber, there were an independent A/C system and a load generation unit (LGU), to create and maintain its experimental thermal environment.

The main components on the refrigerant-side of the experimental TS-DXAC system included a VS compressor, an air-cooled condenser, and a two-sectioned cooling coil with their matching EEVs. Although in the research project reported in this Thesis, a fixed compressor speed was employed, to facilitate the further study of the novel TS-DXAC system, a VS compressor was used in this experimental system. In addition, the size of HX1 was 450mm × 200mm, and that for HX2 450mm × 300mm. The compressor's rated cooling capacity was 5 kW at an input frequency of 70 Hz and the refrigerant was R410A. On the other hand, as seen in Fig. 4.2, the air-side of the experimental TS-DXAC system included two independent air ducts with two VS supply fans and air flow rate measuring apparatus (FRMA). While the condenser was installed inside the outdoor environmental chamber, the rest of the experimental TS-DXAC system the indoor environmental chamber. Also, the two supply fans can be VS operated to ensure a constant total supply air flow rate. In addition, all controllable components, including the EEVs, the compressor, supply fans were all connected to a control unit, shown as C1 in Fig. 4.2. The specifications for the major components used in the experimental TS-DXAC system are listed in Table 4.1.

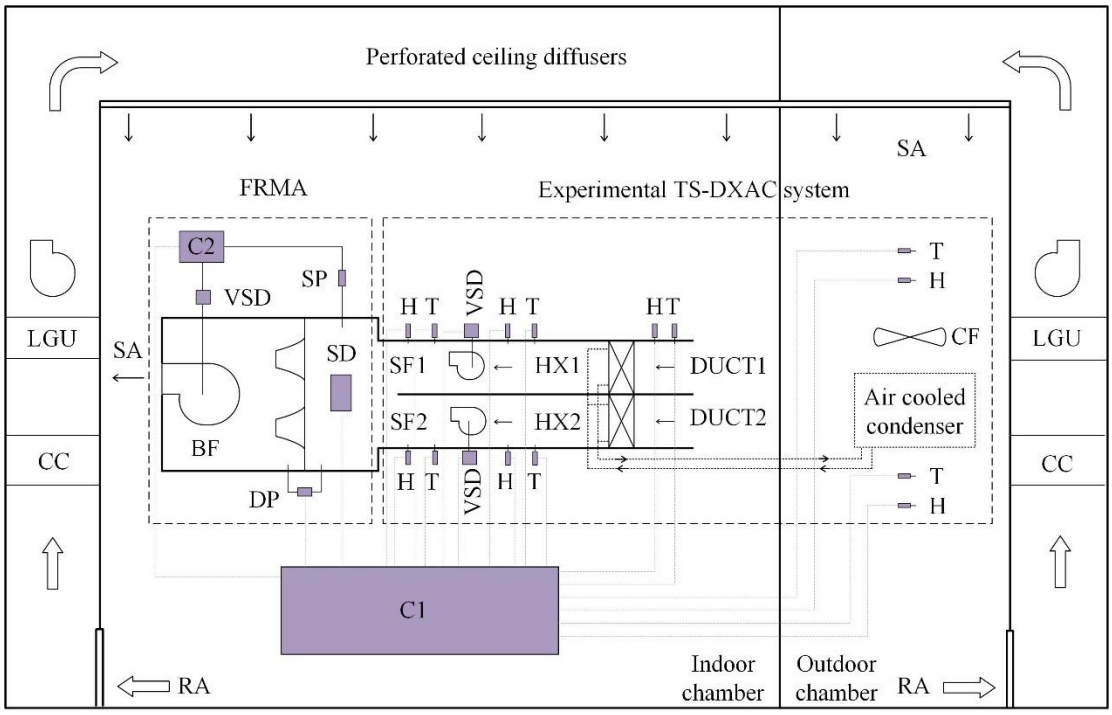

A/C- air conditioning
BF - booster fan
CC - cooling coil
CF - condenser fan
C1 - data acquisition and control unit
C2 - controller for FRMA
DP - differential pressure transducer
FRMA - airflow rate measuring apparatus
H - air humidity sensor
HX - heat exchanger
LGU - load generating unit
RA - return air
SA - supply air
SF - supply fan
SD - sampling device
SP - static pressure measuring device
T - air dry-bulb temperature sensor
VSD - variable speed drives

Fig. 4.2 The schematics of the experimental TS-DXAC system

Table 4.1 Specifications of the main components in the experimental TS-DXAC system

Components	Specifications	
Compressor	Type	Rotary
	Number of cylinder / Polarity	2/6
	Allowable frequency range	10-120 Hz
	Rated input frequency	70 Hz
	Rated cooling capacity	5 kW
	Displacement	14 mL/rev
EEV1	Pulse range	0 −500 pulse
	Rated capacity	2.5 kW
	Port diameter	1.3 mm
EEV2	Pulse range	0 −500 pulse
	Rated capacity	3.5 kW
	Port diameter	1.65 mm
HX1	Fin type	Louver
	Transverse/Longitude pipe spacing	21/12.7mm
	Fin pitch/thickness	1.2/0.115mm
	Coil width/height	450 /200 mm
	Internal/external tube diameter	6.4 / 7 mm
	Total coil length	14.4 m
	Number of the tube row	4
	Number of refrigerant loop	2
HX2	Fin type	Louver
	Transverse/Longitude pipe spacing	21/12.7mm
	Fin pitch/thickness	1.2/0.115mm
	Coil width/height	450/300 mm
	Internal/external tube diameter	6.4 / 7 mm
	Total coil length	21.6 m
	Number of the tube row	5
Condenser	Fin type	Louver
	Internal/external tube diameter	8.82 / 9.52 mm
	Total coil surface area	25 m^2
SF1/SF2	Type	Centrifugal fan
	Air flow rate	0.1–0.3 m^3 /s
Condenser fan	Air flow rate	0.1–0.6 m^3 /s

4.4 Computerized instrumentation and data acquisition system

The operating parameters of the experimental TS-DXAC system were measured by high-precision sensors and transducers. As seen in Fig. 4.2, a computerized data acquisition unit was provided to monitor and record signals from all sensors and measuring devices. For the measurement on the refrigerant-side, Platinum Resistance Temperature Device (RTD) was used to measure the refrigerant temperatures, and the pressure transducers for refrigerant had an accuracy of ± 0.3% of full scale reading. The approximate locations for installing temperature and pressure transducers can be found in Fig. 4.1. Furthermore, two refrigerant mass flow meters were included in the experimental TS-DXAC system, with one located downstream of the condenser, and the other upstream of EEV1, as shown Fig. 4.1.

For the measurements on the air-side of the experimental TS-DXAC system, as seen in Fig. 4.2, the air dry-bulb (T_{db}) and wet-bulb (T_{wb}) temperatures inside the two chambers were measured using the sampling devices which had an ANSI/ASHRAE Standard 41.1 (ASHRAE, 1986) specified psychrometer using platinum resistance (PT100) temperature sensors. Furthermore, six pairs of temperature and humidity probes were used to measure air states at the inlets to HX1, HX2 and condenser, the outlets from HX1, HX2 and condenser. Since the two supply fans and the two sections of the cooling coil were arranged in parallel, the total supply air may be divided into two independent streams using appropriate air ducts. The air flow rates in the experimental system were measured by an FRMA (ASHRAE, 1987), as shown in Fig. 4.2, which was consisted of a differential pressure transducer with a measuring accuracy of ±0.1% of the full scale reading, diffusion baffles and a set of nozzles with different sizes. In addition, one

set of air T_{db} and T_{wb} sensors (PT100) was placed in the FRMA to obtain the status of air leaving the experimental TS-DXAC system.

Finally, the compressor's energy consumption was got from its variable frequency drive, and the total energy consumption of the experimental TS-DXAC system including the two supply fans and the compressor was obtained from a power meter. Detailed instrumentation and sensors incorporated in the experimental TS-DXAC system are listed in Table 4.2.

Table 4.2 Details of instrumentation and sensors used in the experimental TS-DXAC system

Parameters	Instrument Type	Range	Accuracy
Space T_{db} and T_{wb}	Tree and aspirating psychrometer	-50-100 °C	±0.1 °C
Air T_{db}	T&RH probe	-40-60 °C	±0.3 °C
Air RH	T&RH probe	10-95%	±2% RH
Air flow rate	FRMA	0-1 kg/s	±1.2%
Refrigerant temperature	Platinum RTD	-50-100 °C	±0.1 °C
Refrigerant pressure	Pressure transducer	-1-34 bar	±0.3%
Refrigerant pressure	Pressure transducer	-1-20 bar	±0.3%
Refrigerant mass flow rate	Coriolis mass flow meter	0.3-18 kg/min	±0.15%
Power consumption	Single-phase power meter	1-40 A	±0.1%

A data acquisition unit was used in this experimental TS-DXAC system to monitor and collect different types of system operating parameters. It provided up to 60 channels with a minimum data sampling interval of two seconds. The collected direct current or voltage signals from the measuring devices / sensors can be transformed into their real physical values using a data logging & control supervisory program which was developed by LabVIEW programming platform, as detailed before.

4.5 LabVIEW logging & control supervisory program

LabVIEW, a commercially available programming package, was used to develop the data logging & control supervisory program for this experimental TS-DXAC system. The developed program can be used to monitor, record and control all the operating parameters of the experimental TS-DXAC system by communicating the data acquisition unit and the control unit of the experimental TS-DXAC system. All measured system parameters were real time monitored, and the data can be displayed, recorded and processed. In addition, all recorded data can also be retrieved, queried and graphed in trend logs through this program. A personal computer was used to run this program, and therefore, this computer was worked as a central supervisory control unit for both data logging and control for the experimental TS-DXAC system.

4.6 Summary

An experimental TS-DXAC system was purposely established to enable carrying out the research project reported in this Thesis.

All of the operating parameters of the experimental TS-DXAC system, composed of its refrigerant-side and air-side, were measured with high precision sensors and transducers. A data acquisition unit having 60 channels to monitor and record all parameters was used. A data logging & control supervisory program was developed for this experimental TS-DXAC system using LabVIEW, and all measured system parameters were real time monitored, and the data can be displayed, recorded and processed.

This availability of the experimental TS-DXAC system was expected to be essential for carrying out the research project proposed in Chapter 3, such as investigating the operational characteristics of the TS-DXAC system, validating a mathematical model for the experimental TS-DXAC system to be developed and developing a control strategy for the TS-DXAC system.

Photos showing the experimental TS-DXAC system are given in Appendix.

Chapter 5

Operational characteristics of the experimental TS-DXAC system

5.1 Introduction

As mentioned in previous Chapters, the novel TS-DXAC system to be studied in the research project presented in this Thesis was actually originated from a previously developed EDAC system and its development was intended to address the drawbacks associated with the EDAC system. Hence, an experimental TS-DXAC system has been established as detailed in Chapter 4 to enable carrying out the research project in Chapters 5 to 7 of this Thesis, three pieces of the research work corresponding to the objectives of the research project will be respectively presented. In this Chapter, an experimental study on the operational characteristics of the experimental TS-DXAC system is presented to examine whether such a novel TS-DXAC system can provide variable cooling and dehumidification capacities when both its refrigerant and air flow rates passing through the two-sectioned cooling coil were varied.

The details of the experimental TS-DXAC system are given in Chapter 4. In this Chapter, firstly, the experimental procedures and cases are specified. Secondly, experimental results on the operational characteristics of the experimental TS-DXAC system at all experimental cases are presented and analyzed. Finally, conclusions are given.

5.2 Experimental procedures and cases

As mentioned earlier, when the experimental TS-DXAC system was operated, its compressor speed was maintained constant and the total supply air flow rate passing the two sections also constant at 0.3 m^3/s. In this experimental study, two important ratios, R_r and R_a, were defined as follows:

The ratio of the HX1's refrigerant mass flow, m_{r1}, to the total refrigerant mass flow rate, m_r:

$$R_r = m_{r1} / m_r \tag{5.1}$$

and the ratio of HX1's air mass flow rate, m_{a1}, to the total air mass flow rate, m_a:

$$R_a = m_{a1} / m_a \tag{5.2}$$

R_r could be changed by adjusting the degree of opening of EEV1. Correspondingly, the degree of opening of EEV2 needed to be varied at the same time to maintain the setting of *DS* at compressor suction. R_a could be changed by adjusting the operational speeds of two supply fans, but the total supply air flow rate remained unchanged at 0.3 m^3/s.

During the experiments, the experimental TS-DXAC system was operated at five different inlet air states, or the five air states at the simulated indoor space expressed in terms of T_{db} and T_{wb}, as shown in Table 5.1. As seen from Table 5.1, the five inlet air states may be divided into two groups: a constant T group but with varying RH from

40% to 60%, at an interval of 10% RH, and a constant RH group with T_{db} from 22 ℃ to 26 ℃, at an interval of 2 ℃. At each inlet air state, the experimental TS-DXAC system was operated at different values of R_a and R_r, as shown in Table 5.2.

Table 5.1 The experimental inlet air states

Group	Case	T_{db} (°C)	T_{wb} (°C)	RH (%)
Constant T	RH-40	26.0	17.0	40
	RH-50*	26.0	18.7	50
	RH-60	26.0	20.3	60
Constant RH	T_{db} -22	22.0	15.4	50
	T_{db} -24	24.0	17.1	50
	T_{db} -26*	26.0	18.7	50

* Same inlet state

Table 5.2 Combinations of R_a and R_r used in all the experimental cases

R_a						
No.	1		2		3	4
%	30		40		50	60
R_r						
No.	1	2	3	4	5	6
%	15	26	35	44	53	67

When the variations for T_{db} and T_{wb} were both less than 0.1 ℃, respectively, the experimental TS-DXAC system was considered to arrive at a steady operating state. Its inherent operational characteristics were evaluated, as follows.

The output SCC from the TS-DXAC system, Q_s, was evaluated by

$$Q_s = m_a C_{pa} \left(T_{db,i} - T_{db,o} \right) \tag{5.3}$$

where m_a is the total air mass flow rate, C_{pa} specific heat of air, $T_{db,i}$ the inlet air dry-bulb temperature to the TS-DXAC system, $T_{db,o}$ the outlet dry-bulb temperature from the TS-DXAC system.

The output TCC of the TS-DXAC system was evaluated by

$$TCC = m_a \left(h_{a,i} - h_{a,o} \right) \tag{5.4}$$

where $h_{a,i}$ is the inlet air enthalpy to the TS-DXAC system, $h_{a,o}$ the outlet air enthalpy from the TS-DXAC system.

Therefore, Equipment SHR can be evaluated by

$$E\ SHR = \frac{Q_s}{TCC} = \frac{C_{pa} \left(T_{db,i} - T_{db.o} \right)}{h_{a,i} - h_{a,o}} \tag{5.5}$$

In all experimental cases, the simulated outdoor space was maintained at 33 ℃ and 68% [ASHRAE, 2009], and *DS* at the compressor suction at 7 ℃, respectively. The uncertainties [Holman, 2001] for the R_r, R_a, TCC and E SHR are given in Table 5.3.

Table 5.3 The uncertainties for the operating parameters of the TS-DXAC system

Parameter	uncertainty	unit
R_a	0.71-1.16%	-
R_r	0.15-0.28%	-
TCC	0.93-1.52%	kW
E SHR	0.79-1.18%	-

5.3 Experimental results and discussions

In this section, firstly, the results for the experimental TS-DXAC system at T_{db}-26 or RH-50 case are detailed. Secondly, the experimental results at all cases are presented to exam the influences of different inlet air states on the inherent operational characteristics of the TS-DXAC system.

5.3.1 The inherent operational characteristics of the experimental TS-DXAC system at the inlet air state of 26 ℃ and 50% RH

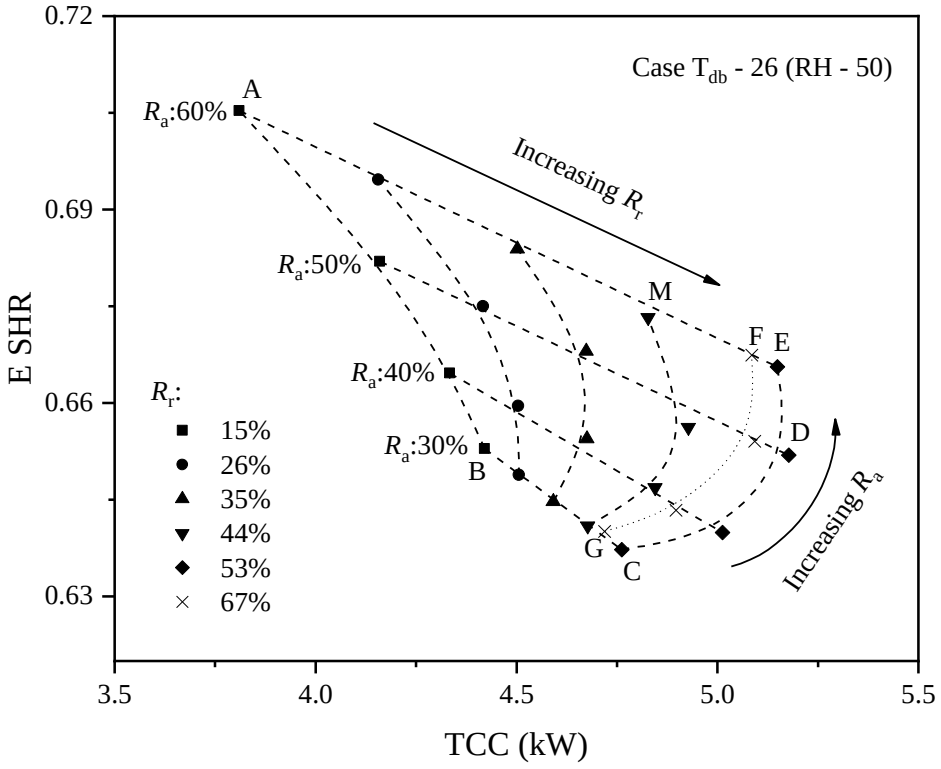

Fig. 5.1 The inherent operational characteristics of the TS-DXAC system at varying R_r and R_a (Case T_{db} - 26 / RH-50)

In Fig. 5.1, the measured output TCC and E SHR under different values of R_a and R_r at the inlet air state of T_{db}-26 or RH-50 are presented. As seen, the output TCC and E SHR were constrained within an irregular area of ABCDE, where R_a varied from 30% to 60% and R_r from 15% to 67%.

In Fig. 5.1, for the area of ABCDE, its borderlines AB and CDE represent the relationships between output TCC and E SHR when varying R_a from 30% to 60%, at two R_r values of 15% and 53%, and curve FG represents those when varying R_a from 30% to 60%, but at a fixed R_r of 67%, respectively. It should however be noted that curve FG is actually located on the left hand side of borderline CDE. This means that further increasing R_r from 53% to 67% would not enlarge the irregular area but the

resulted TCC / E SHR relationship actually duplicated some existing ones inside the area of ABCDE. This was because when R_r was increased to a certain level, such as 53% in the current study, the functions for the two sections would actually be reversed depending on their surface area ratio.

Actually, HX1 as a supplementary section was intended to provide extra cooling and dehumidification capacities. However, when R_r was increased to more than 53%, more refrigerant flowed into HX1. Thus, HX1 would actually function as a main cooling and dehumidifying coil section, and HX2 as a supplementary section. Hence, as R_r was further increased to over 53%, the resulted curves for the TCC / E SHR relationships would continue to move towards the left hand side of the area of ABCDE. This would be further explained later.

On the other hand, borderlines BC and AE are for TCC / E SHR relationships when R_r values were varied from 15% to 53%, at two R_a values of 30% and 60%. As illustrated in Fig. 5.1, at a constant total supply air flow rate, varying R_a and R_r values could contribute to significant variations in output TCC from 3.81 kW to 5.18 kW, and in E SHR from 0.64 to 0.71, respectively.

In the following two sub-sections, the influences of varying R_a and R_r on the inherent operational characteristics in terms of the relationships between TCC and E SHR, are respectively detailed.

5.3.1.1 The influences of varying R_r on TCC / E SHR relationship, at a constant R_a

As seen in Fig. 5.1, for all R_a values from 30% to 60%, at a constant R_a value, an increase in R_r from 15% to 53% led to a decrease in E SHR but an increase in TCC for the experimental TS-DXAC system. Using AE line in Fig. 5.1 as an example, the variation trend in TCC / E SHR relationship based on key operating parameters of the experimental TS-DXAC system as shown in Figs. 5.2 - 5.4 can be explained.

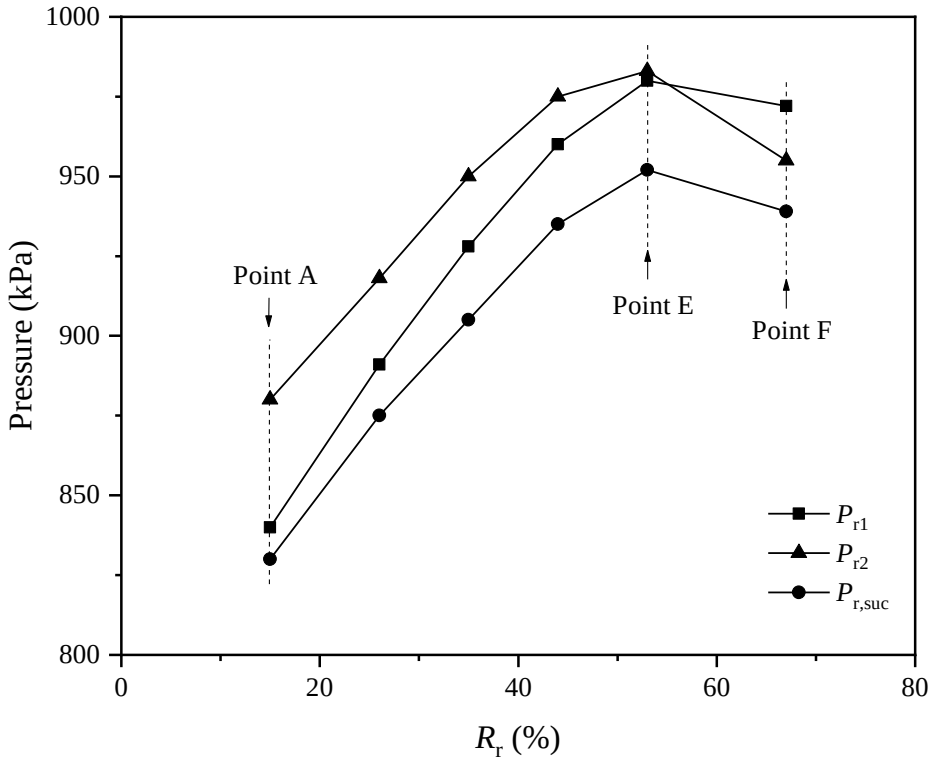

Fig. 5.2 The influences of R_r on the evaporating pressures of HX1 and HX2 and the compressor suction pressure

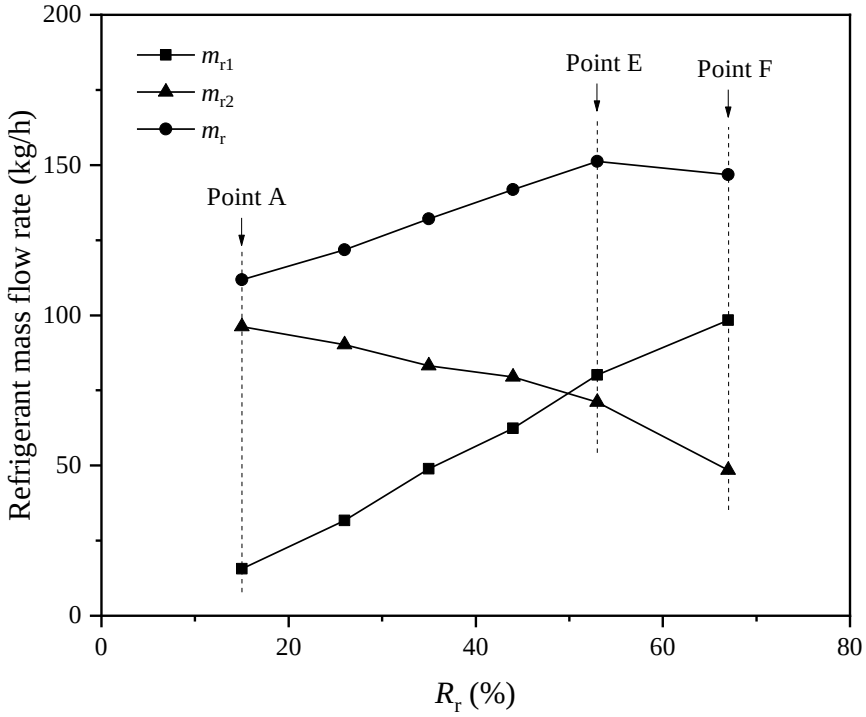

Fig. 5.3 The influences of R_r on the refrigerant mass flow rates in the TS-DXAC system

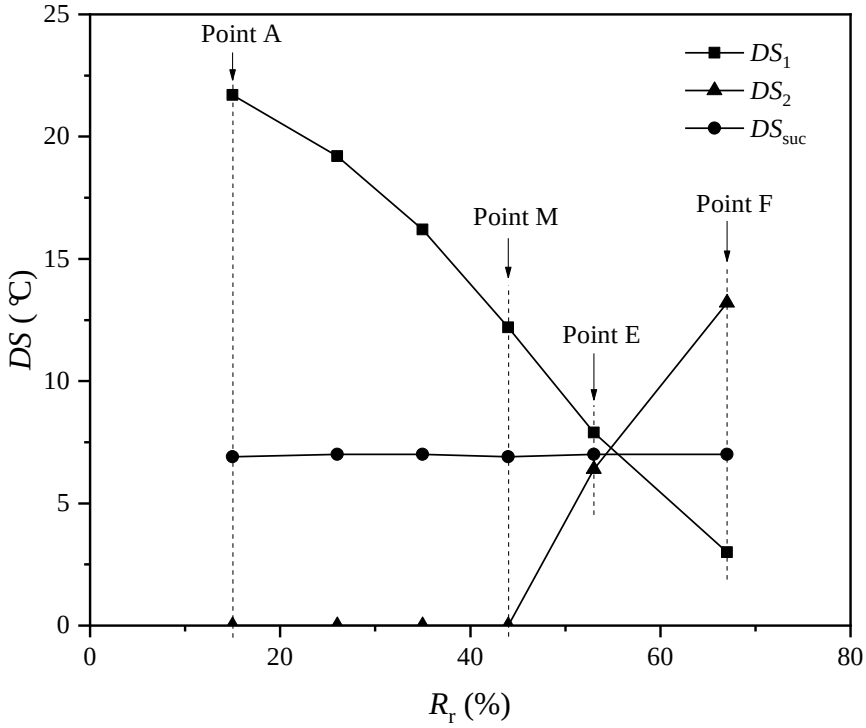

Fig. 5.4 The influences of R_r on the *DS*s

Firstly, the output TCC of the experimental TS-DXAC system was mainly determined by the total refrigerant mass flow rate when other conditions remained unchanged. The refrigerant mass flow rate was closely related to the compressor suction pressure. In the experimental TS-DXAC system, the two sections of the cooling coil were arranged in parallel and their operating conditions would therefore interact with each other. As seen in Fig. 5.2, the compressor suction pressure of the experimental TS-DXAC system was increased with an increase in R_r from 15% (Point A) to 53% (Point E), but decreased as R_r continued to increase from 53% (Point E) to 67% (Point F). The evaporating pressures for two sections experienced similar variation trends of increasing, peaking at R_r = 53%, and decreasing thereafter.

In the TS-DXAC system, the evaporating pressures of two sections were jointly effected by opening degrees and inlet pressures of two EEVs, their refrigerant mass flow rates and the inlet air state and air flow rate on the air side of the cooling coil, which remained unchanged at a fixed R_a. However, as seen from Figs. 5.2 - 5.4, the variation trends in evaporating pressures, refrigerant mass flow rates and *DS* values when R_r was ranged from 15% to 53% were different from those when R_r from 53% to 67%. They are separately analyzed as follows.

When R_r was increased from 15% to 53%, the opening degree of EEV1 was increased, and that of EEV2 decreased correspondingly to maintain a constant *DS* at compressor suction. During this process, the opening degrees of the two EEVs became closer to each other, which helped reduce the overall system refrigerant flow resistance and thus increase compressor suction and discharge pressures. Since the two sections of the cooling coil were arranged in parallel, the refrigerant pressures at the inlets to both

EEVs were increased. Hence, for HX1, when the opening degree of EEV1 was increased, the pressure drop across EEV1 was reduced and more refrigerant would flow into HX1 (Fig. 5.3), which tended to lead to a lower evaporating pressure in HX1. However, the evaporating pressure in HX1 was actually increased (Fig. 5.2), because the impact of reducing evaporating pressure due to more refrigerant flowing into HX1 was less significant than that of increased refrigerant pressure at the inlet of EEV1. For HX2, its opening degree of EEV2 was reduced, so that its refrigerant mass flow rate was also decreased (Fig. 5.3). Hence, together with the increase in refrigerant pressure in the inlet to EEV2, the evaporating pressure in HX2 was also increased (Fig. 5.2). In addition, as seen from Fig. 5.3, when R_r was increased from 15% to 53%, with gradual reduction in system refrigerant flow resistance, the total refrigerant mass flow rate, m_r, was also increased.

On the other hand, when R_r was increased from 53% to 67%, the opening degrees of the two EEVs started to deviate from each other, so that the overall system refrigerant flow resistance was increased. This resulted in a reduced compressor suction pressure and a reduced total refrigerant mass flow rate (Figs. 5.2 - 5.3), although the refrigerant mass flow rate to HX1 continued to grow as the opening of EEV1 continued to increase (Fig. 5.3).

Secondly, as stated above, an increase in refrigerant mass flow rate would lead to an increase in output TCC, at a constant air flow rate on the air side. Consequently, the surface temperature of a cooling coil would drop, which was beneficial to output enhanced dehumidification capacity from the TS-DXAC system, i.e., a lower E SHR. As shown in Fig. 5.1, at a fixed R_a of 60% (Line AE) when R_r was increased from 15%

to 53%, E SHR was decreased because of the increase in the total refrigerant mass flow rate. However, when R_r was continuously increased from 53% to 67%, E SHR was actually increased as a result of the decrease in total refrigerant mass flow rate.

The effects for changing the refrigerant mass flow rates to the two sections on E SHR are analyzed as follows. As known, the *DS* at the exit of a cooling coil can indicate its effective dehumidifying area. A smaller *DS* suggested a larger effective dehumidifying area, thus a better dehumidification capacity of a DX cooling coil, and vice versa. As seen in Fig. 5.4, when R_r was increased from 15% (Point A) to 44% (Point M), the *DS* at the exit of HX2, i.e., DS_2 remained at 0, so that the refrigerant at the exit of HX2 maybe two-phase stable. Moreover, the *DS* at the exit of HX1, i.e., DS_1 was decreased due to the increase in refrigerant mass flow rate. Therefore, the overall dehumidification capacity of the experimental TS-DXAC system was enhanced, as reflected by the reduced E SHR.

Furthermore, when R_r was increased from 44% (Point M) to 53% (Point E), the *DS* for HX1 continued to decrease, implying an improved dehumidification capacity from HX1. But *DS* for HX2 was slightly increased, reflecting a weakening dehumidification capacity from HX2. However, the total system refrigerant mass flow rate was increased, with reduction in refrigerant mass flow rate to HX2 being less than the increase in refrigerant mass flow rate to HX1. Therefore, the increase in the dehumidification capacity from HX1 was greater than the reduction in the dehumidification capacity from HX2, and the system E SHR continued to decrease. However, when R_r was further increased from 53% (Point E) to 67% (Point F), although *DS* for HX1 continued to reduce, *DS* for HX2 was greatly increased. Since the decrease in refrigerant mass flow

rate to HX2 was more than the increase refrigerant mass flow rate to HX1, a poorer total dehumidification capacity of the experimental TS-DXAC system was resulted in, as reflected by an increased E SHR.

5.3.1.2 The influences of varying R_a on TCC / E SHR relationship, at a constant R_r

Firstly, as seen in Fig. 5.1, for all R_r values, the values of E SHR were increased when R_a was increased from 30% to 60%. Using curve CDE in Fig. 5.1 as an example to explain the variation trend of E SHR when R_a was varied. Generally, an increase in airflow rate, or a higher Reynolds Number of airflow would result in a higher heat transfer between the air and cold surface of the cooling coil. The increase in airflow rate may therefore lead to a higher output TCC. On the other hand, as pointed out by Chuah et al. [1998], the dehumidification capacity of a cooling coil was decreased with increased air face velocity because of the increase in air bypass. On the contrary, when air velocity was decreased, the output dehumidification capacity from the system would be increased.

Therefore, as R_a was increased from 30% to 60%, E SHR of HX1 was increased but that for HX2 reduced. However, for the experimental TS-DXAC system, its dehumidification capacity was actually reduced, as R_a was increased from 30% to 60%. This was because the increase in air flow rate for HX1 was equal to the reduction in air flow rate for HX2 because of the constant total air flow rate. However, given the fixed surface area ratio of the two sections at 2:3, the increase in face velocity for HX1 was always 1.5 times greater than the reduction in face velocity for HX2. Therefore, when increasing R_a, the extent of reducing dehumidification capacity from HX1 would be

greater than that of increasing dehumidification capacity from HX2, leading to an increase in E SHR, or reduced dehumidification capacity of the experimental TS-DXAC system.

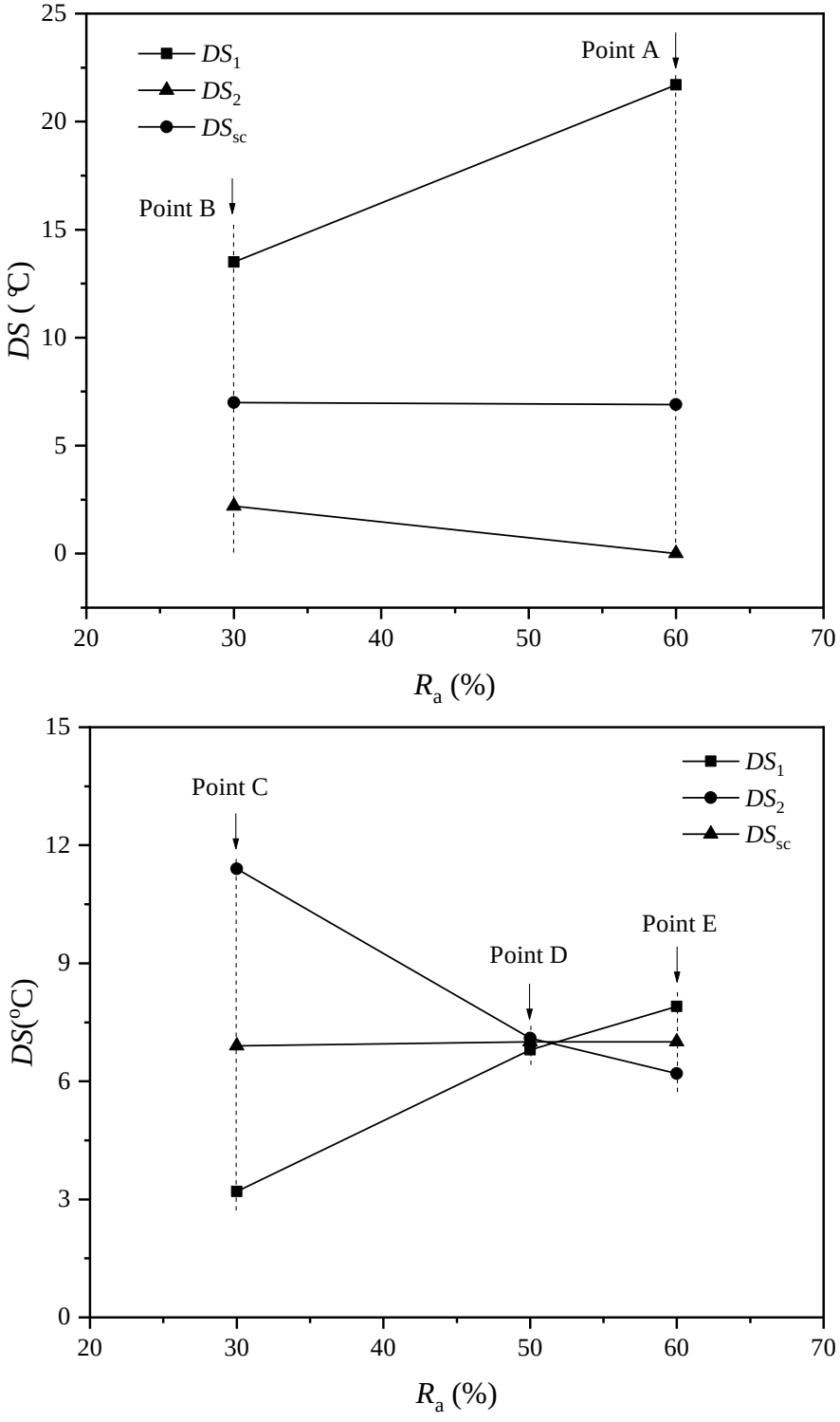

Fig. 5.5 The influences of R_a on the *DS*s

Secondly, as seen in Fig. 5.1, when changing R_a, there were two variation trends for TCC. At a R_r value of < 36%, the output TCC was decreased monotonously with an increased R_a. However, at a R_r of > 36%, the output TCC was firstly increased, then peaked, and decreased thereafter, with an increased R_a. Curves AB and CDE in Fig. 5.1 are taken as examples to explain the variation trends of TCC. As known, *DS* at the exit of a cooling coil may be used to indicate the relative share of the two-phase surface area of the total surface area in a DX cooling coil, i.e., a larger *DS* value reflected less two-phase surface area, and vice versa. As stated above, when R_a was increased and other conditions remained unchanged, an increase in air flow rate for HX1 would enhance the heat transfer taking place in HX1, so that the *DS* at its exit was increased. On the contrary, the *DS* at the exit of HX2 would be decreased.

As seen in Fig. 5.5, for curve AB, at Point B, the *DS* for HX1 was already greater than that for HX2, because of R_a and R_r values, for unit refrigerant mass flow, there was more air mass flow in HX1 than HX2. With an increased R_a from Point B to Point A, the *DS* for HX1 was further increased. As a result, the evaporating pressure in HX1 was increased, so that the pressure difference across EEV1 was reduced, leading to more refrigerant flowing into HX1. However, to maintain a constant R_r, EEV1 should be slightly closed, and EEV2 correspondingly slightly opened further. During the process, the difference in the opening degrees for the two EEVs was increased, leading to an increase in the overall system refrigerant flow resistance. Hence, the total refrigerant mass flow rate was reduced and so was the output TCC. However, for curve CDE, at Point C, the *DS* for HX1 was smaller than the *DS* for HX2, because of R_a and R_r values, for unit refrigerant mass flow rate, there was less air mass flow rate in HX1 than in HX2. With an increased R_a from Point C to Point D and finally to E, the value of *DS*

for HX1 was increased and that for HX2 was decreased. At Point D, the values of *DS* for the two sections were very close to each other, so that the overall system refrigerant flow resistance was the smallest. Hence, both refrigerant mass flow rate and output TCC were the largest. When R_a was further increased from Point D to Point E, the difference in *DS* for the two sections started to increase. Hence, both system refrigerant mass flow rate and output TCC were reduced as the overall system refrigerant flow resistance was increased again.

5.3.2 The influences of different inlet air states on the inherent operational characteristics of the experimental TS-DXAC system

Experimental results at the inlet conditions shown in Table 5.1 other than those at RH-50 / T-26 test case are illustrated in Fig. 5.6 and Fig. 5.7. Fig. 5.6 shows the results for constant RH test group and Fig. 5.7 those for constant T test group. As seen, different inlet air states would influence the high-low limits of TCC and E SHR to different degrees, and the ranges between the limits.

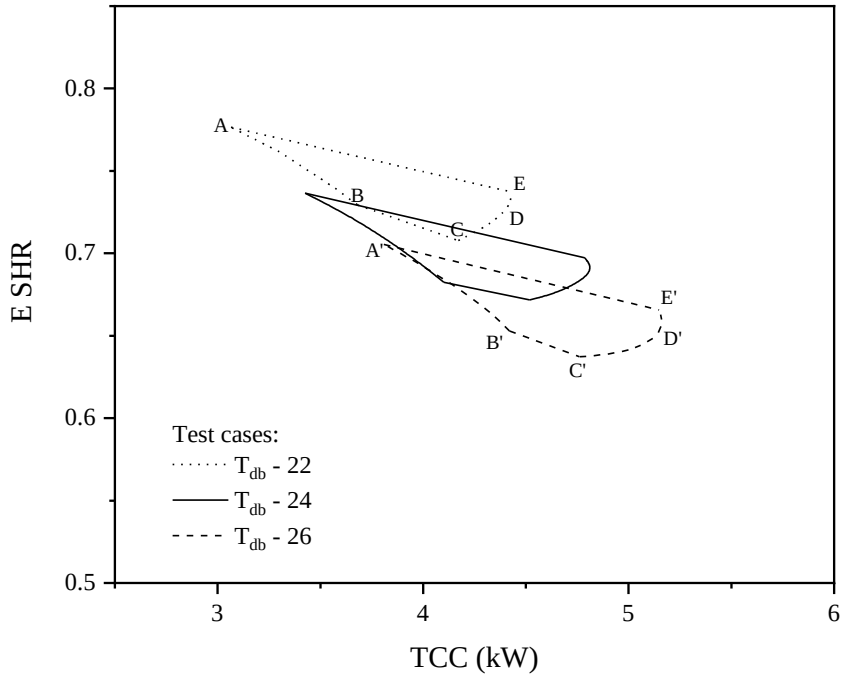

Fig. 5.6 The measured TCC-E SHR relationships of the experimental TS-DXAC system at Constant inlet air RH Groups

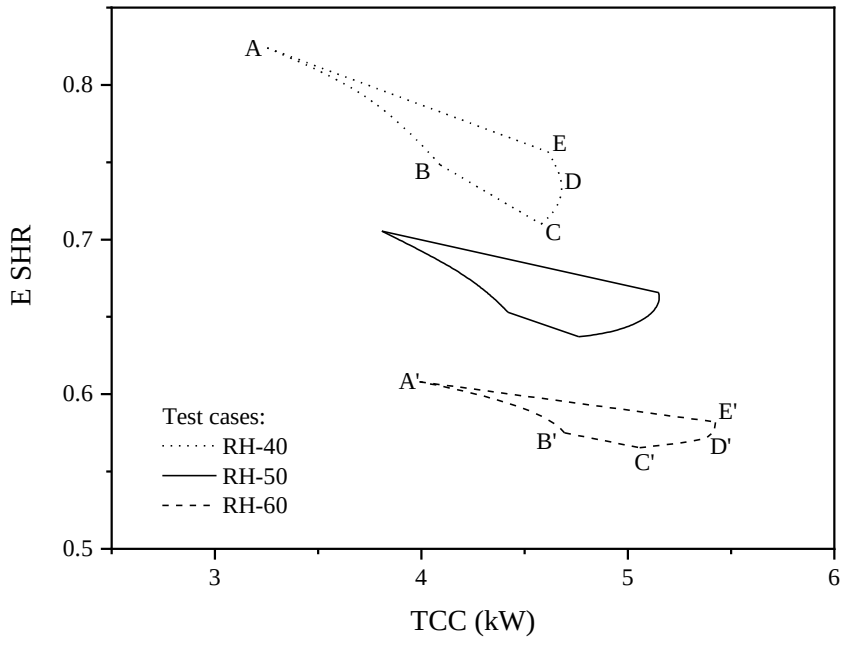

Fig. 5.7 The measured TCC-E SHR relationships of the experimental TS-DXAC system at Constant inlet air T Groups

As seen in Fig. 5.6, at constant RH cases, with the increase in T_{db} from 22 ℃ to 26 ℃, both of the output SCC and LCC of the experimental TS-DXAC system were increased. However, because of a greater increase in LCC, in Fig. 5.6, E SHR values were reduced. Therefore, the positions of the irregular areas of ABCDE were shifted from up-left corner with high E SHR and low TCC values to down-right corner with low E SHR and high TCC values in Fig. 5.6. In addition, when T_{db} was increased from 22 ℃ to 26 ℃, the ranges of output TCC and E SHR were not remarkably changed, so the changes in inlet air dry-bulb temperatures would not affect much the ranges of the output TCC and E SHR from the experimental TS-DXAC system when RH remained constant in Fig. 5.6. The shapes of the irregular areas at different inlet air dry-bulb temperatures were similar, although their positons were shifted.

Fig. 5.7 shows that the high-low ranges for output TCC were increased and that of E SHR decreased, with an increase in RH. However, when RH was increased, the output LCC from the experimental TS-DXAC system was increased significantly, but its output SCC did not change much. As a result, E SHR values were decreased significantly. In addition, the curvatures of borderlines AB and CDE became increasingly obvious and slopes for curves BC and AE were decreased, with an increase in RH. This suggested that TCC was influenced more than E SHR when changing R_a or R_r at a higher RH. Unlike the results in the constant RH group, at a constant T_{db} of 26 ℃, as inlet air RH was changed from 40% to 60%, not only the positions but also the shapes of these irregular areas were changed, suggesting that the changes in RH influenced more on the inherent operational characteristics of the experimental TS-DXAC system those that in T_{db}.

5.4 Discussions

As presented in Sections 5.2 and 5.3, the use of the novel TS-DXAC system could achieve different combinations of output TCC and E SHR, by merely varying the values of R_a and R_r. Therefore, it became possible for the TS-DXAC system to deal with different latent space cooling loads and SCLs, to simultaneously control T_i and RH_i. For this experimental TS-DXAC system, although a constant speed of the compressor was used, unlike a conventional DX A/C system, variable cooling and dehumidification capacities could still be provided. Hence, it was reasonable to expect that a TS-DXAC system when it was variable speed operated would have an even wider variation range of output cooling and dehumidification capacity. Furthermore, the experimental results demonstrated that for the TS-DXAC system, a higher R_r would lead to a higher TCC and a lower R_a a lower E SHR.

5.5 Conclusions

In this Chapter, the inherent operational characteristics of the experimental TS-DXAC system were experimentally studied. In the TS-DXAC system, the compressor speed and the total air flow rate were constant, but the mass flow rates for both refrigerant and air to the two sections may be varied.

The experimental results showed that by varying R_a and R_r values, different combinations of TCC and E SHR were obtained. The output TCC and E SHR values were strongly correlated but mutually constrained in an irregular area in a TCC - E SHR diagram. Under a fixed inlet air state of 26 ℃ and 50% RH, at a constant R_r, varying

R_a impacted more on the E SHR, and at a constant R_a, varying R_r impacted more on the output TCC. Moreover, a larger R_r, and a lower R_a, would lead to a higher TCC and a lower E SHR, and vice versa. In addition, inlet air states also impacted the inherent operational characteristics of the experimental TS-DXAC system, resulting in the changes in both the shape and positon of an irregular area for the relationship of TCC - E SHR in a TCC - E SHR diagram, and the variations in inlet air RH would influence more on the shapes and positions of the irregular areas.

However, in the experimental study presented in this Chapter, given its nature, the configurations and specifications for the experimental TS-DXAC system, such as the surface ratio of the two sections of the cooling coil, were all fixed. Therefore, for further optimizing the configurations of the experimental TS-DXAC system, and studying its operating characteristics at other non-experimental conditions, it became highly necessary to develop a steady-state physical-based mathematical model for the experimental TS-DXAC system, which will be reported in Chapter 6.

Chapter 6

Development of a steady-state mathematical model for the experimental TS-DXAC system

6.1 Introduction

In Chapter 5, the experimental results for the inherent operational characteristics of the experimental TS-DXAC system are presented. For the experimental study presented in Chapter 5, given the nature of an experimental study, the configurations for the experimental TS-DXAC system were fixed, such as the surface ratio for HX1 and HX2 being at about 1:1.5, and the experimental conditions limited. However, different system configurations could have great influences on the operational characteristics of the experimental TS-DXAC system. On the other hand, as reported in Chapter 2, mathematical modeling has been widely used for optimizing the configurations of A/C systems including DX A/C systems [Sami, 1993; Sami and Zhou, 1995]. Therefore, to enable studying the operational characteristics of a TS-DXAC system with different configurations, a steady-state physical-based mathematical model for the experimental TS-DXACA system should be developed.

In this Chapter, therefore, the development of a steady-state physical-based model for the experimental TS-DXAC system, which was based on the previously developed sub-models of DX A/C systems detailed in Section 2.5 of Chapter 2, is presented. Firstly, the development and experimental validation of the steady-state model for the experimental TS-DXAC system are reported. Secondly, the results of a numerical study on the ratio of surface areas of the two sections of the cooling coil in the experimental

TS-DXAC system using the validated model are presented. Finally, conclusions are given.

6.2 The steady-state mathematical model for the TS-DXAC system

A conceptual diagram for the novel TS-DXAC system is shown in Fig. 5.1. In Fig. 6.1, for the purpose of developing the mathematical model, a modified conceptual diagram showing the numbered key locations on the refrigerant side of the experimental TS-DXAC system is shown. Furthermore, a conceptual model for the experimental TS-DXAC system, with the numbered key locations corresponding to those in Fig. 6.1, is illustrated in Fig. 6.2.

The model developed was made of a number of steady-state sub-models for key system components, such as compressor, condenser, two sections of the cooling coil, and EEVs, etc. These sub-models were similar to those developed by Pan et al. [2012] and Chen and Deng [2006], and were already used in a modeling study for the EDAC system [Chen et al., 2018b]. Hence, those sub-models [Pan et al., 2012] and [Chen and Deng, 2006] were also directly used in the developed model for the experimental TS-DXAC system.

As seen in the conceptual model shown in Fig. 6.2, actually these sub-models were systematically linked by the refrigerant flow on the refrigerant side, and the outputs from one sub-model were the inputs to the next sub-model connected. For example, the outputs from the sub-model of compressor, such as the refrigrant mass flow rate and the enthalpy and pressure of refrigerant, were used as the inputs to condenser sub-model.

In addition, the equations for the thermal properties of refrigerant R410A were obtained from Refprop [Lemmon et al., 2010] and the State Equations for humid air from ASHRAE Handbook [ASHRAE, 2009].

Furthermore, in this model, the assumptions and boundary conditions were as follows:

On the refrigerant-side of the experimental TS-DXAC system:

- A fixed setting of degree of refrigerant sub-cooling, T_{sc}, at 5 ℃;
- A constant *DS* at compressor suction, at 7 ℃;
- Isenthalpic expansion in the EEVs.

On the air-side of the experimental TS-DXAC system:

- The air streams passing through HX1 and HX2 were well mixed;
- The air mixing process was adiabatic;
- Counter-flow heat exchange between air and refrigerant in HX1 and HX2 was assumed.

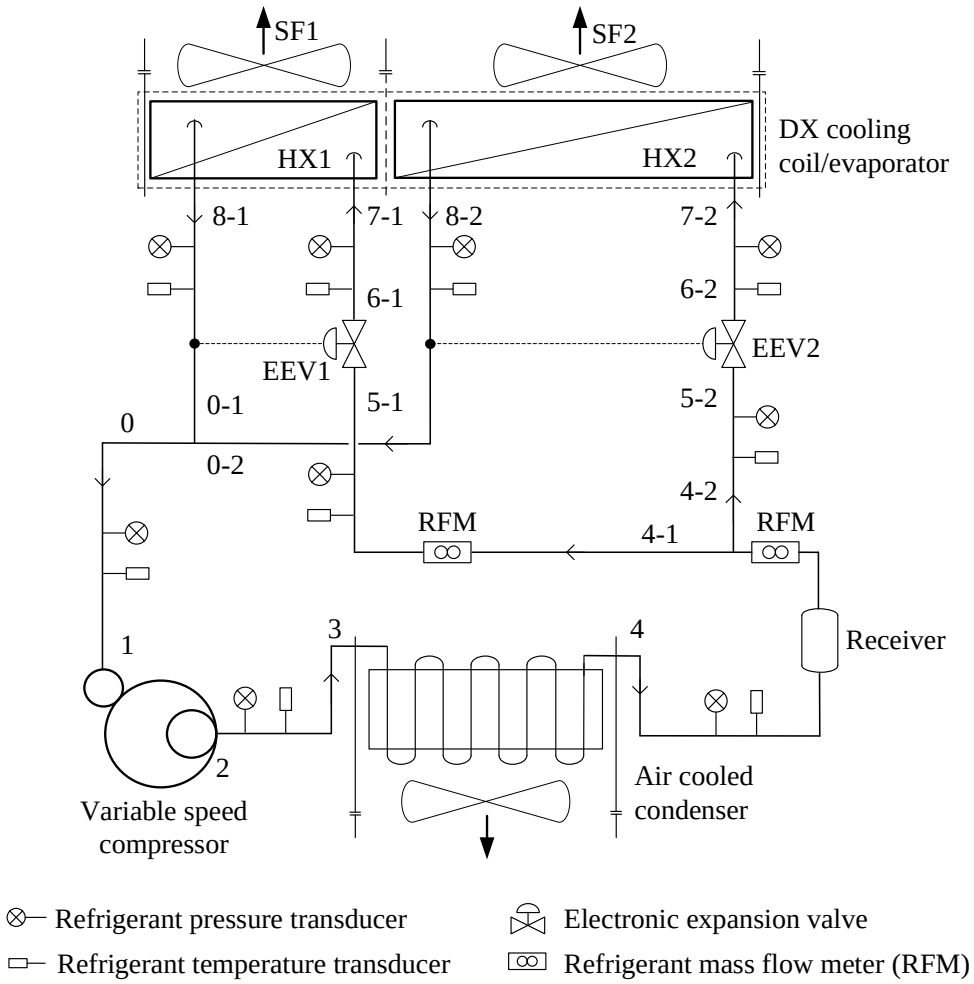

Fig. 6.1 A revised conceptual diagram of a TS-DXAC system

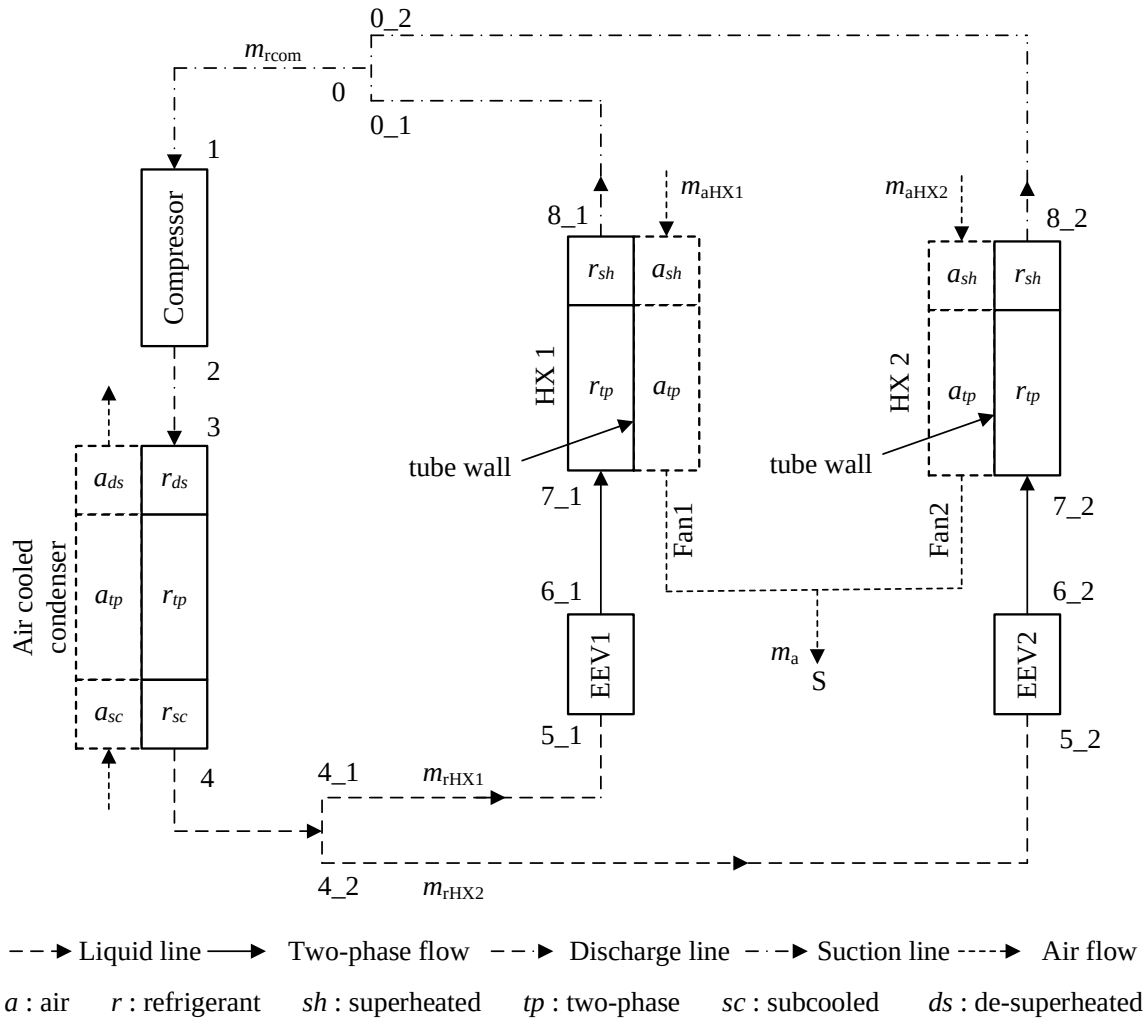

Fig. 6.2 A conceptual model for the experimental TS-DXAC system

Although the model of the experimental TS-DXAC system was developed by referring to the previously developed sub-models, for the completeness of this thesis, the equations for the sub-models of the key system components were given as follows. In all equations in this Section, for better illustration, the numbers in the subscript correspond to those shown in Fig. 6.2.

6.2.1 Sub-model for compressor

An isentropic compression process and quasi-steady conditions for the compressor were assumed. The compressor was modeled based on the principle of energy and mass balance. The refrigerant mass flow rate of the compressor was calculated by:

$$m_{com} = \eta \frac{V_{com}}{v_{r1}} \tag{6.1}$$

where V_{com} is the refrigerant theoretical volumetric flow rate; v_{r1} the refrigerant specfic volume at compressor suction; η the overall displacement coefficient, determined by:

$$\eta = \eta_v \eta_p \eta_t \eta_l \tag{6.2}$$

where η_p is the pressure loss coefficient with an approximate value of 1.0; η_l the leakage coefficient, 0.92~0.98; η_v the compressor volumetric coefficient, given by:

$$\eta_v = 1 - 0.015 \times \left[\left(P_{r2} / P_{r1} \right)^{1/n} - 1 \right] \tag{6.3}$$

where n is the polytropic index of compression.

The temperature coefficient, η_t, was evaluated by:

$$\eta_t = 0.00257\left(T_c + 273.15\right) + 0.00106(T_{r1} - T_e) \tag{6.4}$$

where T_c is the condensing temperature; T_e the evaporating temperature.

The theoretical isentropic work done by the compressor, W, was given by:

$$W = \nu_{r1} P_{r1} n/\left(n-1\right)\left[\left(P_{r2}/P_{r1}\right)^{\text{n-1/n}} - 1\right] \tag{6.5}$$

The indicated coefficient, η_i, was evaluated by:

$$\eta_i = \eta_t \eta_l \Bigg/ \left(1 + \frac{1.5\Delta P_{dm}(\mathrm{P_{r2}}/\mathrm{P_{r1}})^{1/n}}{(h_{r2} - h_{r1})/v_{r1}}\right) \tag{6.6}$$

where ΔP_{dm} is the compressor discharge pressure loss, and was evaluated by:

$$\Delta P_{dm} = 25(T_c - 273.15)^{-1.01} 10^{-0.15\mathrm{P_{r2}}/\mathrm{P_{r1}}} \tag{6.7}$$

The enthalpy of the vapor refrigerant leaving the compressor, h_{r2}, was evaluated by:

$$h_{r2} = h_{r1} + W/\eta_i \tag{6.8}$$

6.2.2 Sub-model for EEVs

The refrigerant mass flow rate passing through an EEV could be represented by an orifice equation. Although there were two EEVs in the experimental TS-DXAC system, the modeling for the two EEVs was the same. Therefore, only the modeling for EEV1 was detailed in this section, and EEV2 may be similarly modelled.

For EEV1, its mass flow rate, $m_{r,EEV1}$, was calculated by:

$$m_{r,EEV1} = C_{d,EEV1} A_{EEV1} \sqrt{2\rho_{r5\_1}(P_{r5\_1} - P_{r6\_1})} \tag{6.9}$$

where A_{EEV1} is the opening of EEV1; $C_{d,EEV1}$, the flow coefficient of the EEV1, given by

$$C_{d,EEV1} = 0.02005\sqrt{\rho_{r5\_1}} + 6.34 v_{r6\_1} \tag{6.10}$$

6.2.3 Sub-model for evaporator

In the experimental TS-DXAC system, a DX evaporator of louver-fin-tube type was used, where counter-flow heat exchange between the refrigerant and air may be assumed. The DX evaporator was divided into two parts, HX1 and HX2, both functioning like an evaporator and the modeling for both HX1 and HX2 was the same. Therefore, in the section, only the modeling for HX1 is detailed and that of HX2 can be carried out in the same way as that for HX1.

For HX1, its refrigerant side was divided into a two-phase region and a superheated region. Furthermore, in the two-phase region, dry-cooling and wet-cooling conditions on the air side were separately modeled.

6.2.3.1 Refrigerant side in the two-phase region

The heat transfer between the two-phase refrigerant and the tube wall was evaluated as:

$$Q_{r,HX1,tp} = \alpha_{r,HX1,tp} A_{r,HX1,tp} \Delta T_{r,HX1,tp} \tag{6.11}$$

where $A_{r,HX1,tp}$ is the internal heat transfer area in the two-phase region; $\Delta T_{r,HX1,tp}$ the temperature difference between the average temperature of the refrigerant and that of the tube; $\alpha_{r,HX1,tp}$ the α (convective heat transfer coefficient) on the refrigerant side, determined by:

$$\alpha_{r,HX1,tp} = \left\{ X_1 X_0{}^{X_2} (25 Fr_r)^{X_5} + 2 X_3 B_0{}^{X_4} \right\} \alpha_{r,l} \tag{6.12}$$

where the assumed α for liquid refrigerant in the two-phase region, $\alpha_{r,l}$, was calculated by:

$$\alpha_{r,l} = 0.023 \left[\frac{g_r (1 - x_e) D_{i,HX1}}{\mu_{r,l}} \right]^{0.8} \frac{Pr_{r,l}{}^{0.4} \lambda_r}{D_{i,HX1}} \tag{6.13}$$

where g_r is the refrigerant mass flux; χ_e the refrigerant dryness fraction; $D_{i,HX1}$ the inside diameter of the tube; $\mu_{r,l}$ the dynamic viscosity of the liquid refrigerant; λ_r the refrigerant thermal conductivity.

The refrigerant convection characteristic number, X_0, was:

$$X_0 = \left(\frac{1-\chi_e}{\chi_e}\right)^{0.8}\left(\frac{\rho_{r,v}}{\rho_{r,l}}\right) \tag{6.14}$$

where $\rho_{r,v}$ is the density of vapor refrigerant; $\rho_{r,l}$ the density of liquid refrigerant. For the constant X_1 to X_5 in Eq. (6.12),

when $X_o \leq 0.65$, $X_1 = 1.1360$, $X_2 = -0.9$, $X_3 = 667.2$, $X_4 = 0.7$, $X_5 = 0.30$; and

when $X_o > 0.65$, $X_1 = 0.6683$, $X_2 = -0.2$, $X_3 = 1058.0$, $X_4 = 0.7$, $X_5 = 0.30$.

The refrigerant *Froude* number, Fr_r, was given by:

$$Fr_r = \frac{g_r^{\,2}}{9.8\rho_{r,l}^{\,2}D_{i,HX1}} \tag{6.15}$$

The refrigerant boiling characteristic number, B_o, was:

$$B_o = \frac{q_{r,tp}}{g_r\gamma_e} \tag{6.16}$$

where $q_{r,tp}$ is the heat flux in the two-phase region; γ_e the refrigerant latent heat of vaporization.

6.2.3.2 Refrigerant side in the superheated region

The heat transfer between superheated refrigerant and the tube wall in the superheated region was given as:

$$Q_{r,HX1,sh} = \alpha_{r,HX1,sh} A_{r,HX1,sh} LMTD_{r,HX1,sh} \tag{6.17}$$

where $A_{r,HX1,sh}$ is the internal transfer area in the superheated region; $LMTD_{r,HX1,sh}$ the log mean temperature difference(LMTD) between the superheated refrigerant and the tube; the α for vapor refrigerant, $\alpha_{r,HX1,sh}$, was evaluated by:

$$\alpha_{r,HX1,sh} = \frac{0.23\lambda_r}{D_{i,HX1}} Re_{r,sh}^{0.8} Pr_{r,sh}^{0.4} \tag{6.18}$$

6.2.3.3 Air side

On the air side of both the superheated region and two-phase region, dry-cooling of air occurred when the tube-fin surface temperature was above the dew point temperature of air entering the respective region; otherwise, wet-cooling of air occurred. In this Section, the modeling of dry-cooling and wet-cooling of air in the two-phase region of HX1 is presented separately, while the modeling of the air side in the superheated region might be similarly treated, and no more details would be provided.

a) Wet-cooling

The heat transfer between air and the tube-fin surface could be expressed as:

$$Q_{a,HX1,wt} = U_{a,HX1,wt} A_{a,HX1,tp} LMTD_{a,HX1,wt} \tag{6.19}$$

where $A_{a,HX1,tp}$ is the air side heat transfer area; $LMTD_{a,HX1,wt}$ the LMTD between the tube-fin and air; the overall heat transfer coefficient, $U_{a,HX1,wt}$, is:

$$U_{a,HX1,wt} = \frac{1}{\frac{1}{\alpha_{a,HX1,wt} \zeta_a \eta_{a,HX1,wt}} + R_{HX1}} \tag{6.20}$$

where R_{HX1} is the combined total thermal resistance from the evaporator tube wall, surface contact and fouling; ζ_a the dehumidifying factor; $\eta_{a,HX1,wt}$ the fin surface efficiency under wet-cooling conditions; $\alpha_{a,HX1,wt}$ the theoretical sensible α for the cooling coil under wet-cooling conditions.

b) Dry-cooling

The heat transfer between air and tube-fin metal in HX1 could be expressed as:

$$Q_{a,HX1,dr} = U_{a,HX1,dr} A_{a,HX1,tp} LMTD_{a,HX1,dr} \tag{6.21}$$

where the overall heat transfer coefficient, $U_{a,HX1,dr}$, is:

$$U_{a,HX1,dr} = \frac{1}{\frac{1}{\alpha_{a,HX1,dr}\eta_{a,HX1,dr}} + R_{HX1}} \tag{6.22}$$

where $\eta_{a,HX1,dr}$ is the fin surface efficiency under dry-cooling conditions; $\alpha_{a,HX1,dr}$ the theoretical sensible α for the louver-finned cooling coil under dry-cooling conditions.

6.2.3.4 Energy equation

The energy balance equation between the air side and the refrigerant side of HX1 could be expressed as:

$$m_{a,HX1}\left(h_{a,i,HX1} - h_{a,o,HX1}\right) = m_{r,HX1}\left(h_{r,o,HX1} - h_{r,i,HX1}\right) \tag{6.23}$$

where $m_{a,HX1}$ and $m_{r,HX1}$ are the air and refrigerant mass flow rates to HX1, respectively, $h_{a,i,HX1}$ and $h_{r,i,HX1}$ inlet air and refrigerant enthalpy to HX1, respectively, $h_{a,o,HX1}$ and $h_{r,o,HX1}$ outlet air and refrigerant enthalpy from HX1, respectively;

6.2.4 Sub-model for condenser

According to the refrigerant's state, the condenser was divided into three regions, i.e., a de-superheating region, a two-phase region and a sub-cooling region. The modeling processes in the de-superheating and the two-phase regions of the condenser on refrigerant side were similar to that in the superheated and two-phase regions of HX1.

The heat transfer equations for the air side of the condenser were similar to those on the air side of HX1 under a dry-cooling condition.

6.2.4.1 Refrigerant side of de-superheating region

The heat transfer in the de-superheating region in the condenser could be evaluated by:

$$Q_{r,c,ds} = \alpha_{r,c,ds} A_{r,c,ds} LMTD_{r,c,ds} \tag{6.24}$$

where $A_{r,c,ds}$ is the internal heat transfer area in the de-superheating region; $LMTD_{r,c,ds}$ the LMTD between the de-superheating refrigerant and the tube; $\alpha_{r,c,ds}$ the α in the de-superheating region, calculated by:

$$\alpha_{r,c,ds} = \lambda_r \times \frac{Nu_{r,ds}}{D_{i,c}} \tag{6.25}$$

where λ_r is the thermal conductivity of refrigerant;

The *Nusselt* number was:

$$Nu_{r,ds} = 0.023 Re_{ds}^{0.8} Pr_{ds}^{0.3} \tag{6.26}$$

6.2.4.2 Refrigerant side of two-phase region

The heat transfer in the two-phase region in the condenser, $Q_{r,c,tp}$, was calculated by:

$$Q_{r,c,tp} = \alpha_{r,c,tp} A_{r,c,tp} \Delta T_{r,c,tp} \tag{6.27}$$

where $A_{r,c,tp}$ is the internal heat transfer area in the two-phase region; $\Delta T_{r,c,tp}$ the temperature difference between the average temperature of the refrigerant and that of the tube.

The corresponding α, $\alpha_{r,c,tp}$, could be expressed by:

$$\alpha_{r,c,tp} = \alpha_{r,c,l} \left[\left(1-\chi_c\right)^{0.8} + \frac{3.8\chi_c^{0.76}\left(1-\chi_c\right)^{0.04}}{Pr^{0.38}} \right] \tag{6.28}$$

where $\alpha_{r,c,l}$ is the α in the liquid phase; χ_c the refrigerant dryness fraction in the two-phase region.

6.2.4.3 Refrigerant side of sub-cooling region

The heat transfer in the sub-cooling region in the condenser was calculated as:

$$Q_{r,c,sc} = \alpha_{r,c,sc} A_{r,c,sc} LMTD_{r,c,sc} \tag{6.29}$$

where $A_{r,c,sc}$ is the internal heat transfer area in the sub-cooling region; $LMTD_{r,c,sc}$ the LMTD between the sub-cooling refrigerant and the tube; $\alpha_{r,c,sc}$, the α for the sub-cooled liquid refrigerant, calculated by:

$$\alpha_{r,c,sc} = \lambda_r \times \frac{Nu_{r,sc}}{D_{i,c}} \tag{6.30}$$

The *Nusselt* number was:

$$Nu_{r,sc} = 0.023 Re_{sc}^{0.8} Pr_{sc}^{0.3} \tag{6.31}$$

6.2.4.4 Air side

Since in a condenser the moisture content of cooling air forced across the condenser remained unchanged, it was assumed that the same overall heat transfer coefficient, $U_{a,c}$, between the tube-fin and cooling air was applied to all the regions in the condenser, and the heat transfer between air and tube-fin metal could be expressed as:

$$Q_{a,c} = U_{a,c} A_{a,c} LMTD_{a,c} \tag{6.32}$$

where $A_{a,c}$ is the external heat transfer area of the condenser; $LMTD_{a,c}$ the LMTD between the tube and air; $U_{a,c}$, the overall heat transfer coefficient, calculated by:

$$U_{a,c} = \frac{1}{\frac{1}{\alpha_{a,c}\eta_{a,c}} + R_c} \tag{6.33}$$

where R_c is the combined total thermal resistance from the tube wall, surface contact and fouling; $\eta_{a,c}$ the fin surface coefficient of the condenser tube-fin and air; $\alpha_{a,c}$ the air heat transfer coefficient for forced convection.

6.2.4.5 Energy balance equation

The energy balance equation between the air side and the refrigerant side of the condenser could be expressed as:

$$m_{a,c}\left(h_{a,o,c} - h_{a,i,c}\right) = m_{r,c}\left(h_{r,i,c} - h_{r,o,c}\right) \tag{6.34}$$

where $m_{a,c}$ and $m_{r,c}$ are the air and refrigerant mass flow rates to the condenser, respectively, $h_{a,i,c}$ and $h_{r,i,c}$ inlet air and refrigerant enthalpy to the condenser, respectively, $h_{a,o,c}$ and $h_{r,o,c}$ outlet air and refrigerant enthalpy from the condenser, respectively;

6.2.5 Calculation procedure of the complete experimental TS-DXAC system model

The flow chart for solving the complete experimental TS-DXAC system model is shown in Fig. 6.3. Five iteration loops existed when solving the model. The first one (Loop I) was for evaluating the compressor discharge pressure, P_{r2}, by solving the

compressor sub-model. The second and third loops (Loop II and Loop III) were for calculating refrigerant mass flow rates passing through HX1 and HX2, m_{rHX1} and m_{rHX2}, respectively. The fourth and fifth loops (Loop IV and Loop V) were used to obtain refrigerant pressure and enthalpy at compressor suction, P_{r1} and h_{r1}, respectively. Detailed explanations for calculation procedures are as follows:

Before running the model, system configuration details such as the surface areas of HX1 and HX2, compressor displacement and other initial operating parameters including the opening degrees for EEV1 and EEV2, inlet air temperature and relative humidity, $T_{a,i}$ and RH, the degree of refrigerant sub-cooling, T_{sc}, were input to the model. Also the initial values of refrigerant enthalpy at compressor suction, h_{r1}, refrigerant pressures at compressor suction and discharge, P_{r1} and P_{r2}, were assumed.

The calculation procedures were started from solving the sub-model of compressor with the assumed initial values of h_{r1}, P_{r1}, P_{r2}, to obtain the total refrigerant mass flow rate, m_{rcom}. Meanwhile, the refrigerant pressure at compressor suction, or P_{r0}, could also be obtained by solving the pressure drop equations for pipelines. Afterwards, by solving the condenser sub-model, the degree of refrigerant sub-cooling at condenser outlet, T_{sc}', could be evaluated and was compared with its initial setting T_{sc}, with the difference between the two to decide if the calculation in this iterative loop should be ended or otherwise continued by updating the initial value of P_{r2} until the difference was less than a preset value.

After ending the calculations in Loop I, the calculations in Loop II and Loop III were started, by assuming the initial values of m_{rHX1} and m_{rHX2}. By solving the sub-models

for HX1, HX2 and their matching EEVs, the refrigerant pressures at the end of the respective branch for HX1 and HX2, P_{r0_1} and P_{r0_2}, could be obtained. Since two branches were in parallel and connected to the suction of a common compressor, the values of P_{r0_1} and P_{r0_2} should be same and further equal to P_{r0} by adjusting the assumed values of m_{rHX1} and m_{rHX2}. In addition, m_{rcom}', which was the sum of m_{rHX1} and m_{rHX2}, should also be equal to the initially assumed m_{rcom} and the difference between m_{rcom}' and m_{rcom} was used to either end the iterative calculation process of Loop IV, or update a new initial value of P_{r1}. During this procedure, certain key parameters on the air-sides of HX1 and HX2, such as supply air temperature and enthalpy, $T_{a,o}$, $h_{a,o}$, could also be obtained by solving the sub-models for the air-sides of HX1 and HX2.

After the calculations of Loop IV were ended, the refrigerant enthalpy at compressor suction, h_{r1}' was obtained by solving the sub-model for mixing the refrigerant from the two branches. The iterative calculation process in Loop V was ended until the difference between h_{r1}' and h_{r1} was within a preset range, or a new value of h_{r1} was assumed. When all iterative calculations were ended, the calculation process for solving the complete model of the experimental TS-DXAC system was finished.

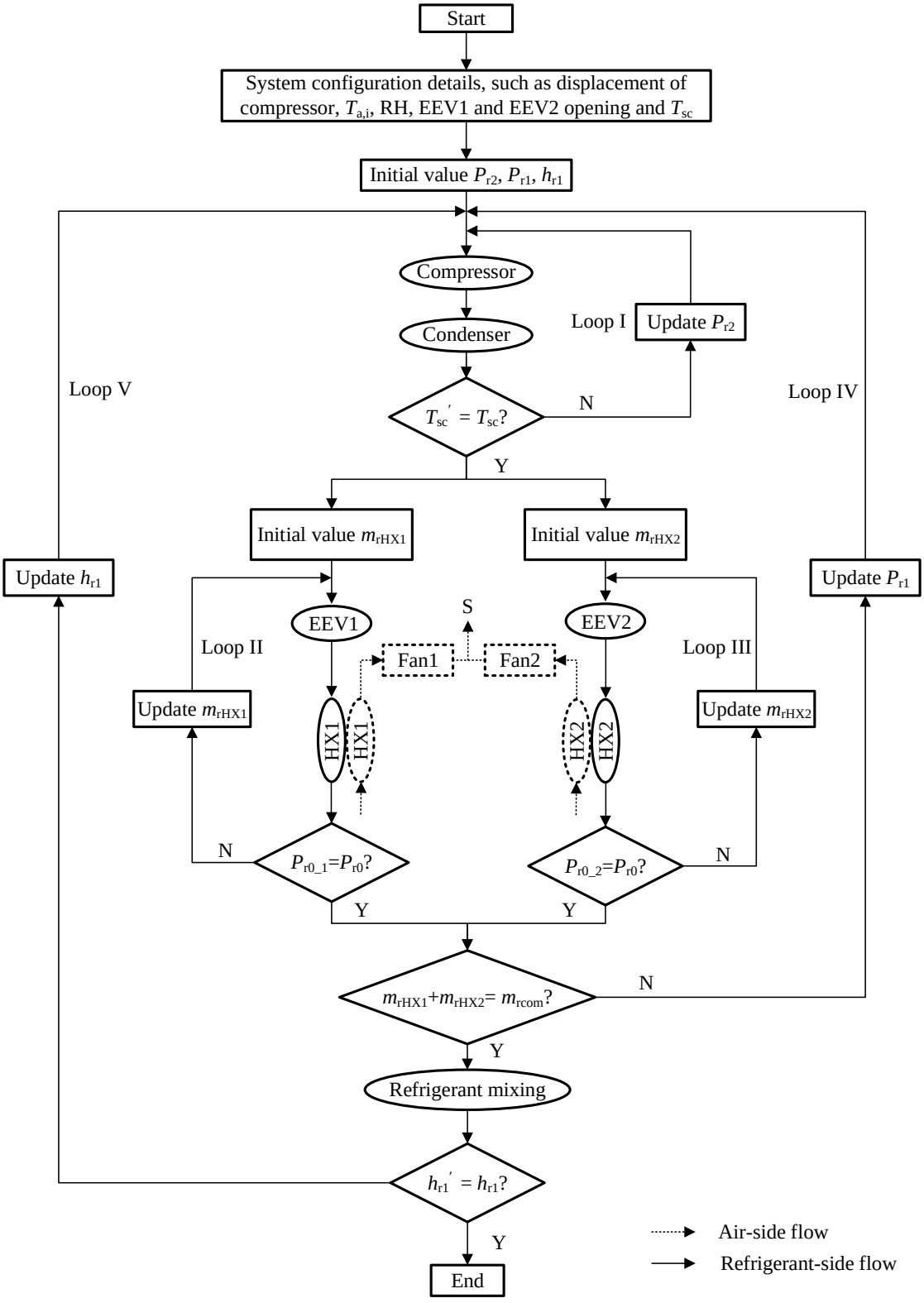

Fig. 6.3 Flow chart of the calculation procedure of the complete experimental TS-DXAC system model

6.3 Experimental validation of the developed mathematical model

The parameters of output TCC and E SHR of a DX A/C system were commonly used to represent its operational characteristics [Xu et al., 2010], since they could reflect its overall cooling and dehumidification ability. Therefore, in this Chapter, output TCC and E SHR values predicted by the developed model for the experimental TS-DXAC system were compared with the experimental results of output TCC and E SHR values reported in Chapter 5 for the purpose of validating the developed mathematical mode.

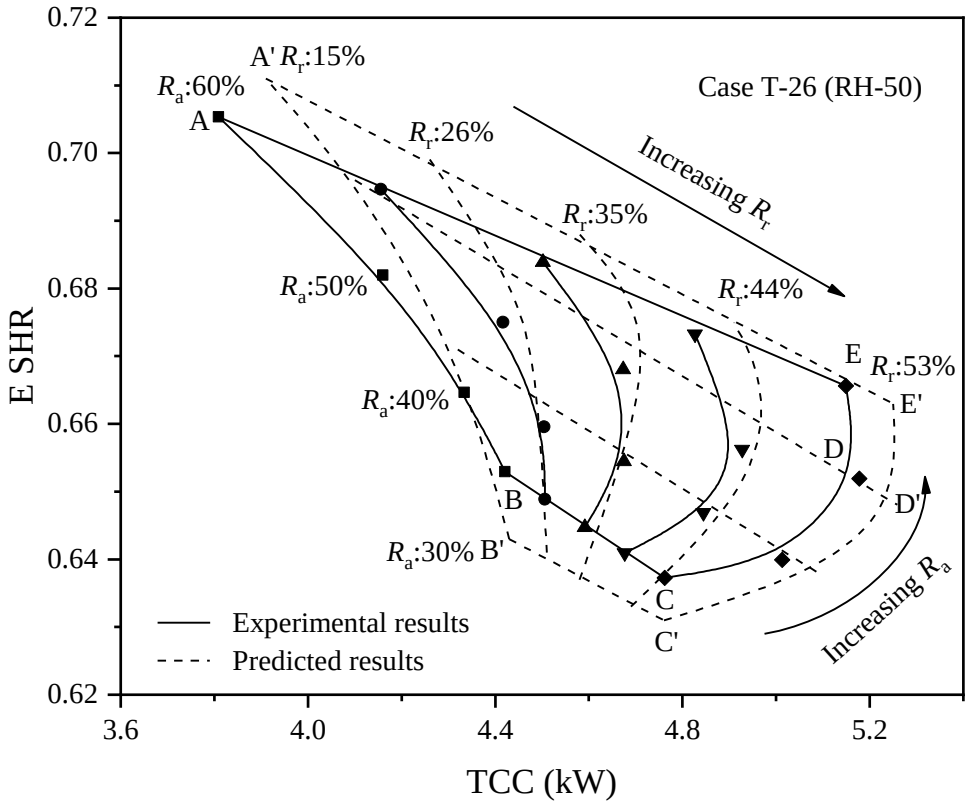

Fig. 6.4 Comparison of the experimental and predicted output TCC and E SHR values at the inlet air state of 26 °C and 50% RH

Fig. 6.4 shows the comparisons between the experimental results and the corresponding model predicted TCC / E SHR relationships plotted in a TCC - E SHR diagram at the inlet air state of 26 ℃ and 50% RH with the combinations of R_a (from 30% to 60%) and R_r (from 15% to 53%) shown in Table 5.2. As seen, both experimental and predicted relationships demonstrated that the values of TCC / E SHR were mutually constrained within two irregular areas of ABCDE (experimental) and A′B′C′D′E′ (predicted). For the two irregular areas, Points A (A′), B (B′), E (E′) and C (C′) correspond to the experimental (predicted) output TCC / E SHR values when the experimental TS-DXAC system was operated at its highest R_a values of 60% and lowest R_r value of 15%, lowest R_a values of 30% and lowest R_r value of 15%, highest R_a values of 60% and highest R_r value of 53%, and lowest R_a values of 30% and highest R_r value of 53%, respectively. Points D (D′) correspond to the experimental (predicted) output TCC / E SHR values with the maximum output TCC from the experimental TS-DXAC system. Therefore, both the experimental and predicted TCC / E SHR relationships shown in Fig. 6.4 demonstrated that the experimental TS-DXAC system can output variable TCC and E SHR to deal with variable space loads, by varying R_a and R_r values.

As seen from Fig. 6.4, the shapes of the two irregular areas, ABCDE and A′B′C′D′E′ were similar to each other. At a constant R_a, when R_r was increased from 15% to 53%, both the experimental and predicted values of TCC were increased, and both E SHR values decreased. At a fixed R_r, when R_a was increased from 30% to 60%, both the experimental and predicted values of E SHR were increased, and both TCC values experienced similar variation trends of increasing, peaking and decreasing when R_r was greater than 35%, but were decreased continuously when R_r was less than 35%. It can also be found from Fig. 6.4 that the maximum error between predicted and experimental

output TCC values at each R_a / R_r combination was only at 2.6% and that for E SHR at 2.1%, respectively. The predicting accuracy of the developed model was further confirmed by comparing the predicted and experimental output TCC / E SHR values at all the five inlet air temperatures and humidity levels shown in Table 5.1 and the combinations of R_a (from 30% to 60%) and R_r (from 15% to 53%) shown in Table 5.2. Fig. 6.5 shows the comparisons between the experimental and predicted results for TCC values and Fig. 6.6 that for E SHR values, respectively. As seen, the relative errors between the experimental and predicted values for both TCC and E SHR were all within 6%.

From the above comparison results, the steady-state model developed for the experimental TS-DXAC system was experimentally validated and could be further used to predict its operational characteristics in terms of the relationship between TCC and E SHR with an acceptable accuracy. Therefore, the validation model was used in a modeling study to optimize the sizes of the two sections in the cooling coil in a TS-DXAC system.

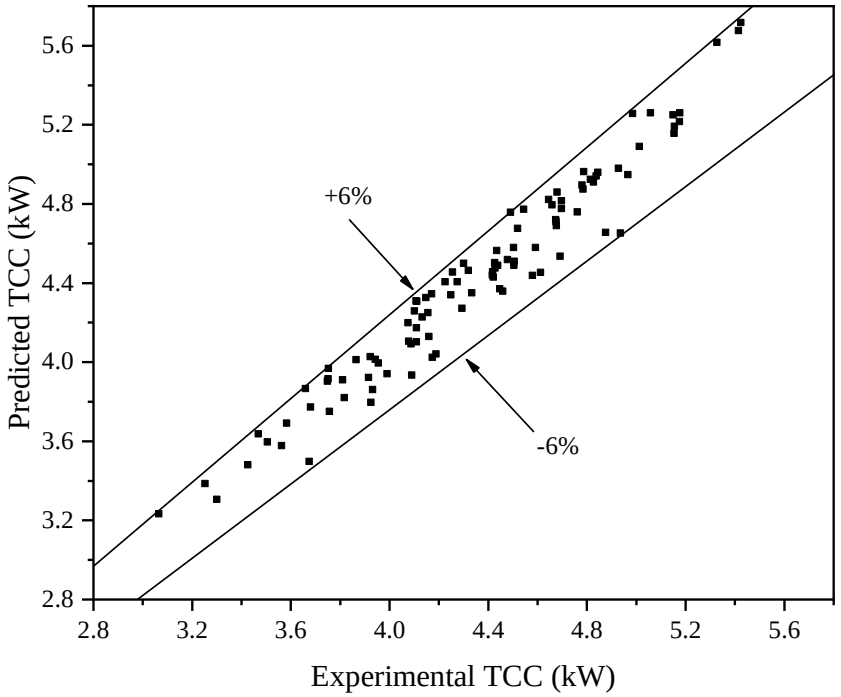

Fig. 6.5 Relative errors between experimental and predicted TCC values at five different inlet air temperatures and humidity levels

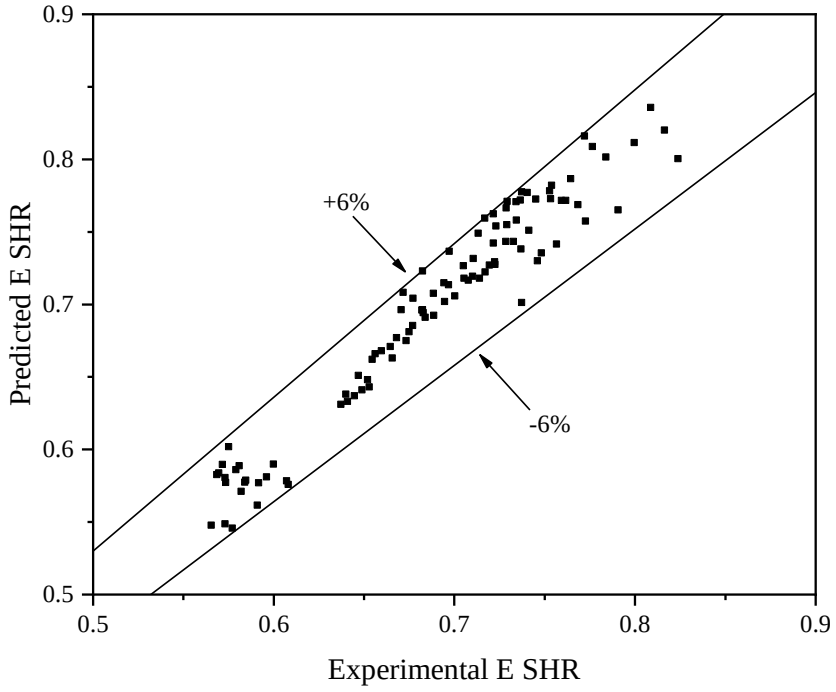

Fig. 6.6 Relative errors between the experimental and predicted E SHR values at five different inlet air temperatures and humidity levels

6.4 The modeling study

For a TS-DXAC system, the relative size for the two sections of the cooling coil, HX1 and HX2, was a key factor that could affect its overall operational characteristics. Hence, it was necessary to study the impacts of different ratios of the two sections on the operational characteristics of the TS-DXAC system. This was numerically studied using the validated model, and the study results are reported in this section.

The ratio of surface areas for the two sections (R_s) in the TS-DXAC system was defined by

$$R_s = A_{HX1} / A_{HX2} \tag{6.35}$$

where A_{HX1} is the HX1's surface area, and A_{HX2} the HX2's surface area.

Fig. 6.7 shows the simulated operational characteristics of the TS-DXAC system in terms of the relationships between output TCC and E SHR at the combinations of R_a (from 30% to 60%) and R_r (from 15% to 53%) shown in Table 5.2, at five different R_s values of 1:3, 2:5, 1:2, 2:3 and 1:1. The inlet air state were fixed at 26 ℃ and 50% RH.

The irregular areas of A′B′C′D′, ABCD and A″B″C″D″ shown in Fig. 6.7 represent the modeling study of the output TCC / E SHR relationships for the TS-DXAC system at three R_s values of 1:1, 2:3 and 1:3, respectively. It can be seen that the shapes of these irregular areas were varied significantly at different R_s values. The high limits of TCC values stayed almost unchanged at 5.27 kW. However, the low limits of TCC values

were increased from 3.61 kW at R_s of 1:3 to 4.02 kW at R_s of 1:1, reflecting a 33% increase in the high-low ranges for output TCC from 1.25 kW at R_s of 1:1 to 1.66 kW at R_s of 1:3. On the other hand, the high limits of E SHR values were decreased from 0.727 at R_s of 1:3 to 0.706 at R_s of 1:1, and the low limit was decreased from 0.636 at R_s of 1:1 to 0.621 at R_s of 1:3. Hence, the high-low ranges for E SHR were significantly increased by 51% from 0.07 at R_s of 1:1 to 0.106 at R_s of 1:3.

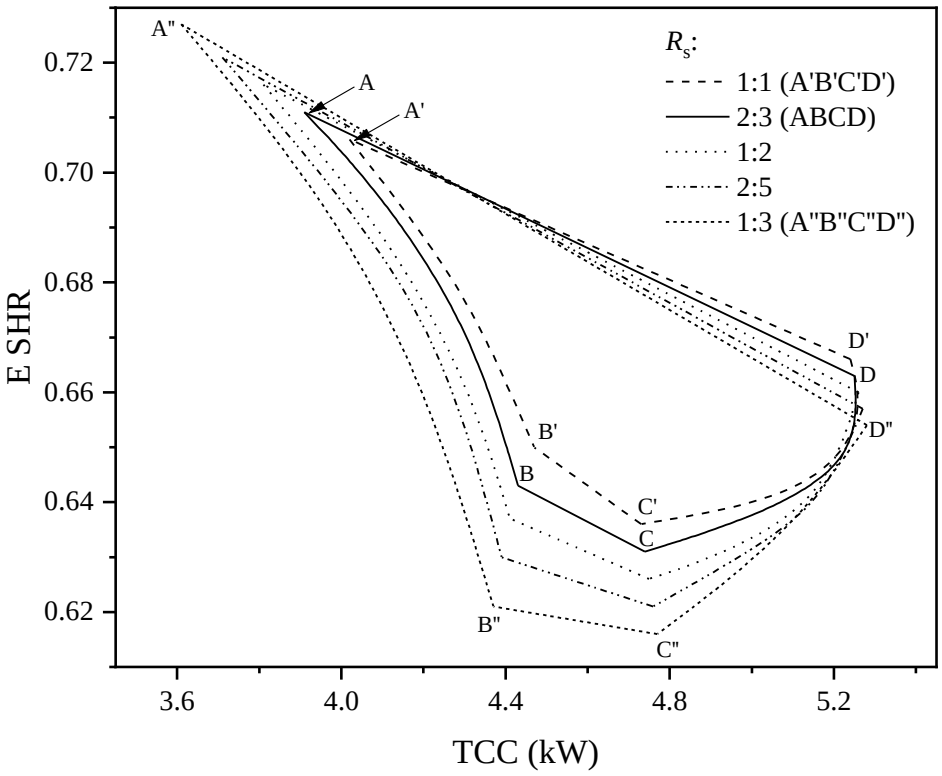

Fig. 6.7 The operational characteristics of the TS-DXAC system at different R_s values at a fixed inlet air state of 26 °C and 50% RH

Furthermore, different R_s values would also have different impacts on the operational characteristics in terms of the relationship between output TCC and E SHR of the TS-DXAC system when varying R_r and R_a. As seen from Fig. 6.7, since the curvatures of borderline C′D′ became more obvious than borderline C″D″ when increasing R_s value,

the changes in R_a at a higher R_s would impact more on output TCC values than E SHR values at a high R_r level. In addition, the slope of line B″C″ was smaller than that of line B′C′, suggesting that the changes in R_r at a higher R_s impacted more on E SHR values than TCC values at a low R_a level.

The above simulation results suggested that a lower R_s could help enlarge the variation ranges of output TCC and E SHR, which was beneficial to better dehumidification, and that the changes in R_s would influence more on E SHR than TCC. However, a low R_s would deteriorate the efficiency of the TS-DXAC system because the surface area of HX1 was too small to provide enough heat to evaporate the refrigerant passing through it. Therefore, the degree of refrigerant superheat at the exit of HX1 would become unreasonably low, but that at the exit of HX2 unreasonably high, thus maintaining a constant *DS* at compressor suction was difficult.

6.5 Conclusions

In this Chapter, based on previously developed sub-models for DX A/C systems, a steady-state physical-based mathematical model for the experimental TS-DXAC system was established. The model was further experimentally validated using the experimental data reported in Chapter 5, with differences between experimental and predicted results of less than 6%. Both the experimental and modeling results suggested that the experimental TS-DXAC system can output variable TCC and E SHR to deal with variable space loads.

With the availability of the validated experimental TS-DXAC system model, a follow-up modeling study on optimizing the sizes of the two sections was carried out. The modeling results demonstrated that a lower ratio for the surface areas of the two sections (R_s) could lead to enlarged variation ranges in both TCC and E SHR. For example, at the inlet state of 26 ℃ and 50% relative humidity, when R_s was altered from 1:1 to 1:3, the variation range for TCC was increased by 33%, and that for E SHR by 51%, which was beneficial to better dehumidification. In addition, the changes in R_s would influence more on E SHR than TCC. Further, with the validated model, the operational characteristics of the experimental TS-DXAC system at other inlet air states and system configurations may also be studied.

The experimental work reported in Chapter 5 and the modeling work reported in this Chapter enabled the better understandings of the experimental TS-DXAC system. Furthermore, in order to operate the experimental TS-DXAC system, a control strategy was needed. Therefore, in Chapter 7, the development of a control strategy for operating the experimental TS-DXAC system, and the controllability tests for the control strategy are reported.

Chapter 7

Development of a control strategy of the experimental TS-DXAC system for improved indoor thermal environmental control

7.1 Introduction

In Chapter 5, an experimental study on the operational characteristics of the experimental TS-DXAC system is reported, and in Chapter 6, a modeling study where a steady-state mathematical model for the TS-DXAC system was developed presented. Both the experimental and modeling studies enabled the better understandings of the experimental TS-DXAC system.

However, as mentioned in Chapter 3, the experimental TS-DXAC system was intended to be operated at different indoor conditions in buildings located in hot-humid climates. Therefore, in order to operate the experimental TS-DXAC system at all possible indoor conditions in hot-humid climates, in this Chapter, the development of a simple control strategy that enabled operating the experimental TS-DXAC system is reported. Firstly, the developed control strategy, which included two control algorithms, for the experimental TS-DXAC system is detailed. Secondly, using the experimental TS-DXAC system described in Chapter 4, two sets of experiments to test the controllability of the developed control strategy were carried out, and the controllability test results and their related analysis and discussion are presented. Finally, conclusions are given.

7.2 Development of the control strategy for the experimental TS-DXAC system

Although the TS-DXAC system was primarily developed for obtaining simultaneously control of T_i and RH_i at a hot and humid indoor condition, it was also possible that it may be operated at a hot- dry indoor condition. Therefore, the control strategy to be developed would also cover this hot and dry indoor condition. Hence, it would include two control algorithms, one for hot and humid indoor condition, as Algorithm I, and the other hot and dry indoor condition, as Algorithm II.

In this Section, the experimental results of the experimental TS-DXAC system obtained in the experimental study presented in Chapter 5, which were used as the basis for the development of Algorithm I, are briefly reviewed first, and then Algorithm I detailed. This is followed by discussing Algorithm II. Thirdly, with the availability of the two Algorithms, the developed control strategy for the experimental TS-DXAC system is detailed.

7.2.1 Algorithm I

The experimental results of the experimental TS-DXAC system obtained from the experimental study in Chapter 5 were used as the basis for developing Algorithm I. The experimental results shown in Fig. 5.1 suggested that at a fixed compressor speed, by varying R_a and R_r values, different combinations of TCC and E SHR could be obtained from the experimental TS-DXAC system, and these combinations were restricted within an irregular area. Furthermore, at the fixed inlet air state of 26 ℃ / 50% RH, at a constant R_r, E SHR was affected more by varying R_a, and at a constant R_a, the output

TCC was affected more by varying R_r. In addition, a higher TCC and a lower E SHR were obtained at a larger R_r and a lower R_a, and vice versa. Hence, it was experimentally proved that the experimental TS-DXAC system had an ability to output different SCC and LCC so as to handle different indoor space SCL and LCL. This has paved a way to develop Algorithm I to enable the experimental TS-DXAC system to be operated at a hot and humid indoor condition to control T_i and RH_i simultaneously.

Based on the experimental results of the experimental TS-DXAC system briefly discussed above, Algorithm I has been developed. For Algorithm I, a fixed compressor speed was used as these operational characteristics were obtained under a fixed compressor speed. SF1 and SF2 would respond to the change in RH_i, EEV1 to those in T_i and EEV2 to those in the *DS* of the experimental TS-DXAC system.

Fig. 7.1 shows the flowchart for Algorithm I. At first, the experimental TS-DXAC system would be operated at a high R_r value and low R_a value. For example, according to Table 5.2, R_r could be set at 44%, and R_a at 40%, respectively. This was because at a hot and humid indoor condition, both cooling and dehumidification were required. Then depending on the actual T_i and RH_i values, if they were within their respective dead-bands, no changes to the operation of the experimental TS-DXAC system would be introduced. Once T_i was lower than the low boundary of its dead-band, a lower R_r value would be used by reducing the opening degree of EEV1. Likewise, if RH_i was lower than the low boundary of its dead-band, a higher value of R_a would be used by increasing the fan speed of SF1. It can be seen that for Algorithm I, the values of R_a and R_r needed to be regularly real-time updated to respond timely the changes in T_i and RH_i. It should be noted that Algorithm I was currently based on a fixed compressor speed,

which may effectively restrict the actual output cooling capacities from the experimental TS-DXAC system. Therefore, in the controllability tests, if R_r or R_a are changed, boundary values of R_r or R_a shown in Fig. 5.1 will be used. Hence, as shown in Fig. 7.1, operating Status 1 was defined where there were four different actions for R_a and R_r. In addition, under Algorithm I, a constant total air flow rate would also be kept by adjusting speeds of the two fans according to the required R_a values.

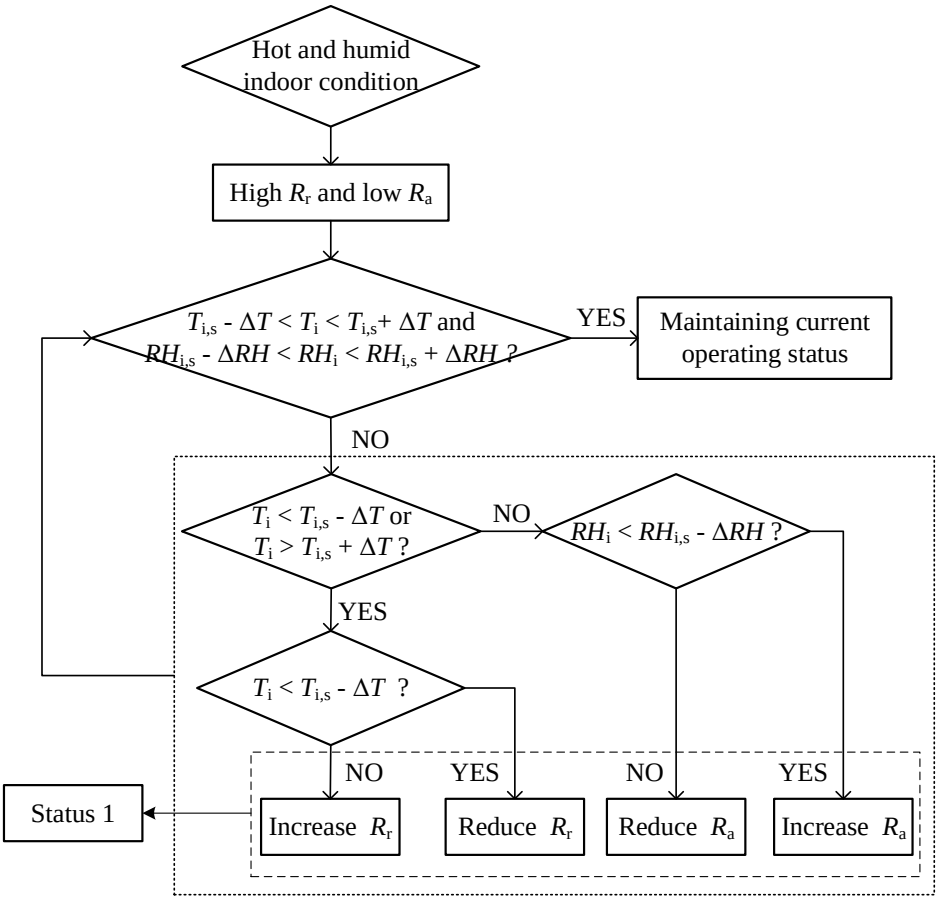

Fig. 7.1 The flowchart for Algorithm I

7.2.2 Algorithm II

For the experimental TS-DXAC system, its improved output LCC under Algorithm I would deteriorate the indoor thermal environment when used at a hot and dry indoor condition. Actually, at a hot and dry indoor condition, only indoor dry-bulb air temperature needed to be controlled. Hence, using a traditional On-Off control should have been adequate. However, to fully take the advantages of the configuration of an experimental TS-DXAC system, and alleviate the magnitudes of fluctuation in T_i associated with the traditional On-Off control, a traditional On-Off control was optimized into Algorithm II, as shown in Fig. 7.2, and is detailed as follows.

When the setting of indoor air dry bulb temperature was not satisfied, the experimental TS-DXAC system was operated at Status 2, when only HX2 was operated, and the variable speed compressor was operated at 80 Hz and SF2 at 1400 rpm. Otherwise, it was operated at Status 3, when only HX1 was used, and the compressor was operated at 40 Hz and SF1 at 700 rpm. It can be seen that there were only two operating statuses under Algorithm II, and the experimental TS-DXAC system can be operated alternatively between the two statuses depending on only T_i, which can be easily implemented.

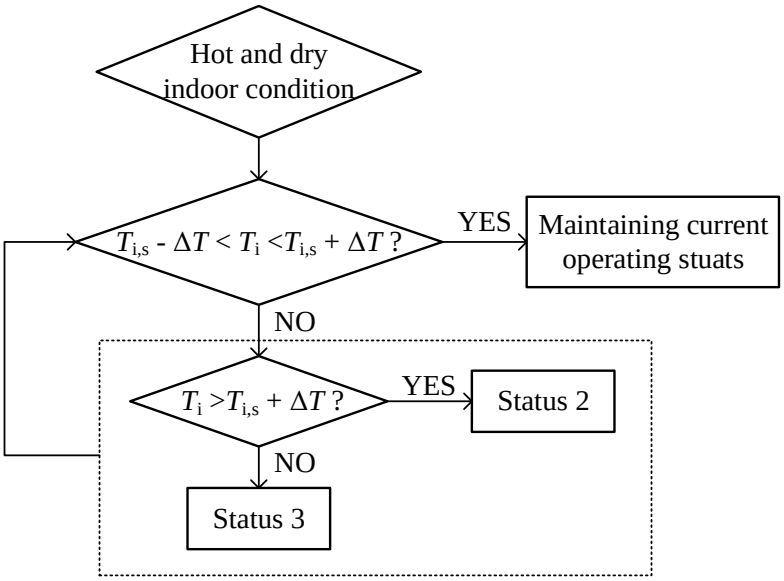

Fig. 7.2 The flowchart for Algorithm II

7.2.3 The developed control strategy of the experimental TS-DXAC system

The flowchart of the developed control strategy consisting of the two Algorithms for the experimental TS-DXAC system is shown in Fig. 7.3. The strategy enabled the experimental TS-DXAC system to be operated at the two indoor conditions that may be encountered in hot-humid climates, i.e., hot and humid, and hot and dry. Depending on the actual indoor air states, there were three different operating statuses of the experimental TS-DXAC system using this control strategy, i.e., Status 1 under Algorithm I, and Status 2 and Status 3 under Algorithm II. Table 7.1 details the operating conditions for EEVs, compressor and supply fans at the three Statuses. To start with, the experimental TS-DXAC system was operated at Status 2, as a default status. Then the actual T_i and RH_i values were measured and the measured values were used in the follow up control actions. Once T_i was lower than the low boundary of its dead-band, the operating status would be switched to Status 3. When both T_i and RH_i

were higher than the high boundaries of their respective dead-bands, the experimental TS-DXAC system would be operated at Status 1.

Hence, it can be seen that the control strategy developed was not complex, but simple and straightforward as compared to other previous controllers, such as a fuzzy logic controller or a controller based on artificial neural network model, and can therefore be easily implemented.

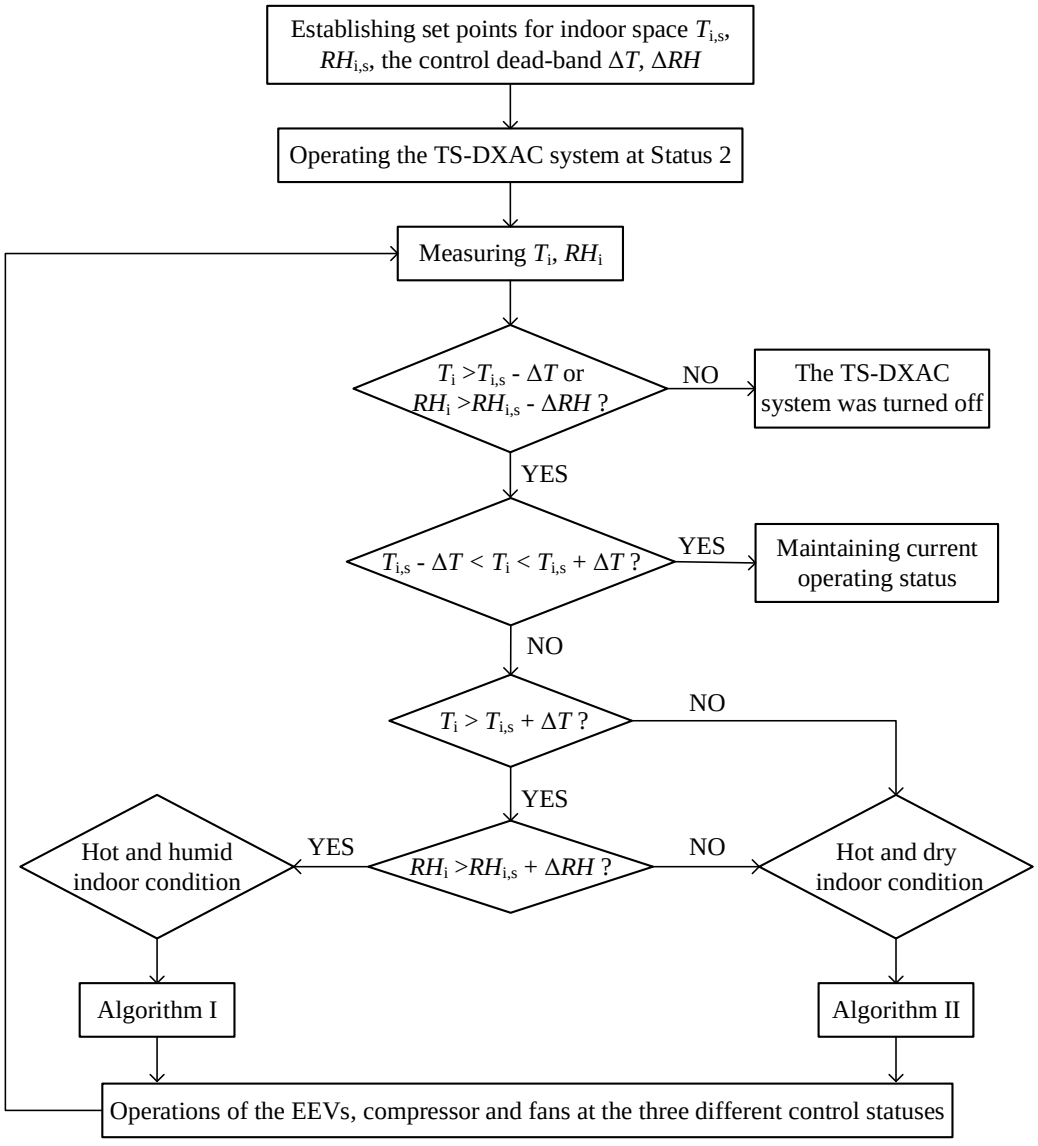

Fig. 7.3 Flowchart of the developed control strategy for the experimental TS-DXAC system

Table 7.1 The operations of the components in the experimental TS-DXAC system at different operating statuses

Operating Status	Components				
	EEV1	EEV2	SF1	SF2	compressor
1	B	A	V	V	80 Hz
2	0	A	S	1400 rpm	80 Hz
3	A	0	700 rpm	S	40 Hz

Notes:
0: to close EEVs; A: to control *DS*; B: to adjust refrigerant flow rates passing through the two sections; S: shut down; V: variable speed operated;

7.3 Controllability tests of the developed control strategy for the experimental TS-DXAC system

To examine the controllability of the experimental TS-DXAC system under the developed control strategy, two sets of test conditions, Set A and Set B, were designated, as shown in Table 7.2. In Set A, there were two tests (A1, A2), where the set-point of T_i, $T_{i,s}$, and that of RH_i, $RH_{i,s}$, were kept constant at 26 ℃ and 50%, respectively, but the space SCL and LCL were altered. In Set B (B1 to B4), the space SCL and LCL remained unchanged, but only $T_{i,s}$ was changed from 26 ℃ to 25 ℃ or only $RH_{i,s}$ from 55% to 45%, or both were changed simultaneously, from 26 ℃ / 60% to 25 ℃ / 50%, respectively.

Furthermore, as shown in Table 7.2, in each Set, two different indoor conditions, i.e., hot and dry and hot and humid, were included. Discrete values for indoor SCL and LCL

were used to represent the typical space cooling loads at the two different indoor conditions. For example, a combination of an indoor SCL of 2430 W and a LCL of 780W was used to represent a hot and dry indoor condition, and 3060 W/1500 W a hot and humid indoor condition. In addition, a constant outdoor air state at 33 ℃ / 68% was maintained at the outdoor space, based on typical outdoor air conditions in hot-humid climates. It should be noted that in this controllability tests, the high setting of indoor RH was 60%, which may be lower than the indoor RH under the hot and humid climates. However, the focus of this study is on the controllability of the developed control strategy, and the range of control may be expanded in future study.

Table 7.2 Test conditions and cases

Test set	Case	Fixed settings	Changed settings		Algorithm
		T_{is}/RH_{is}	SCL/LCL (W)		
			From	To	
A	A1[a]	26 ℃/~	2430/780	2520/960	II
	A2[b]	26 ℃/50%	3060/1500	3240/1680	I
		SCL/LCL (W)	T_{is}/RH_{is}		
			From	To	
B	B1[a]	2340/900	26 ℃/~	25 ℃/~	II
	B2[b]	3060/1620	26 ℃/50%	25 ℃/50%	I
	B3[b]	3060/1620	26 ℃/55%	26 ℃/45%	I
	B4[b]	2970/1800	26 ℃/60%	25 ℃/50%	I

[a] Hot and dry indoor condition; [b] Hot and humid indoor condition

For each test, its duration was 10000 s. The experimental TS-DXAC system was operated long enough to reach a steady state before the intended changes were

introduced, usually at between 2750 s and 4350 s into the tests. In addition, to prevent frequent switch amongst different operating statuses, a dead-band of ± 0.35 °C for T_i and that of $\pm 5\%$ for RH_i were set.

7.4 Test results and related analysis

Using the experimental TS-DXAC system and following the test conditions presented in Table 7.2, extensive controllability tests have been conducted, and the test results expressed in the term of the variations in T_i and RH_i are presented in this section. When both indoor SCL and LCL were high in Tests A2, B2, B3, B4, the experimental TS-DXAC system was controlled by Algorithm I. On the other hand, in Tests A1 and B1, when indoor SCL was high but indoor LCL was low, the experimental TS-DXAC system was controlled by Algorithm II. These are detailed in Sections 7.4.1 to 7.4.2.

7.4.1 Test results under Algorithm I

Figs. 7.4 - 7.7 show the results in Tests A2, B2, B3 and B4, respectively. As seen, both T_i and RH_i could be simultaneously controlled within the dead-bands of their respective set points.

Fig. 7.4 shows the test results in Test A2. Before the changes in cooling loads, as detailed in Table 7.2, were introduced at 4350 s into the test, both T_i and RH_i were controlled within their respective dead-bands. After the changes, the experimental TS-DXAC system can adjust its output SCC and LCC by increasing R_r from 44% to 53% and decreasing R_a from 60% to 50%, to match the change in cooling loads. As a result,

the required T_i and RH_i could be maintained within the dead-band of their set points, respectively, till the end of the test.

Fig. 7.5 shows the test results in Test B2. In this test, only $T_{i,s}$ was lowered from 26 ℃ to 25 ℃ at 3150 s, but with all others remaining unchanged, as detailed in Table 7.2. As shown, under Algorithm I, the experimental TS-DXAC system responded to the change by increasing R_r from 48% to 53% to output more cooling capacity, as T_{is} was lowered. However, the RH_i would be correspondingly increased, because of the insignificant changes in its output dehumidification capacity when only R_r was varied. Hence, when RH_i was over the upper boundary of its dead-band, R_a was reduced from 50% to 40% to output more latent cooling capacities to maintain the RH_i within its dead-band. Furthermore, it can also be observed that it took approximately 1000 seconds for T_i and RH_i to reach the new set points. This was because the range of the output cooling capacity was restricted by the fixed speed operation of the compressor. Therefore, if a larger output cooling capacity was required, consideration should be given to the variable speed operating of the compressor, so as to improve the control sensitivity of Algorithm I.

In Test B3, only $RH_{i,s}$ was changed from 55% to 45% at 2750 s, but with all others remaining unchanged, as detailed in Table 7.2 for the purpose of verifying the humidity control using the experimental TS-DXAC system. As shown in Fig. 7.6, after the $RH_{i,s}$ was reduced, under Algorithm I, the experimental TS-DXAC system could respond to the change by reducing R_a from 55% to 45% to output more LCC. However, in this test, it took approximately 2000 s to restore T_i and RH_i to their new set points, respectively. This was also because the fixed compressor speed operation restricted the output LCC.

Moreover, as observed from the operational characteristics shown in Fig. 5.1, the variation range in TCC from the experimental TS-DXAC system at a fixed compressor speed was larger than that in E SHR, so that a longer time duration was required in restoring $RH_{i,s}$. To improve this, again, variable speed operation of the compressor may be considered.

In addition, Fig. 7.7 shows the test results in Test B4. In this test, both $T_{i,s}$ and $RH_{i,s}$ were altered from 26 ℃ to 25 ℃ and from 60% to 50% at 3500 s, respectively, with indoor cooling loads remaining unchanged, as shown in Table 7.2. Under Algorithm I, the experimental TS-DXAC system responded to the changes by increasing R_r from 40% to 53% and reducing R_a from 60% to 40% to provide more SCC and LCC, so that both T_i and RH_i could be controlled within the dead-bands of their new respective set points. However, it took approximately 2200 s for T_i and RH_i to reach their new set points. It can also be observed that the T_i reached the new set point earlier than RH_i, which was explained already when presenting Test B3 results.

The test results shown in Figs. 7.4 - 7.7 suggested that, at hot and humid indoor conditions, under Algorithm I, the experimental TS-DXAC system can output variable sensible and latent cooling capacities to handle the changes in indoor SCLs and LCLs, and simultaneously control T_i and RH_i within the dead-band of their respective set points. However, it can be also observed that in all tests, both T_i and RH_i fluctuated, but within their respective dead-bands. This was basically due to the discrete nature of the control action when varying both R_a and R_r. Furthermore, under Algorithm I, currently, a fixed compressor speed was used, resulting in a smaller range of the output SCCs and LCCs from the experimental TS-DXAC system. Hence, since a variable

speed compressor was actually used, to have a larger range of the TCC, variable speed operation of the compressor may be considered and incorporated into Algorithm I.

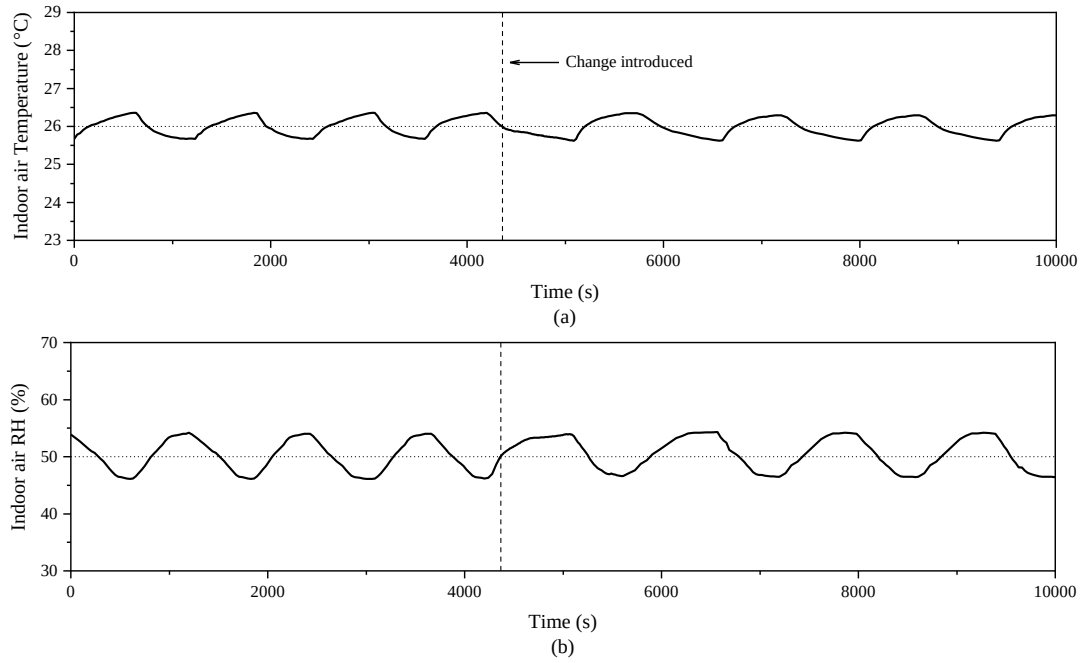

Fig. 7.4 Controllability test results in Test A2

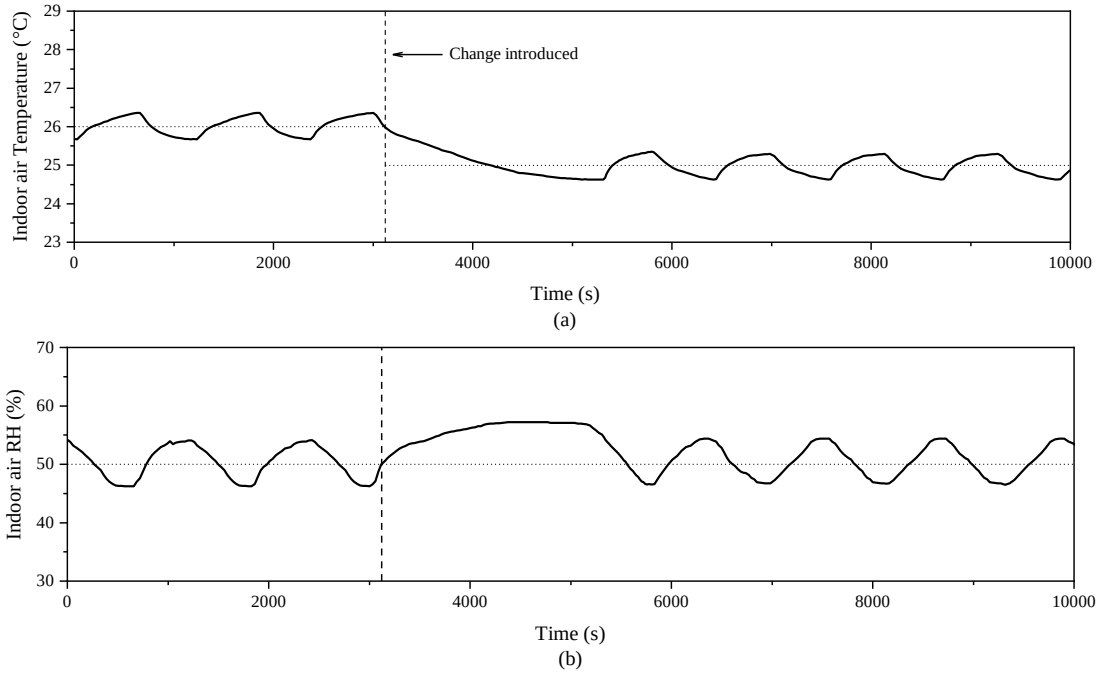

Fig. 7.5 Controllability test results in Test B2

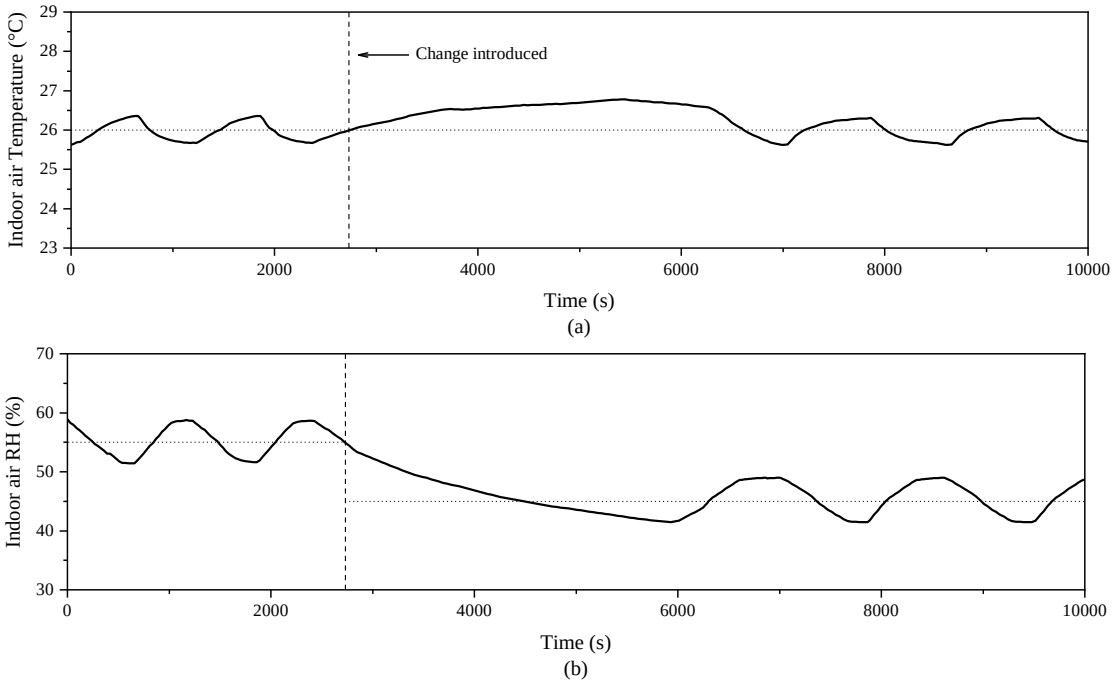

Fig. 7.6 Controllability test results in Test B3

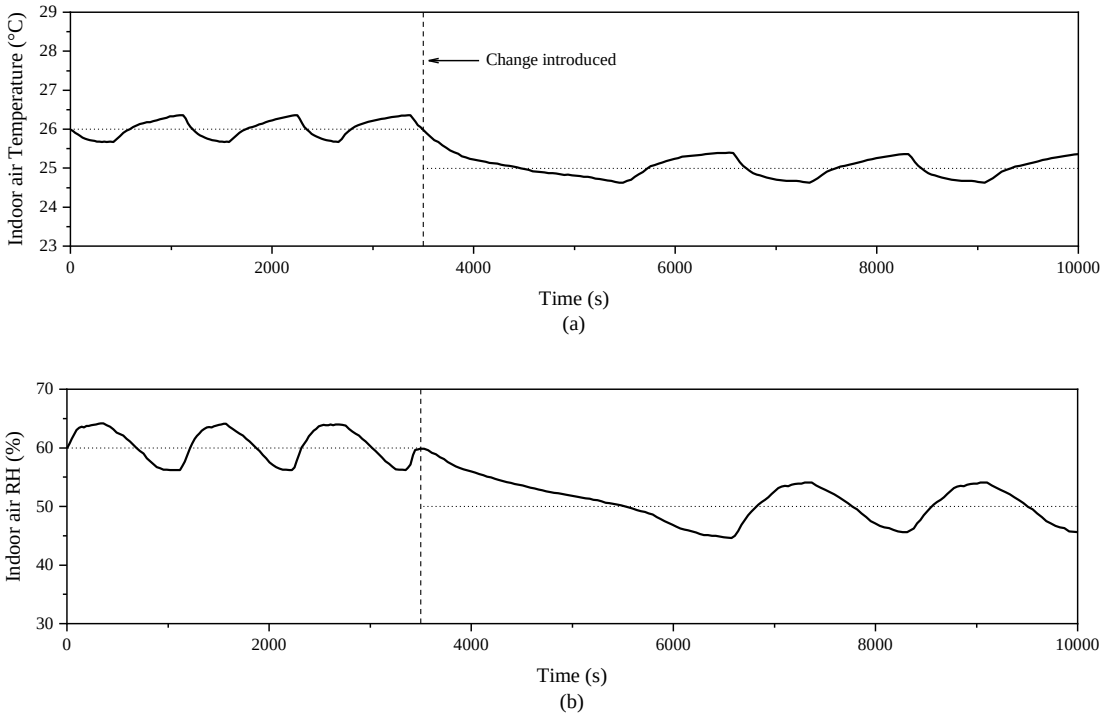

Fig. 7.7 Controllability test results in Test B4

7.4.2 Test results under Algorithm II

Fig. 7.8 shows the test results of Test A1. Before the changes in space cooling loads were introduced at 4180 s, under Algorithm II, the experimental TS-DXAC system was operated alternatively between Status 2 and Status 3, with the former having a shorter duration. T_i was stably maintained within the dead-band of its set point at 26 ℃. After the changes, however, the duration of Status 2 was increased to provide more cooling capacity to handle the increased space SCLs and LCLs, so as to maintain T_i still at 26 ℃. On the other hand, due to the increase in space LCL, averaged RH_i was increased from 44.3% to 47.8%, because the output LCC from the experimental TS-DXAC system did not change much, as a result of a longer duration of Status 2 and shorter duration of Status 3.

Furthermore, the test results of B1 are shown in Fig. 7.9. As seen, a 1 ℃ reduction in T_i from 26 ℃ to 25 ℃ was introduced at 3900 s, with all others remaining unchanged. Under Algorithm II, similar to that in Test B1, after the change, the duration of Status 2 was increased but that of Status 3 shortened, so that more cooling capacity could be obtained from the experimental TS-DXAC system to deal with an increased space cooling load as $T_{i,s}$ was reduced. As a result, T_i was controlled within the dead-band of 25 ℃ T_i setting. On the other hand, RH_i was slightly increased from 48.9% to 50.8%, similar to that in Test A1.

From Figs. 7.8 - 7.9, it could be also seen that the T_i fluctuated within the dead-band of it settings, as a result of the experimental TS-DXAC system being operated between the two statuses under Algorithm II, similar to that under a conventional On-Off control.

However, as compared to the traditional On-Off control, the use of Algorithm II may help further effectively reduce the magnitude of fluctuations in T_i, as a result of the low compressor speed operation of the experimental TS-DXAC system (i.e., Status 3) when T_i reached the lower boundary of the dead-band. On the other hand, the use of Algorithm II may also lead to a more energy efficient operation of the experimental TS-DXAC system at a hot and dry indoor condition, as the switching between high-low compressor speed operation can effectively avoid space over cooling. Consequently, a lower indoor-outdoor air temperature difference would result in a smaller indoor cooling load, thus requiring less energy to deal with.

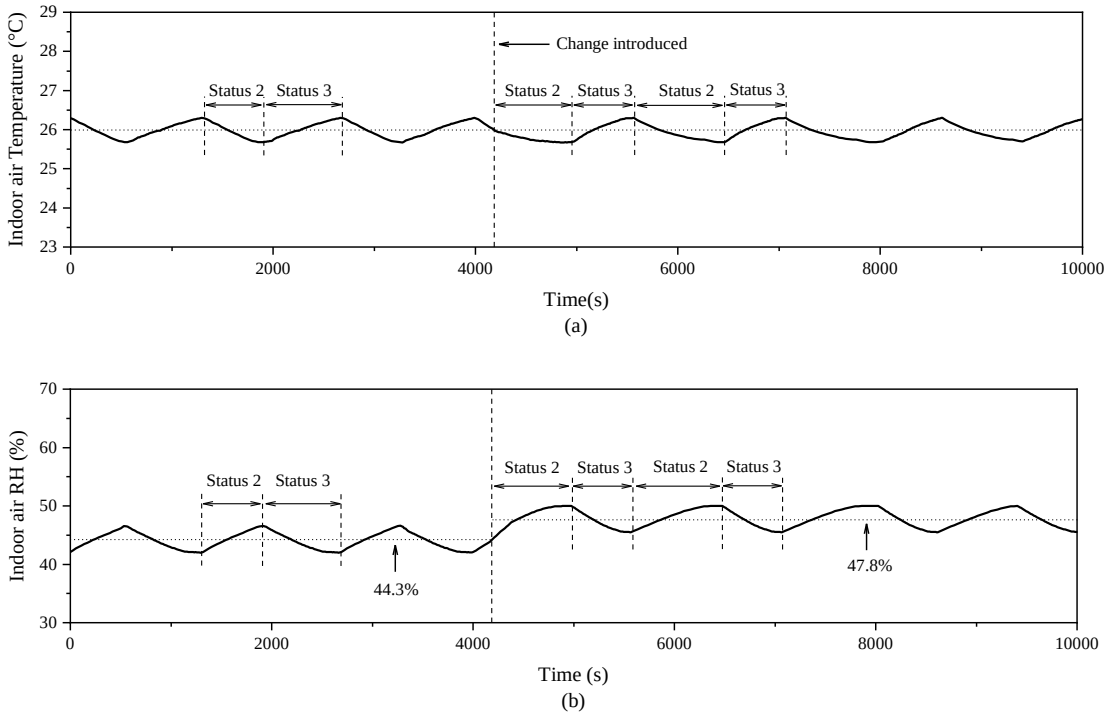

Fig. 7.8 Controllability test results in Test A1

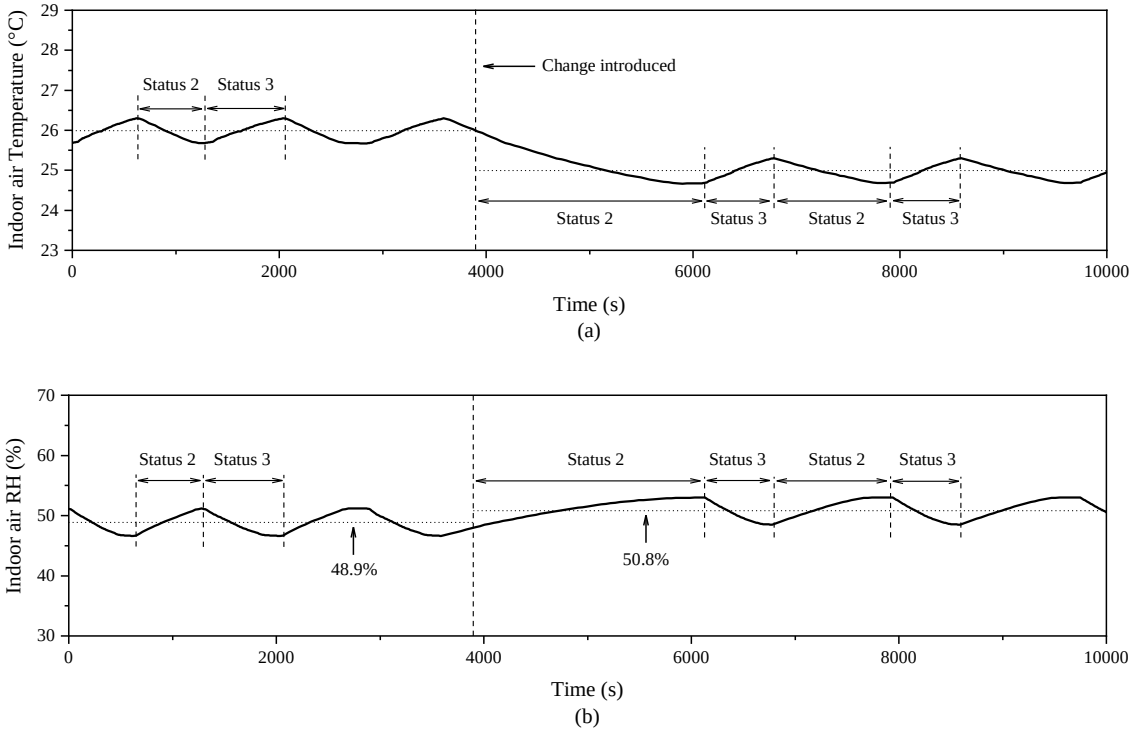

Fig. 7.9 Controllability test results in Test B1

7.4.3 Discussions

The test results presented in Sections 7.4.1 and 7.4.2 suggested that when controlled by the control strategy developed, the experimental TS-DXAC system was able to respond the changes in either indoor settings or cooling loads by outputting variable sensible and latent cooling capacities, at two different indoor conditions, i.e., hot and humid, and hot and dry. With the two algorithms specifically developed, the two sections of the cooling coil in a TS-DXAC system may be operated separately or jointly, according to different indoor air states. In addition, T_i could be directly controlled at the two indoor conditions using both algorithms, while RH_i could be directly controlled at a hot and humid indoor condition using Algorithm I, but controlling RH_i was not necessary at a hot and dry indoor condition.

It can also be seen that the control strategy developed for the experimental TS-DXAC system was much simpler and straightforward, when compared to other advanced controllers, and can therefore be easily implemented. Furthermore, a constant total supply air flow rate could also be kept. However, it should be noted that, currently, Algorithm I was actually based on a fixed compressor speed, which may effectively restrict the actual output SCCs and LCCs from the experimental TS-DXAC system. As a result, the control sensitivity may be impaired by taking a longer time to reach new indoor settings. Hence, consideration should be given to further improving Algorithm I by incorporating variable speed compressor operation.

7.5 Conclusion

In this Chapter, the development of a control strategy to operate the experimental TS-DXAC system is presented. The control strategy included two algorithms, i.e., Algorithm I for hot and humid indoor conditions, and Algorithm II for hot and dry indoor conditions. Algorithm I was developed based on the experimentally obtained inherent operational characteristics of the experimental TS-DXAC system at a fixed compressor speed, as reported in Chapter 5, and Algorithm II by optimizing the conventional On-Off control. Extensive controllability tests for the control strategy have been carried out using an experimental TS-DXAC system. The controllability test results suggested that the control strategy enabled the experimental TS-DXAC system to respond the changes in either indoor settings or cooling loads by outputting variable sensible and latent cooling capacities. During all the tests, T_i could be directly controlled at the two indoor conditions using both algorithms, while RH_i could be directly controlled at a hot and humid indoor condition using Algorithm I. However, it

was also observed that under Algorithm I, it tended to take a longer duration to restore indoor settings after changes, as restricted by the fixed compressor speed operation. To improve control sensitivity, variable speed compressor operation should be considered and implemented into Algorithm I.

The results of controllability tests presented in this Chapter demonstrated that the experimental TS-DXAC system was able to be operated, under the control of the developed control strategy, in buildings located in hot-humid climates for improved indoor thermal environmental control.

Chapter 8

Conclusion and future work

8.1 Conclusions

A research project on firstly proposing a DX A/C system having a two-sectioned cooling coil (TS-DXAC), without employing any additional provisions to provide variable cooling and dehumidifying capacities and establishing an experimental TS-DXAC system, secondly experimentally investigating the operational characteristics of the experimental TS-DXAC system, thirdly developing and validating a steady-state physical-based mathematical model for the experimental TS-DXAC system, and finally developing a simple and straightforward control strategy for the experimental TS-DXAC system for improved indoor thermal environmental control, has been successfully carried out and is reported in this Thesis. The conclusions of the Thesis are:

Firstly, the operational characteristics of the experimental TS-DXAC system have been experimentally studied, and the relevant experimental results are reported in Chapter 5. The study results demonstrated that the experimental TS-DXAC system was able to provide variable output cooling and dehumidification capacities at a constant compressor speed and a fixed total supply air flow rate when refrigerant and air flow rates to the two-sectioned cooling coil were varied. In addition, the experimental results showed that the output TCC and E SHR values from the experimental TS-DXAC system were strongly correlated but mutually constrained within an irregular area in a TCC - E SHR diagram. Furthermore, inlet air states also influenced the operational

characteristics of the experimental TS-DXAC system, resulting in the changes in both the shape and positon of an irregular area for the relationship of TCC - E SHR in a TCC - E SHR diagram, and the variations in inlet air RH would influence more on the shapes and positions of the irregular areas.

Secondly, the development of a steady-state physical-based mathematical model for the experimental TS-DXAC system is presented in Chapter 6. The model was experimentally validated using the experimental data reported in Chapter 5, with the differences between experimental and predicted results of being less than 6%. Using the validated model, a follow-up modeling study on the surface area ratio of the two sections in the cooling coil was carried out and the modeling study results are reported. The modeling results demonstrated that a lower ratio for the surface areas of the two sections (R_s) could lead to enlarged variation ranges in both TCC and E SHR. For example, at the inlet state of 26 ℃ and 50% RH, when R_s was altered from 1:1 to 1:3, the variation range for TCC was increased by 33%, and that for E SHR by 51%, which was beneficial to better dehumidification. In addition, the changes in R_s would influence more on E SHR than TCC.

Finally, the control strategy developed for the experimental TS-DXAC system is detailed in Chapter 7. This control strategy enabled the experimental TS-DXAC system to be operated at two typical indoor air conditions in buildings located in hot-humid climates for improved indoor thermal environmental control. Two algorithms were incorporated into the control strategy, i.e., Algorithm I for hot and humid indoor conditions, and Algorithm II for hot and dry indoor conditions. T_i could be directly controlled at the two indoor conditions using both algorithms, while RH_i could be

directly controlled at a hot-humid indoor condition using Algorithm I. Controllability tests for the control strategy have been carried out and the test results demonstrated that the experimental TS-DXAC system was able to be operated, under the control of the developed control strategy, in buildings located in hot-humid climates for improved indoor thermal environmental control.

The successful carrying out of the research project presented in this Thesis helped achieve improved indoor thermal environmental control and IAQ, and reduced energy use through better RH_i control using DX air conditioning technology. The developed TS-DXAC system was less complicated and costly as compared to the other approaches used for enhancing the dehumidification performances for DX A/C systems. The outcomes from the research project has also contributed to the advancements of DX A/C technologies.

8.2 Proposed further work

Following the successful completion of the research project reported in this Thesis, a number of future possible studies are proposed as follows:

Firstly, in Chapter 5, the experimental results suggested that the flow rates of both refrigerant and air passing through the two-sectioned cooling coil and different inlet air states impacted greatly the operational characteristics of the experimental TS-DXAC system. However, other system operating parameters such as compressor speed and the total supply air flow rate could also affect the operational characteristics of the

experimental TS-DXAC system. Therefore, future experimental work should be organized to study the influences of these parameters.

Secondly, the developed steady-state TS-DXAC model was experimentally validated with an acceptable predicting accuracy, as reported in Chapter 6. Nonetheless, a dynamic model for a TS-DXAC system to simulate the transient system responses should be further developed, as a dynamic model is more useful in developing control strategies, and detecting and removing faults for a TS-DXAC system.

Thirdly, a simple and straightforward control strategy consisting of two algorithms to enable the experimental TS-DXAC system to respond the changes in either indoor settings or cooling loads by outputting variable sensible and latent cooling capacities was developed, as presented in Chapter 7. However, it was also observed that under Algorithm I, it likely took a long duration to restore indoor settings after changes were introduced, as restricted by the fixed compressor speed operation. To improve the control sensitivity, variable speed compressor operation should be considered and implemented into Algorithm I. Therefore, future related studies should be carried out.

Fourthly, due to the parallel connection of the two sections in the TS-DXAC system, the refrigerant pressure drop along the two branches was forced to be equal, which impaired the energy efficiency of the system. Therefore, it is possible to carry out the investigation of the TS-DXAC system with ejector and take advantage of the high refrigerant pressure in a certain section to increase the suction pressure of the compressor, thus improving the energy efficiency of the whole system.

Finally, for the research project of studying a TS-DXAC system presented in this Thesis, no fresh air was introduced into the system. However, because the two sections in the cooling coil were actually connected in parallel, it was possible to designate one of the two sections to process specifically the fresh air for more effectively moisture removal. Therefore, to fully take advantages of the characteristics of the TS-DXAC system and expand its application ranges, a provision for introducing fresh air into the TS-DXAC system should be incorporated.

Appendix

Photos of the experimental TS-DXAC system

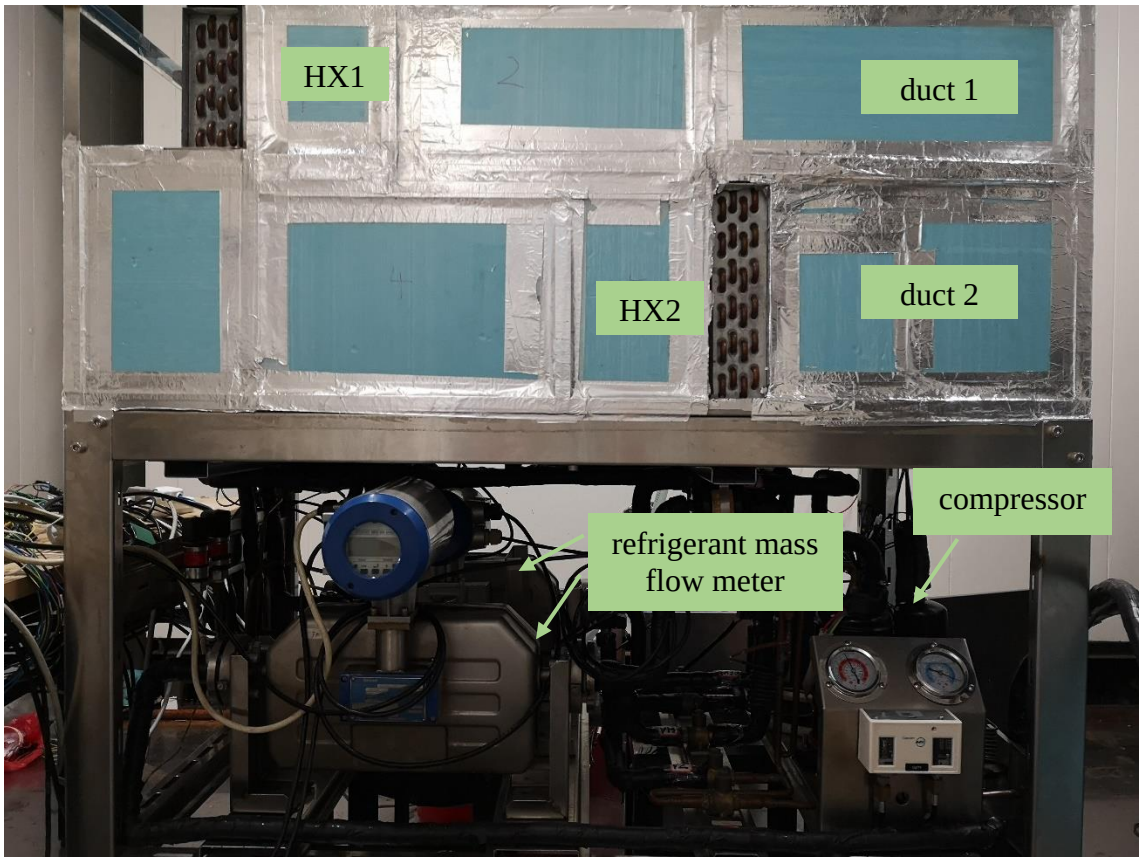

Photo 1 The experimental TS-DXAC system (1)

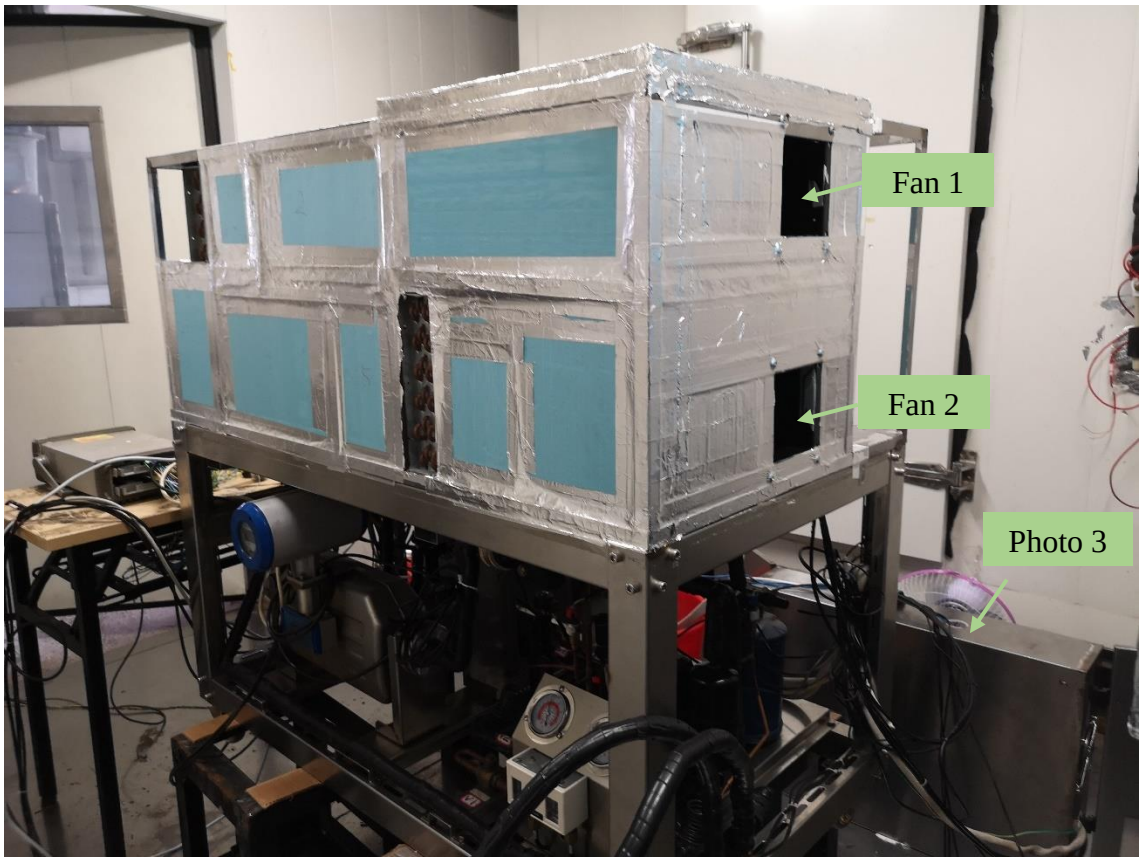

Photo 2 The experimental TS-DXAC system (2)

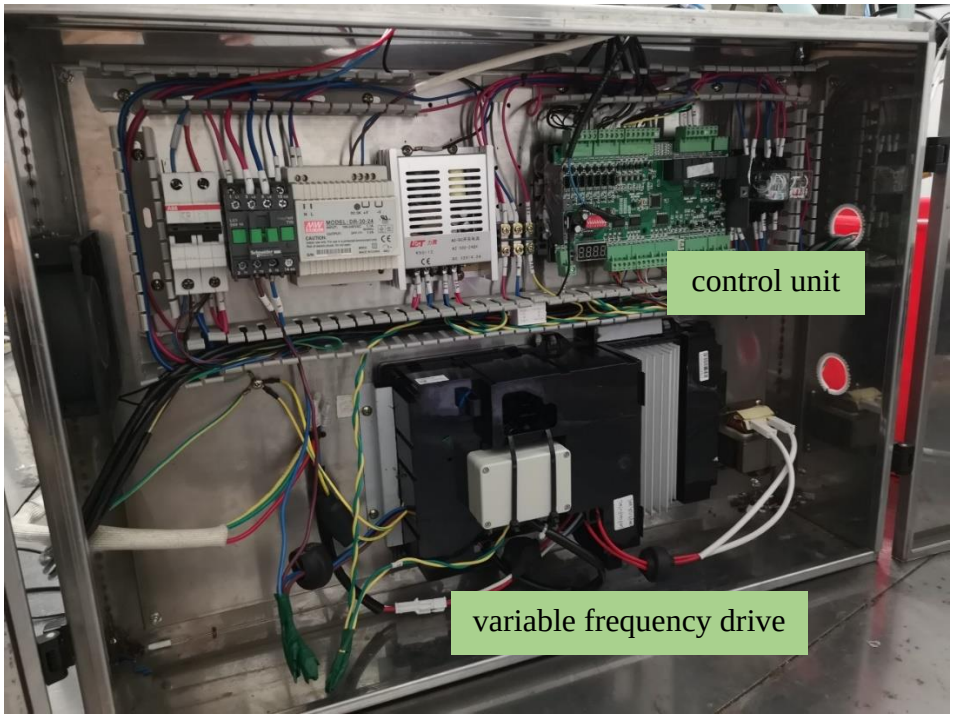

Photo 3 The electric box of the experimental TS-DXAC system

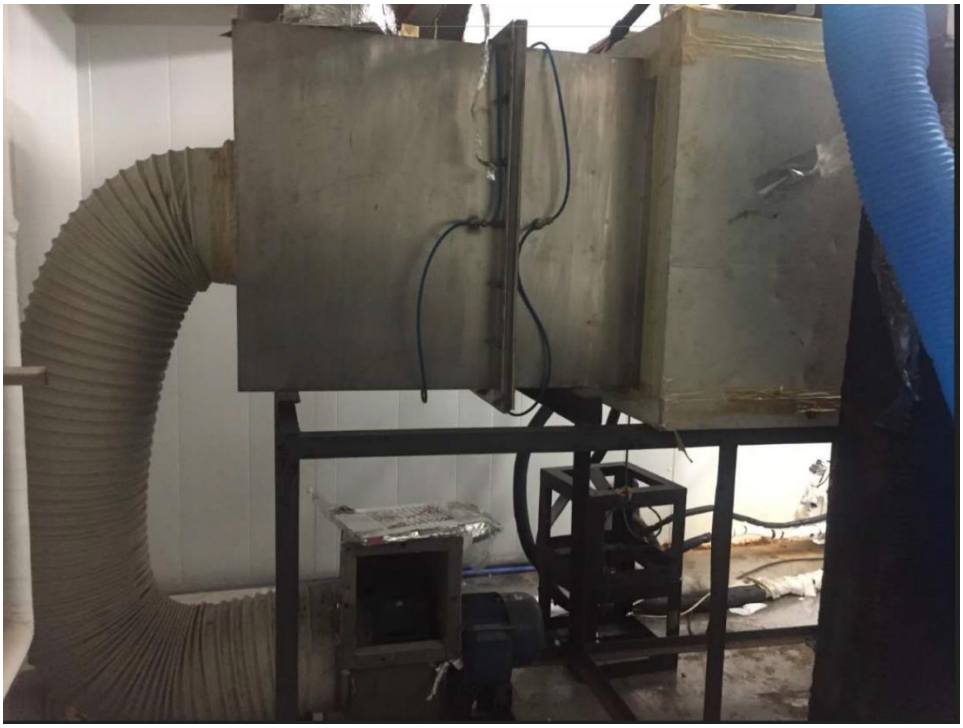

Photo 4 Airflow rate measuring apparatus

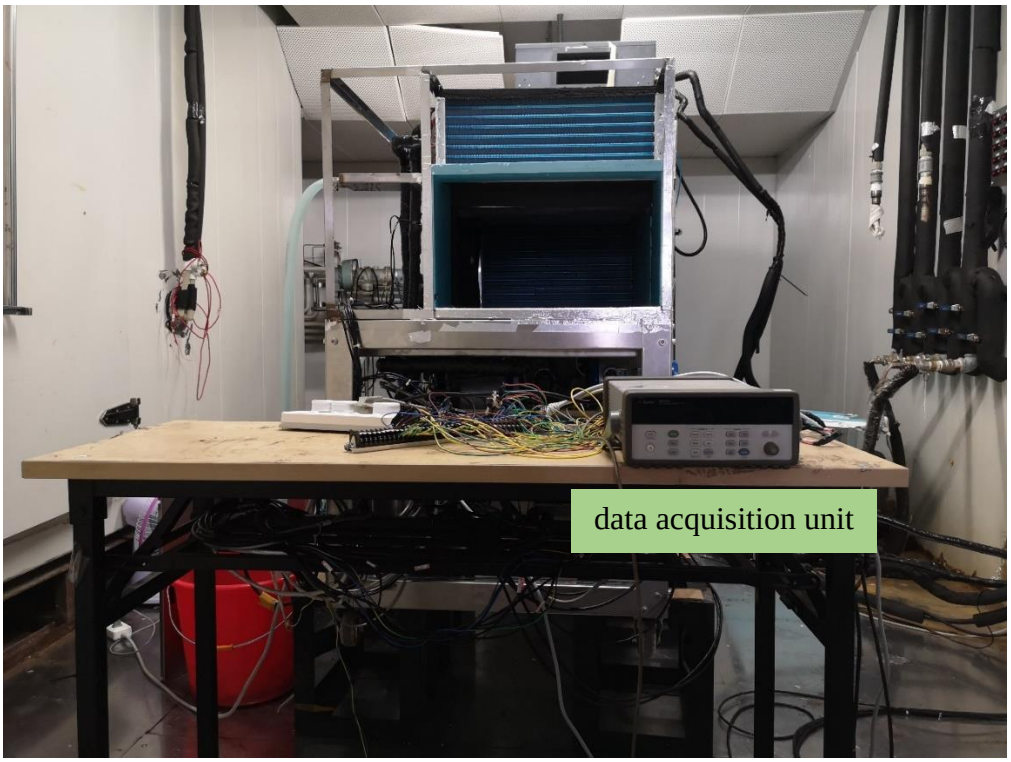

Photo 5 Data acquisition system of the experimental TS-DXAC system

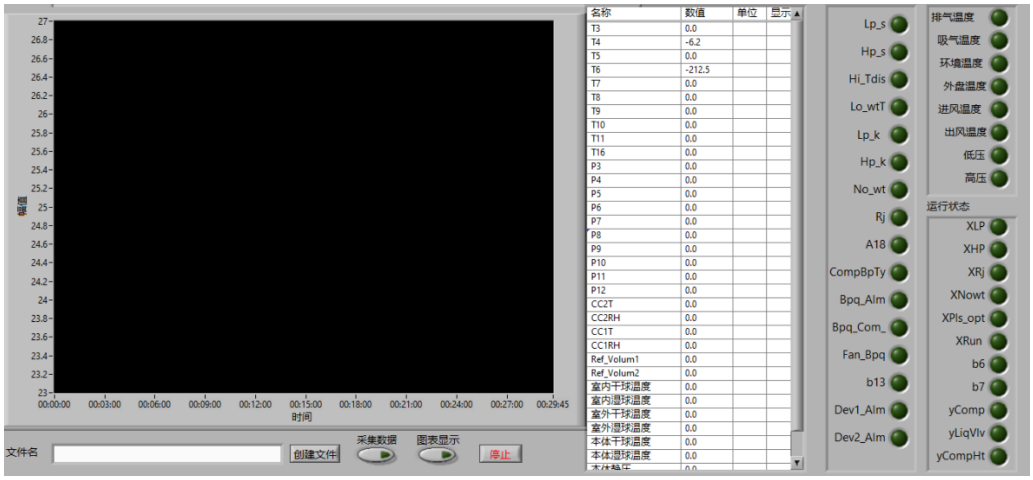

Photo 6 LabVIEW logging & control supervisory program

Photo 7 Indoor chamber of the laboratory

Photo 8 Outdoor chamber of the laboratory

References

[1] Amrane et al. 2003

Amrane, K., Hourahan, G.C. and Potts, G.

Latent performance of unitary equipment. ASHRAE Journal, 45 (2003): 28.

[2] Andrade and Bullard 2002

Andrade, M.A. and Bullard, C.W.

Modulating blower and compressor capacities for efficient comfort control/Discussion. ASHRAE Transactions, 108 (2002): 631.

[3] Arens et al. 2009

Arens, E., Turner, S., Zhang, H. and Paliaga, G.

Moving air for comfort. (2009).

[4] Arens and Baughman 1996

Arens, E.A. and Baughman, A.

Indoor humidity and human health: part II--buildings and their systems. ASHRAE Transactions, 102 (1996): 212-221.

[5] ASHRAE 1986

ASHRAE Standard 41.1.

Standard Method for Temperature Measurement. American Society of Heating, Refrigerating and Air-Conditioning Engineers, Atlanta, GA, USA, (1986).

[6] ASHRAE 1987

ASHRAE Standard 41.2.

Standard methods for laboratory airflow measurement. American Society of Heating Refrigeration and Air Conditioning Engineers, Atlanta, GA, USA, (1987).

[7] ASHRAE 2009

ASHRAE Handbook: Fundamentals.

American Society of Heating Refrigerating and Air-Conditioning Engineers, Atlanta, GA, USA, (2009).

[8] Ataer et al. 1995

Ataer, Ö.E., Ileri, A. and Göğüş, Y.

Transient behaviour of finned-tube cross-flow heat exchangers. International Journal of Refrigeration, 18 (1995): 153-160.

[9] Aynur et al. 2008

Aynur, T.N., Hwang, Y. and Radermacher, R.

Experimental evaluation of the ventilation effect on the performance of a VRV system in cooling mode—Part I: Experimental evaluation. HVAC&R Research, 14 (2008): 615-630.

[10] Bensafi et al. 1997

Bensafi, A., Borg, S. and Parent, D.

CYRANO: a computational model for the detailed design of plate-fin-and-tube heat exchangers using pure and mixed refrigerants. International Journal of Refrigeration, 20 (1997): 218-228.

[11] Berglund and Cunningham 1986

Berglund, L. and Cunningham, D.

Parameters of human discomfort in warm environments. ASHRAE Transactions, 92 (1986).

[12] Berglund 1994

Berglund, L.G.

Common elements in the design and operation of thermal comfort and ventilation systems. ASHRAE Transactions, 100 (1994): 776-776.

[13] Berglund 1998

Berglund, L.G.

Comfort and humidity. ASHRAE Journal, 40 (1998): 35.

[14] Browne and Bansal 1998

Browne, M.W. and Bansal, P.K.

Challenges in modeling vapor-compression liquid chillers. ASHRAE Transactions, 104 (1998): 474.

[15] Burns et al. 1985

Burns, P., Mitchell, J. and Beckman, W.

Hybrid desiccant cooling systems in supermarket applications. ASHRAE Transactions, 91 (1985): 457-468.

[16] Chen et al. 2018a

Chen, W., Chan, M., Deng, S., Yan, H. and Weng, W.

A direct expansion based enhanced dehumidification air conditioning system for improved year-round indoor humidity control in hot and humid climates. Building and Environment, 139 (2018a): 95-109.

[17] Chen et al. 2018b

Chen, W., Chan, M., Weng, W., Yan, H. and Deng, S.

Development of a steady-state physical-based mathematical model for a direct expansion based enhanced dehumidification air conditioning system. International Journal of Refrigerationm, 91 (2018b): 55-68.

[18] Chen et al. 2018c

Chen, W., Chan, M., Weng, W., Yan, H. and Deng, S.

An experimental study on the operational characteristics of a direct expansion based enhanced dehumidification air conditioning system. Applied Energy, 225 (2018c): 922-933.

[19] Chen and Deng 2006

Chen, W. and Deng, S.

Development of a dynamic model for a DX VAV air conditioning system. Energy Conversion and Management, 47 (2006): 2900-2924.

[20] Chi and Didion 1982

Chi, J. and Didion, D.

A simulation model of the transient performance of a heat pump. International Journal of Refrigeration, 5 (1982): 176-184.

[21] Chuah et al. 1998

Chuah, Y., Hung, C. and Tseng, P.

Experiments on the dehumidification performance of a finned tube heat exchanger. HVAC&R Research, 4 (1998): 167-178.

[22] Damasceno et al. 1990

Damasceno, G., Goldschmidt, V. and Rooke, S.

Comparison of three steady-state heat pump computer models. ASHRAE Transactions, 96 (1990).

[23] Diaz et al. 1999

Diaz, G., Sen, M., Yang, K. and McClain, R.L.

Simulation of heat exchanger performance by artificial neural networks. HVAC&R Research, 5 (1999): 195-208.

[24] Ding et al. 2004a

Ding, G., Zhang, C. and Lu, Z.

Dynamic simulation of natural convection bypass two-circuit cycle refrigerator–freezer and its application: Part I: Component models. Applied Thermal Engineering, 24 (2004a): 1513-1524.

[25] Ding et al. 2004b

Ding, G.L., Zhang, C.L. and Zhan, T.

An approximate integral model with an artificial neural network for heat exchangers. Heat Transfer—Asian Research: Co‐sponsored by the Society of Chemical Engineers of Japan and the Heat Transfer Division of ASME 33, (2004b): 153-160.

[26] Domanski 1991

Domanski, P.A.

Simulation of an evaporator with nonuniform one-dimensional air distribution. (1991)

[27] Domanski and McLinden 1992

Domanski, P.A. and McLinden, M.O.

A simplified cycle simulation model for the performance rating of refrigerants and refrigerant mixtures. International Journal of Refrigeration, 15 (1992): 81-88.

[28] Elliott and Rasmussen 2008

Elliott, M.S. and Rasmussen, B.P.

Model-based predictive control of a multi-evaporator vapor compression cooling cycle, American Control Conference, 2008. IEEE, 1463-1468.

[29] Elliott and Rasmussen 2013

Elliott, M.S. and Rasmussen, B.P.

Decentralized model predictive control of a multi-evaporator air conditioning system. Control Engineering Practice, 21 (2013): 1665-1677.

[30] Elmahdy et al. 1977

Elmahdy, A., AH, E. and GP, M.

A simple model for cooling and dehumidifying coils for use in calculating energy requirements for buildings. (1977).

[31] Fan et al. 2014

Fan, H., Shao, S. and Tian, C.

Performance investigation on a multi-unit heat pump for simultaneous temperature and humidity control. Applied Energy, 113 (2014): 883-890.

[32] Fang et al. 2004

Fang, L., Wyon, D.P., Clausen, G. and Fanger, P.O.

Impact of indoor air temperature and humidity in an office on perceived air quality, SBS symptoms and performance. Indoor Air, 14 (2004): 74-81.

[33] Green 1982

Green, G.

The positive and negative effects of building humidification. ASHRAE Transactions, 88 (1982).

[34] Guan et al. 2020

Guan, B., Liu, X., Zhang, Q. and Zhang, T.

Performance of a temperature and humidity independent control air-conditioning system based on liquid desiccant for industrial environments. Energy and Buildings, 214 (2020): 109869.

[35] Gwosdow et al. 1986

Gwosdow, A., Stevens, J., Berglund, L. and Stolwijk, J.

Skin friction and fabric sensations in neutral and warm environments. Textile Research Journal, 56 (1986): 574-580.

[36] Han and Zhang 2011

Han, X. and Zhang, X.

Experimental study on a residential temperature–humidity separate control air-conditioner. Energy and Buildings, 43 (2011): 3584-3591.

[37] Han et al. 2013

Han, X., Zhang, X., Wang, L. and Niu, R.

A novel system of the isothermal dehumidification in a room air-conditioner. Energy and Buildings, 57 (2013): 14-19.

[38] Harriman 2002

Harriman III, L.G.

Dehumidification equipment advances. ASHRAE Journal, 44 (2002): 22.

[39] ASHRAE 2004

Thermal environmental conditions for human occupancy

American Society of Heating Refrigerating and Air-Conditioning Engineers, Atlanta, GA, USA, (2004).

[40] Henderson et al. 2014

Henderson Jr, H.I. and Rudd, A.

Energy Efficiency and cost assessment of humidity control options for residential buildings. ASHRAE Transactions, 120 (2014): 163.

[41] Hernandez et al. 2020

Hernandez III, A.C. and Fumo, N.

A Review of Variable Refrigerant Flow HVAC System Components for Residential Application. International Journal of Refrigeration, 110 (2020): 47-57.

[42] Holman 2001

Holman, J.P.

Experimental methods for engineers. (2001)

[43] Hourahan 2004

Hourahan, G.C.

How to properly size unitary equipment. ASHRAE Journal, 46 (2004): 15.

[44] Hu and Niu 2012

Hu, R. and Niu, J.

A review of the application of radiant cooling & heating systems in Mainland China. Energy and Buildings, 52 (2012): 11-19.

[45] Huh and Brandemuehl 2008

Huh, J.H. and Brandemuehl, M.J.

Optimization of air-conditioning system operating strategies for hot and humid climates. Energy and Buildings, 40 (2008): 1202-1213.

[46] Jacobi and Goldschmidt 1990

Jacobi, A.M. and Goldschmidt, V.

Low Reynolds number heat and mass transfer measurements of an overall counterflow, baffled, finned-tube, condensing heat exchanger. International Journal of Heat and Mass Transfer, 33 (1990): 755-765.

[47] Jain and Bansal 2007

Jain, S. and Bansal, P.

Performance analysis of liquid desiccant dehumidification systems. International Journal of Refrigeration, 30 (2007): 861-872.

[48] Jeong et al. 2010

Jeong, J., Yamaguchi, S., Saito, K. and Kawai, S.

Performance analysis of four-partition desiccant wheel and hybrid dehumidification air-conditioning system. International Journal of Refrigeration, 33 (2010): 496-509.

[49] Jia et al. 2006

Jia, C., Dai, Y., Wu, J. and Wang, R.

Analysis on a hybrid desiccant air-conditioning system. Applied Thermal Engineering, 26 (2006): 2393-2400.

[50] Jin et al. 2011

Jin, S., Sung, T., Kim, J. and Seo, T.

Optimal design of a micro-orifice for constant evaporator superheat in a small cooler. Applied Thermal Engineering, 31 (2011): 2631-2635.

[51] Jolly et al. 1990

Jolly, P., Jia, X. and Clements, S.

Heat pump assisted continuous drying part 1: simulation model. International Journal of Energy Research, 14 (1990): 757-770.

[52] Kittler 1996

Kittler R.

Mechanical dehumidification control strategies and psychrometrics. (1996). American Society of Heating, Refrigerating and Air-Conditioning Engineers, Inc., Atlanta, GA (United States).

[53] Krakow et al. 1995

Krakow K.I., Lin S. and Zeng Z.S.

Temperature and humidity control during cooling and dehumidifying by compressor and evaporator fan speed variation. (1995). American Society of Heating, Refrigerating and Air-Conditioning Engineers, Inc., Atlanta, GA (United States).

[54] Kreider et al. 1992

Kreider, J.F., Wang, X.A., Anderson, D. and Dow, J.

Expert systems, neural networks and artificial intelligence applications in commercial building HVAC operations. Automation in Construction, 1 (1992): 225-238.

[55] Kumlutaş et al. 2012

Kumlutaş, D., Karadeniz, Z.H., Avcı, H. and Özşen, M.

Investigation of design parameters of a domestic refrigerator by artificial neural networks and numerical simulations. International Journal of Refrigeration, 35 (2012): 1678-1689.

[56] Kurtz 2003

Kurtz, B.

Being size wise. ASHRAE Journal, 45 (2003): 17.

[57] Lam 1993

Lam, J.

A survey of electricity consumption and user behaviour in some government staff quarters: Survey covering fire services' quarters in Hong Kong found variable use of electricity consumption. Building Research and Information, 21 (1993): 109-116.

[58] Lan et al. 2010

Lan, L., Lian, Z. and Pan, L.

The effects of air temperature on office workers' well-being, workload and productivity-evaluated with subjective ratings. Applied Ergonomics, 42 (2010): 29-36.

[59] Lan et al. 2009

Lan, L., Lian, Z., Pan, L. and Ye, Q.

Neurobehavioral approach for evaluation of office workers' productivity: The effects of room temperature. Building and Environment, 44 (2009): 1578-1588.

[60] Lemmon et al. 2013

Lemmon E., Huber M. and McLinden M.

NIST Standard Reference Database 23: Reference Fluid Thermodynamic and Transport Properties-REFPROP, Version 9.1, National Institute of Standards and Technology, Standard Reference Data Programm, Gaithersburg, (2013)

[61] Li et al. 2012

Li, N., Xia, L., Deng, S., Xu, X. and Chan, M.

Dynamic modeling and control of a direct expansion air conditioning system using artificial neural network. Applied Energy, 91 (2012): 290-300.

[62] Li et al. 2013

Li, N., Xia, L., Deng, S., Xu, X. and Chan, M.

On-line adaptive control of a direct expansion air conditioning system using artificial neural network. Applied Thermal Engineering, 53 (2013): 96-107.

[63] Li 2013

Li, W.

Simplified steady-state modeling for variable speed compressor. Applied Thermal Engineering, 50 (2013): 318-326.

[64] Li et al. 2018

Li, Z., Chen, J., Wang, F., Cui, L. and Qu, M.

A simulation study for evaluating the performances of different types of house-hold radiant air conditioning systems. Applied Thermal Engineering, 131 (2018): 553-564.

[65] Li et al. 2017

Li, Z., Chen, J., Yu, H. and Cui, L.

The development and experimental performance evaluation on a novel household variable refrigerant flow based temperature humidity independently controlled radiant air conditioning system. Applied Thermal Engineering, 122 (2017): 245-252.

[66] Li et al. 2006

Li, Z., Chen, W., Deng, S. and Lin, Z.

The characteristics of space cooling load and indoor humidity control for residences in the subtropics. Building and Environment, 41 (2006): 1137-1147.

[67] Li and Deng 2007a

Li, Z. and Deng, S.

A DDC-based capacity controller of a direct expansion (DX) air conditioning (A/C) unit for simultaneous indoor air temperature and humidity control–Part I: Control algorithms and preliminary controllability tests. International Journal of Refrigeration, 30 (2007a): 113-123.

[68] Li and Deng 2007b

Li, Z. and Deng, S.

An experimental study on the inherent operational characteristics of a direct expansion (DX) air conditioning (A/C) unit. Building and Environment, 42 (2007b): 1-10.

[69] Li et al. 2014

Li, Z., Xu, X., Deng, S. and Pan, D.

Further study on the inherent operating characteristics of a variable speed direct expansion air conditioning system. Applied Thermal Engineering, 66 (2014): 206-215.

[70] Li et al. 2015a

Li, Z., Xu, X., Deng, S. and Pan, D.

A novel neural network aided fuzzy logic controller for a variable speed (VS) direct expansion (DX) air conditioning (A/C) system. Applied Thermal Engineering, 78 (2015a): 9-23.

[71] Li et al. 2015b

Li, Z., Xu, X., Deng, S. and Pan, D.

A novel proportional-derivative (PD) law based fuzzy logic principles assisted controller for simultaneously controlling indoor temperature and

humidity using a direct expansion (DX) air conditioning (A/C) system. International Journal of Refrigeration, 57 (2015b): 239-256.

[72] Lin and Deng 2004

Lin, Z. and Deng, S.

A study on the characteristics of nighttime bedroom cooling load in tropics and subtropics. Building and Environment, 39 (2004): 1101-1114.

[73] Ling et al. 2010

Ling, J., Hwang, Y. and Radermacher, R.

Theoretical study on separate sensible and latent cooling air-conditioning system. International Journal of Refrigeration, 33 (2010): 510-520.

[74] Ling et al. 2011

Ling, J., Kuwabara, O., Hwang, Y. and Radermacher, R.

Experimental evaluation and performance enhancement prediction of desiccant assisted separate sensible and latent cooling air-conditioning system. International Journal of Refrigeration, 34 (2011): 946-957.

[75] Ling et al. 2013

Ling, J., Kuwabara, O., Hwang, Y. and Radermacher, R.

Enhancement options for separate sensible and latent cooling air-conditioning systems. International Journal of Refrigeration, 36 (2013): 45-57.

[76] Liu et al. 2004

Liu, J., Wei, W., Ding, G., Zhang, C., Fukaya, M., Wang, K. and Inagaki, T.

A general steady state mathematical model for fin-and-tube heat exchanger based on graph theory. International Journal of Refrigeration, 27 (2004): 965-973.

[77] Liu et al. 2019

Liu, Z., Li, W., Chen, Y., Luo, Y. and Zhang, L.

Review of energy conservation technologies for fresh air supply in zero energy buildings. Applied Thermal Engineering, 148 (2019): 544-556.

[78] Lorsch 1994

Lorsch, H.G.

The impact of the indoor environment on occupant productivity-Part 2: Effects of temperature. ASHRAE Transactions, 100 (1994): 895-901.

[79] Lowenstein 2008

Lowenstein, A.

Review of liquid desiccant technology for HVAC applications. HVAC&R Research, 14 (2008): 819-839.

[80] Lstiburek 2002

Lstiburek, J.

Residential ventilation and latent loads. ASHRAE Journal, 44 (2002): 18.

[81] Lu et al. 2009

Lu, H., Chen, H., Xie, J., Tao, H. and Hu, Y.

Refrigerant flow distributary disequilibrium caused by configuration of two phase fluid pipe network. Energy Conversion and Management, 50 (2009): 730-738.

[82] Lu et al. 2004

Lu, Z., Ding, G. and Zhang, C.

Dynamic simulation of natural convection bypass two-circuit cycle refrigerator–freezer and its application: Part II: System simulation and application. Applied Thermal Engineering, 24 (2004): 1525-1533.

[83] MacArthur and Grald 1987

MacArthur, J. and Grald, E.

Prediction of cyclic heat pump performance with a fully distributed model and a comparison with experimental data. ASHRAE Transactions, 93 (1987).

[84] MacArthur 1984

MacArthur, J.W.

Transient heat pump behaviour: a theoretical investigation. International Journal of Refrigeration, 7 (1984): 123-132.

[85] Martínez et al. 2017

Martínez, P.J., Llorca, C., Pla, J.A. and Martínez, P.

Experimental validation of the simulation model of a DOAS equipped with a desiccant wheel and a vapor compression refrigeration system. Energies, 10 (2017): 1330.

[86] Matthews et al. 1989

Matthews, T., Thompson, C., Wilson, D., Hawthorne, A. and Mage, D.

Air velocities inside domestic environments: an important parameter in the study of indoor air quality and climate. Environment International, 15 (1989): 545-550.

[87] Mazzei et al. 2005

Mazzei, P., Minichiello, F. and Palma, D.

HVAC dehumidification systems for thermal comfort: a critical review. Applied Thermal Engineering, 25 (2005): 677-707.

[88] McGahey 1998

McGahey, K.

New commercial applications for desiccant-based cooling. ASHRAE Journal, 40 (1998): 41.

[89] McKeon et al. 2004

McKeon, B., Swanson, C., Zagarola, M., Donnelly, R. and SMITS, A.J.

Friction factors for smooth pipe flow. Journal of Fluid Mechanics, 511 (2004): 41.

[90] Mumma 2001a

Mumma, S.

Fresh thinking: dedicated outdoor air systems. Engineered Systems, 18 (2001a): 54-60.

[91] Mumma 2001b

Mumma, S.A.

Designing dedicated outdoor air systems. ASHRAE Journal, 43 (2001b): 28-32.

[92] Mumma 2002

Mumma, S.A.

Chilled ceilings in parallel with dedicated outdoor air systems: Addressing the concerns of condensation, capacity, and cost. ASHRAE Transactions, 108 (2002): 220.

[93] Muñoz et al. 2017

Muñoz, F., Sanchez, E.N., Xia, Y. and Deng, S.

Real-time neural inverse optimal control for indoor air temperature and humidity in a direct expansion (DX) air conditioning (A/C) system. International Journal of Refrigeration, 79 (2017): 196-206.

[94] Murphy 2002

Murphy, J.

Dehumidification performance of HVAC systems. ASHRAE Journal, 44 (2002): 23.

[95] Ndiaye and Bernier 2010

Ndiaye, D. and Bernier, M.

Dynamic model of a hermetic reciprocating compressor in on–off cycling operation (Abbreviation: Compressor dynamic model). Applied Thermal Engineering, 30 (2010): 792-799.

[96] Nevins et al. 1975

Nevins, R., RG, N., RR, G. and AP, G.

Effect of changes in ambient temperature and level of humidity on comfort and thermal sensations. (1975)

[97] Niemelä et al. 2002

Niemelä, R., Hannula, M., Rautio, S., Reijula, K. and Railio, J.

The effect of air temperature on labour productivity in call centres—a case study. Energy and Buildings, 34 (2002): 759-764.

[98] Pacheco-Vega et al. 2001

Pacheco-Vega, A., Sen, M., Yang, K. and McClain, R.L.

Neural network analysis of fin-tube refrigerating heat exchanger with limited experimental data. International Journal of Heat and Mass Transfer, 44 (2001): 763-770.

[99] Pan et al. 2012

Pan, Y., Xu, X., Xia, L. and Deng, S.

A modeling study on the effects of refrigerant pipeline length on the operational performance of a dual-evaporator air conditioning system. Applied Thermal Engineering, 39 (2012): 15-25.

[100] Park et al. 2007

Park, C., Cho, H., Lee, Y. and Kim, Y.

Mass flow characteristics and empirical modeling of R22 and R410A flowing through electronic expansion valves. International Journal of Refrigeration, 30 (2007): 1401-1407.

[101] Pramuang and Exell 2007

Pramuang, S. and Exell, R.

The regeneration of silica gel desiccant by air from a solar heater with a compound parabolic concentrator. Renewable Energy, 32 (2007): 173-182.

[102] Qi and Deng 2008

Qi, Q. and Deng, S.

Multivariable control-oriented modeling of a direct expansion (DX) air conditioning (A/C) system. International Journal of Refrigeration, 31 (2008): 841-849.

[103] Qi and Deng 2009

Qi, Q. and Deng, S.

Multivariable control of indoor air temperature and humidity in a direct expansion (DX) air conditioning (A/C) system. Building and Environment, 44 (2009): 1659-1667.

[104] Qu et al. 2012

Qu, M., Xia, L., Deng, S. and Jiang, Y.

An experimental investigation on reverse-cycle defrosting performance for an air source heat pump using an electronic expansion valve. Applied Energy, 97 (2012): 327-333.

[105] Rambhad et al. 2016

Rambhad, K.S., Walke, P.V. and Tidke, D.

Solid desiccant dehumidification and regeneration methods—A review. Renewable and Sustainable Energy Reviews, 59 (2016): 73-83.

[106] Rasmussen and Alleyne 2004

Rasmussen, B.P. and Alleyne, A.G.

Control-oriented modeling of transcritical vapor compression systems. Journal of Dynamic Systems, Measurement, and Control, 126 (2004): 54-64.

[107] Rhee et al. 2017

Rhee, K., Olesen, B.W. and Kim, K.W.

Ten questions about radiant heating and cooling systems. Building and Environment, 112 (2017): 367-381.

[108] Rudd 2013

Rudd, A.

Supplemental Dehumidification in Warm-Humid Climates. Building America Report, 1310 (2013).

[109] Rudd et al. 2005

Rudd, A., Lstiburek, J. and Ueno, K.

Residential Dehumidification Systems Research for Hot-Humid Climates. Building Science Corporation Research Report, 505 (2005).

[110] Saber et al. 2016

Saber, E.M., Tham, K.W. and Leibundgut, H.

A review of high temperature cooling systems in tropical buildings. Building and Environment, 96 (2016): 237-249.

[111] Sami 1993

Sami, S.

Dynamic performance of heat pumps using refrigerant R-134a. ASHRAE Transactions, 99 (1993): 41-47.

[112] Sami and Zhou 1995

Sami, S. and Zhou, Y.

Numerical prediction of heat pump dynamic behaviour using ternary non-azeotropic refrigerant mixtures. International Journal of Energy Research, 19 (1995): 19-35.

[113] Sekhar 2013

Sekhar, C.

Good humidity control: hot, humid climates. ASHRAE Journal, 55 (2013): 68-71.

[114] Sekhar 2016

Sekhar, S.

Thermal comfort in air‐conditioned buildings in hot and humid climates–why are we not getting it right? Indoor Air, 26 (2016): 138-152.

[115] Seo et al. 2014

Seo, J.M., Song, D. and Lee, K.H.

Possibility of coupling outdoor air cooling and radiant floor cooling under hot and humid climate conditions. Energy and Buildings, 81 (2014): 219-226.

[116] Shah et al. 2004

Shah, R., Alleyne, A.G. and Bullard, C.W.

Dynamic modeling and control of multi-evaporator air-conditioning systems. ASHRAE Transactions, 110 (2004): 109.

[117] Deng 2000

Deng, S.

A dynamic mathematical model of a direct expansion (DX) water-cooled air-conditioning plant. Building and Environment, 35 (2000): 603-613.

[118] Shirey 1993

Shirey, D.

Demonstration of efficient humidity control techniques at an art museum, the 1993 Winter Meeting of ASHRAE Transactions. Part 1, Chicago, IL, USA, 01/23-27/93, 694-703

[119] Shirey et al. 2006

Shirey III, D.B., Henderson Jr, H.I. and Raustad, R.A.

Understanding the Dehumidification Performance of Air-Conditioning Equipment at Part-Load Conditions. University of Central Florida. (2006).

[120] Song et al. 2014

Song, M., Deng, S. and Xia, L.

A semi-empirical modeling study on the defrosting performance for an air source heat pump unit with local drainage of melted frost from its three-circuit outdoor coil. Applied Energy, 136 (2014): 537-547.

[121] Standard 2010

Standard, A.

Standard 55-2010, Thermal environmental conditions for human occupancy. American Society of Heating, Refrigerating and Air Conditioning Engineers (2010).

[122] Tian et al. 2004

Tian, C., Dou, C., Yang, X. and Li, X.

A mathematical model of variable displacement wobble plate compressor for automotive air conditioning system. Applied Thermal Engineering, 24 (2004): 2467-2486.

[123] Toftum 2004

Toftum, J.

Air movement–good or bad? Indoor Air, 14 (2004): 40-45.

[124] Toftum and Fanger 1999

Toftum, J. and Fanger, P.O.

Air humidity requirements for human comfort. ASHRAE transactions, 105 (1999): 641.

[125] Toftum et al. 1998a

Toftum, J., Jørgensen, A.S. and Fanger, P.O.

Upper limits for indoor air humidity to avoid uncomfortably humid skin. Energy and Buildings, 28 (1998a): 1-13.

[126] Toftum et al. 1998b

Toftum, J., Jørgensen, A.S. and Fanger, P.O.

Upper limits of air humidity for preventing warm respiratory discomfort. Energy and Buildings, 28 (1998b): 15-23.

[127] Tuo et al. 2012

Tuo, H., Bielskus, A. and Hrnjak, P.

Experimentally validated model of refrigerant distribution in a parallel microchannel evaporator. SAE International Journal of Materials and Manufacturing, 5 (2012): 365-374.

[128] Vargas and Parise 1995

Vargas, J. and Parise, J.

Simulation in transient regime of a heat pump with closed-loop and on-off control. International Journal of Refrigeration, 18 (1995): 235-243.

[129] Wang and Touber 1991

Wang, H. and Touber, S.

Distributed and non-steady-state modeling of an air cooler. International Journal of Refrigeration, 14 (1991): 98-111.

[130] Westphalen 2004

Westphalen, D.

Energy savings for rooftop AC. ASHRAE Journal, 46 (2004): 38-46.

[131] Worek and Chung 1986

Worek, W.M. and Chung, J.M.

Simulation of an integrated hybrid desiccant vapor-compression cooling system. Energy, 11 (1986): 1005-1021.

[132] Wyon et al. 2006

Wyon, D.P., Fang, L., Lagercrantz, L. and Fanger, P.O.

Experimental determination of the limiting criteria for human exposure to low winter humidity indoors (RP-1160). HVAC&R Research, 12 (2006): 201-213.

[133] Xia et al. 2019

Xia, Y., Ding, Q., Jiangzhou, S., Zhang, X. and Deng, S.

A simulation study on the operational stability of an EEV-controlled direct expansion air conditioning system under variable speed operation. International Journal of Refrigeration, 103 (2019): 115-125.

[134] Xia et al. 2018

Xia, Y., Yan, H., Deng, S. and Chan, M.

A new capacity controller for a direct expansion air conditioning system for operational safety and efficiency. Building Services Engineering Research and Technology, 39 (2018): 21-37.

[135] Xiao et al. 2011

Xiao, F., Ge, G. and Niu, X.

Control performance of a dedicated outdoor air system adopting liquid desiccant dehumidification. Applied Energy, 88 (2011): 143-149.

[136] Xu et al. 2010

Xu, X., Xia, L., Chan, M. and Deng, S.

Inherent correlation between the total output cooling capacity and equipment sensible heat ratio of a direct expansion air conditioning system under variable-speed operation (XXG SMD SHR DX AC unit). Applied Thermal Engineering, 30 (2010): 1601-1607.

[137] Xu et al. 2018

Xu, X., Zhong, Z., Deng, S. and Zhang, X.

A review on temperature and humidity control methods focusing on air-conditioning equipment and control algorithms applied in small-to-medium-sized buildings. Energy and Buildings, 162 (2018): 163-176.

[138] Xu et al. 1996

Xu, Z., Gotham, D., Collins, M., Coney, J., Sheppard, C. and Merdjani, S.

A numerical and experimental study of turbulent flow through the evaporator coil in an air-conditioning unit. International Journal of Refrigeration, 19 (1996): 369-381.

[139] Xue et al. 2008

Xue, Z., Lin, S. and Ou, H.

Refrigerant flow characteristics of electronic expansion valve based on thermodynamic analysis and experiment. Applied Thermal Engineering, 28 (2008): 238-243.

[140] Yadav 1995

Yadav, Y.

Vapour-compression and liquid-desiccant hybrid solar space-conditioning system for energy conservation. Renewable Energy, 6 (1995): 719-723.

[141] Yan et al. 2016

Yan, H., Deng, S. and Chan, M.

A novel capacity controller for a three-evaporator air conditioning (TEAC) system for improved indoor humidity control. Applied Thermal Engineering, 98 (2016): 1251-1262.

[142] Yan et al. 2018

Yan, H., Xia, Y., Xu, X. and Deng, S.

Inherent operational characteristics aided fuzzy logic controller for a variable speed direct expansion air conditioning system for simultaneous

indoor air temperature and humidity control. Energy and Buildings, 158 (2018): 558-568.

[143] Ye et al. 2007

Ye, Q., Chen, J. and Chen, Z.

Experimental investigation of R407C and R410A flow through electronic expansion valve. Energy Conversion & Management, 48 (2007): 1624-1630.

[144] Zhang et al. 2019a

Zhang, G., Xiao, H., Wang, B., Li, X., Shi, W. and Cao, Y.

Review on recent developments of variable refrigerant flow systems since 2015. Energy and Buildings, 198 (2019a): 444-466.

[145] Zhang et al. 1990

Zhang, J., Christianson, L. and Riskowski, G.

Regional airflow characteristics in a mechanically ventilated room under non-isothermal conditions. ASHRAE Transactions, 96 (1990): 751-759.

[146] Zhang et al. 2012

Zhang, X.J., Xiao, F. and Li, S.

Performance study of a constant temperature and humidity air-conditioning system with temperature and humidity independent control device. Energy and Buildings, 49 (2012): 640-646.

[147] Zhang et al. 2011

Zhang, X.J., Yu, C.Y., Li, S., Zheng, Y.M. and Xiao, F.

A museum storeroom air-conditioning system employing the temperature and humidity independent control device in the cooling coil. Applied Thermal Engineering, 31 (2011): 3653-3657.

[148] Zhang et al. 2019b

Zhang, Z., Cao, X., Yang, Z., Shao, L. and Zhang, C.

Modeling and experimental investigation of an advanced direct-expansion outdoor air dehumidification system. Applied Energy, 242 (2019b): 1600-1612.

[149] Zhao et al. 2011

Zhao, K., Liu, X., Zhang, T. and Jiang, Y.

Performance of temperature and humidity independent control air-conditioning system in an office building. Energy and Buildings, 43 (2011): 1895-1903.

[150] Zhong et al. 2017

Zhong, Z., Xu, X., Zhang, X. and Huang, Z.

Simulation based control performance evaluation of a novel fuzzy logic control algorithm for simultaneously controlling indoor air temperature and humidity using a direct expansion (DX) air-conditioning (A/C) system. Procedia Engineering, 205 (2017): 1792-1799.

[151] Zhu et al. 2014a

Zhu, Y., Jin, X., Du, Z., Fan, B. and Fang, X.

Simulation of variable refrigerant flow air conditioning system in heating mode combined with outdoor air processing unit. Energy and Buildings, 68 (2014a): 571-579.

[152] Zhu et al. 2014b

Zhu, Y., Jin, X., Du, Z., Fang, X. and Fan, B.

Control and energy simulation of variable refrigerant flow air conditioning system combined with outdoor air processing unit. Applied Thermal Engineering, 64 (2014b): 385-395.